Theory and application of explicitly correlated Gaussians

Jim Mitroy*

ARC Center for Antimatter-Matter Studies, School of Engineering, Charles Darwin University, Darwin NT 0909, Australia

Sergiy Bubin and Kálmán Varga

Department of Physics and Astronomy, Vanderbilt University, Nashville, Tennessee 37235, USA

Wataru Horiuchi

Department of Physics, Hokkaido University, Sapporo 060-0810, Japan

Yasuyuki Suzuki

Department of Physics, Niigata University, Niigata 950-2181, Japan and RIKEN Nishina Center, Wako 351-0198, Japan

Ludwik Adamowicz

Department of Chemistry and Biochemistry and Department of Physics, University of Arizona, Tucson, Arizona 85721, USA

Wojciech Cencek and Krzysztof Szalewicz

Department of Physics and Astronomy, University of Delaware, Newark, Delaware 19716, USA

Jacek Komasa

Faculty of Chemistry, Adam Mickiewicz University, Grunwaldzka 6, Poznan 60-780, Poland

Doerte Blume

Department of Physics and Astronomy, Washington State University, Pullman, Washington 99164-2814, USA

(Dated: September 3, 2012)

Abstract

The variational method complemented with the use of explicitly correlated Gaussian basis functions is one of the most powerful approaches currently used for calculating the properties of few-body systems. Despite its conceptual simplicity the method offers great flexibility, high accuracy and can be used to study diverse quantum systems, ranging from small atoms and molecules to light nuclei, hadrons, quantum dots, and Efimov systems. The basic theoretical foundations are discussed, recent advances in the applications of explicitly correlated Gaussians (ECG) in physics and chemistry are reviewed, and the strengths and weaknesses of the ECG approach are compared with other few-body techniques.

PACS numbers: 31.15.-p, 31.15.ac, 21.60.De, 03.65.Nk

*Electronic address: jxm107@rsphysse.anu.edu.au

Contents

I. Introduction 6

A. The quantum few-body problem 6

B. Explicitly correlated Gaussians 8

II. Formalism 10

A. Hamiltonian 10

B. The variational principle 12

C. Center of mass reduction 12

D. Choice of basis functions 15

1. Central potentials and states with small total orbital angular momentum 16

2. Global vector representation for states with arbitrary L 17

3. Explicitly correlated Gaussians with shifted centers 18

4. Basis functions for systems in external fields 20

5. Completeness of Gaussian basis sets 21

E. Matrix elements 21

F. Relativistic and QED corrections 23

G. Perturbative treatment of the finite mass effects 25

1. Adiabatic approximation 25

2. Nonadiabatic nuclear equation 27

III. Computational methodologies 28

A. Parameter optimization 28

1. Stochastic optimization 29

2. Why extensive optimization is feasible 30

3. Direct optimization 31

B. Computational requirements 32

C. Improving the convergence of the expectation values of singular operators 33

1. Expectation value identities 33

2. Integral transform technique 34

3. ECG basis functions with linear prefactors 37

D. Strongly repulsive interactions 37
E. Highly excited states 39
F. Linear dependence issues 39
G. Fixed core methods 41
H. The Gaussian expansion method 43
I. Other types of basis functions 44
1. Hylleraas and related functions 44
2. James-Coolidge type functions for H_2 45
3. Single center basis functions 46
J. Many body perturbation theories and coupled cluster methods 47
K. Hyperspherical methods 50
L. Monte Carlo techniques 51

IV. Atomic structure applications 53
A. Benchmark calculations of non-relativistic atoms 53
1. The hydrogen atom 55
2. Two-electron atoms 55
3. Three-electron atoms 55
4. Four-electron atoms 56
5. Five-electron atoms 57
6. Inclusion of relativistic effects 58
B. Atoms in magnetic fields 58
C. Atomic polarizability calculations 59
D. Positronic complexes 61
E. Coulomb few-body systems 66
F. Outlook 67

V. Molecular structure applications 67
A. Geminals and perturbation theory 67
B. Ab-initio Born-Oppenheimer calculations 69
1. Relativistic and QED corrections for light molecules 73
C. Going beyond the Born-Oppenheimer approximation 75

D. Outlook 78
1. Contractions of ECGs 79

VI. Application to nuclear structure calculations 79
A. Nuclear Hamiltonian and wave function 79
B. Alpha particle 80
C. Application to multi-cluster systems 83
D. Baryon spectroscopy 85
E. Outlook 86

VII. Few-body systems in condensed matter 87
A. Excitonic complexes 87
B. 2D and 3D quantum dots and quantum wells 88

VIII. Ultracold bosonic and fermionic few-body systems 91
A. Two-component Fermi gases 93
B. Hyperspherical ECG approach 96
C. Bose systems and Efimov physics 99
D. Outlook 101

IX. Scattering and resonances 102
A. Single channel elastic scattering systems 103
1. Confining potentials 103
2. The asymptotic basis 103
3. Getting scattering information 104
4. Stabilization calculations 104
5. Kohn variational calculations 107
B. Multi-channel scattering 109
1. Continuum discretized coupled-channels method 109
2. R-matrix calculations of few-nucleon reactions 110
C. Complex rotation calculations of resonances 113
1. Antiprotonic helium 115
2. Complex Scaling calculation with SVM 115

3. Electric dipole response of ^{4}He 118
D. Outlook 119
X. Conclusions 120
Acknowledgments 122
References 122

I. INTRODUCTION

A. The quantum few-body problem

This review will discuss the application of explicitly correlated Gaussians (ECGs) to the description of quantum few-body systems. The quantum few-body problem is as old as quantum mechanics. Immediately after the birth of quantum mechanics, one of the most significant problems to be solved was the correct prediction of the ionization energy of helium. This problem was put to E. Hylleraas by M. Born (Hylleraas, 1963). A series of increasingly sophisticated calculations using the Ritz (variational) method were then completed on states of the helium atom and two-electron ions (Hylleraas, 1928; Hylleraas, 1929; Hylleraas, 1929, 1930a). Agreement at the level of about 0.1 part per thousand was achieved (Hylleraas, 1929). One of the key ingredients in these calculations was the use of a correlated basis explicitly involving the electron-electron distance, $r_{12} = |\mathbf{r}_1 - \mathbf{r}_2|$.

Although many different approaches have been devised to solve few-body problems, the present work focuses on those that exploit the Ritz variational principle, namely

$$E_0 = \frac{\langle \Psi_0 | H | \Psi_0 \rangle}{\langle \Psi_0 | \Psi_0 \rangle} \geq E_{\text{exact}} \ . \tag{1}$$

The trial wave function, Ψ_0, is constructed to minimize the energy, E_0. The few-body problem is a subset of the N-body problem with the number of particles typically restricted to lie between three and six. When solving the few-body problem one seeks to develop from the outset techniques to describe precisely the inter-particle correlations between all particles in the systems. In the N-body problem, mean-field approaches, such as the Hartree-Fock (HF) method are often used as the starting point.

Few-body systems occur in many areas of physics and cover range of energy and length scales. In particle physics, i.e., at the sub-nuclear level, the basic constituents are quarks. Assuming effective model interactions consistent with our understanding of the strong force, few-body techniques can help to determine the ordering of the energy levels of hadrons (baryons and mesons) and provide insights into the formation of clusters consisting of more than three quarks. At somewhat lower energy scales, around 1-20 MeV, the basic constituents are nucleons interacting through the strong and coulomb forces. The ^{3}H, ^{3}He and ^{4}He nuclei and other light nuclei including hypernuclei are important systems since a complete understanding of their structures and interactions is a necessary condition for a better understanding of the nuclear interaction.

In atomic physics, the helium and lithium atoms are primary few-body examples. The basic constituents are the electrons, and their interactions are governed by the electromagnetic interactions. While the typical atomic energy scale is around 1-10 eV, interpretation of high precision measurements that are sensitive to relativistic corrections and possibly the shape of the nucleus require calculations that are accurate to an overall precision of 10^{-10} eV.

In molecular physics, one can identify H_2^+, H_2, He_2^+, LiH and He_2 as "simple" few-body systems. Compared to atomic systems, the internuclear distance coordinate introduces new degrees of freedom, i.e., the vibrational and rotational degrees of freedom with typical energy scales of 10^{-1} eV and 10^{-3} eV, respectively. As in atomic physics, the charged particles interact via the electromagnetic interaction. The internuclear distance vector has traditionally been fixed as in the Born-Oppenheimer approximation but recent developments has enabled calculations where this restriction is relaxed.

Examples of few-body systems that occur in soft condensed matter consist of two and three dimensional quantum dots which might only contain electrons and excitonic complexes which are made up of electrons and holes that interact electromagnetically and are confined externally. Just as in atomic systems, the typical energy scales are of the order of 1-10 eV, and the forces predominantly electromagnetic but is influenced by the medium in which the object is immersed.

Finally, recent developments in cold atom physics have greatly stimulated the investigation of Efimov physics and general studies of the stability of few-body systems. In these applications, the basic constituents are neutral atoms interacting through van der Waals

potentials and the typical energy scales are of the order of 10^{-10} eV.

Much work in the field of few-body physics is related to low-energy collision processes. Description of the dynamics of collisions is particularly important for the investigation of nuclear and cold atom systems.

A variety of theoretical techniques have been developed to study such systems, for example, quantum monte carlo methods, configuration interaction methods and the no-core shell model, methods that use hyperspherical coordinate systems, and variational methods using basis sets that represent a development of those originally developed by Hylleraas. These are only mentioned briefly in the present review which is focussed on the application of ECGs which have been successfully applied to the investigations of all the systems described above. Some of these are listed in Table I which contains a list of the acronyms that are used in this review.

B. Explicitly correlated Gaussians

The fundamental results concerning ECGs were first put forward in 1960 by Boys (Boys, 1960) and Singer (Singer, 1960). They proposed to describe the N particle wave function with a basis of exponential functions with an argument involving the square of the distance between every pair of particles. Such a function can be written as

$$\psi = \exp\left(-\sum_{i>j=1}^{N} \alpha_{ij}(\mathbf{r}_i - \mathbf{r}_j)^2\right), \tag{2}$$

where α_{ij} are adjustable parameters. The advantage of this functional form is twofold. First, very high accuracy is achievable since the basis functions are correlated. This advantage is magnified for systems with strongly attractive inter-particle interactions. Secondly, the quadratic form involving inter-particle distances permits the reduction of the Hamiltonian matrix elements to very simple analytic expressions. The algebraic complexity of the matrix elements does not change at all for $N \geq 3$ and this has permitted calculations with correlated basis sets to be performed on systems which were previously inaccessible. They represent a major advantage over exponential functions with linear distance factors since these basis functions lead to matrix elements of increasing intractability as the number of particles increases (King *et al.*, 2011).

Despite the computational advantages, the ECG basis was long regarded as inferior to the

exponential $\exp(-\alpha r)$ form since the ECG basis functions do not have the correct functional form near the $r_{ij} \to 0$ coalescence point for Coulomb interactions. They also have the incorrect forms for the $r_{ij} \to \infty$ asymptote for short range potentials. However, the amazing ease with which matrix elements can be computed has allowed ECGs to be used to describe a number of diverse physical systems. Furthermore, it makes the extensive optimization of the Gaussian exponents computationally feasible (Cencek and Rychlewski, 1993; Kukulin and Krasnopol'sky, 1977; Varga and Suzuki, 1995), leading to very accurate energies and other properties.

While the fundamental results concerning ECGs have been known for a long time, it is mainly since the 1990s that it has been systematically used by a number of different research groups. Fig. 1 shows the citations to the original Boys and Singer papers (Boys, 1960; Singer, 1960) by decade. The citation count increased markedly in the 1991-2000 and 2001-2010 decades. Prior to the 1991-2000 decade, the applications of ECG basis sets to the few-body problem are best described as intermittent. The lack of activity prior to the 1991-2000 decade was probably due to a number of reasons. One contributing factor would have been that prior to the 1990s, much research in few-body physics was focussed on three-body problems where the ECG basis does not have a competitive advantage over other methods.

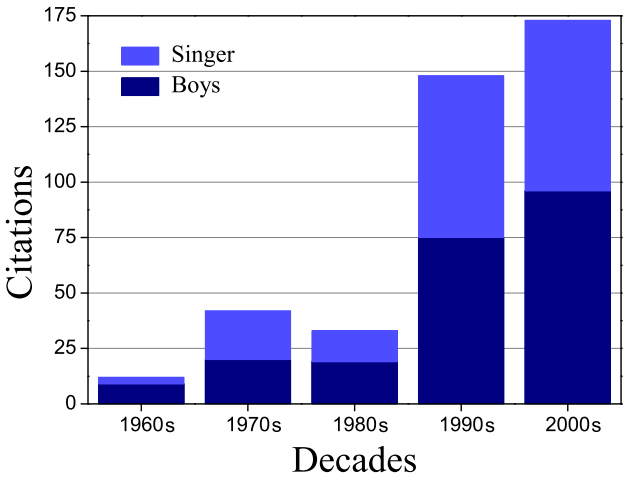

FIG. 1 (Color oline) Number of citations by decade to the original works (Boys, 1960) and (Singer, 1960). The data for both articles is taken from the ISI Web of Knowledge science citation database as of October 1, 2011. The last decade covers the years 2000-2011.

To a certain extent, the development of the ECG basis set for few-body quantum physics

mirrors the development of single particle Gaussian basis sets (Boys, 1950; McWeeny, 1950) for the calculation of electronic structures for molecules. Initially, there were concerns about the accuracy of the wave functions near the nuclear centers and in the $r \to \infty$ limit. However, the pragmatic consideration of simply being able to perform realistic calculations on molecules, regardless of whether they had two or more centers overcame any considerations of the theoretical niceties and the field of quantum chemistry is now dominated by the use of Gaussian basis sets.

Another major advantage of ECGs is that the inter-particle interactions can be treated with all pairs of particles being given equal prominence. This makes the ECG basis sets very suitable for treating systems with attractive interactions that result in strong inter-particle correlations. Examples of such systems include small nuclear systems with tendencies to form α-particle clusters (Varga *et al.*, 1995), exotic positron-atom systems with a tendency to form positronium clusters (Ryzhikh *et al.*, 1998b) and excitonic systems (Riva *et al.*, 2000, 2001). The ECG basis has also been generalized to handle systems with strongly repulsive interactions (or "hard-core" potentials) (Kinghorn and Adamowicz, 1999; Stanke *et al.*, 2006).

II. FORMALISM

A. Hamiltonian

Consider an N-particle system where the i-th particle with mass m_i is described by the position vector $\mathbf{r}_i$. The Hamiltonian of the system reads

$$H = \sum_{i=1}^{N} \frac{\mathbf{p}_i^2}{2m_i} + \sum_{i=1}^{N} U_i(\mathbf{r}_i) + \sum_{j>i=1}^{N} V_{ij}(\mathbf{r}_i, \mathbf{r}_j), \tag{3}$$

where U_i is the one-body potential experienced by the i-th particle in the presence of an external field and V_{ij} is the interaction between particles i and j. It is assumed that all particles interact via two-body forces. In the most general case we can also introduce three- and more body potentials, as well as consider the case of nonlocal interactions. Also, for some systems, the potentials may depend on additional degrees of freedom such as spin, isospin, flavor, etc. The specific interactions relevant to a particular system will be discussed as needed.

TABLE I Glossary of acronyms and abbreviations used in this manuscript.

Abbreviation	Description
AV8	Argonne nucleon-nucleon interaction with 8 operators
AV18	Argonne nucleon-nucleon interaction with 18 operators
BEC	Bose-Einstein condensate
BO	Born-Oppenheimer
CDCC	Continuum discretized coupled channels
CCSD(T)	Coupled cluster method with single,double and non-iterative triple excitations perturbatively
CI	Configuration interaction
CI-R12	Configuration interaction with r_{ij} correlation factors.
CSM	Complex scaling method
DMC	Diffusion Monte Carlo
ECG	Explicitly correlated Gaussian
EVI	Expectation value identities for evaluation of singular operators
FCCI	Fixed core configuration interaction
FCSVM	Fixed core stochastic variational method
GEM	Gaussian expansion method
GFMC	Greens function Monte Carlo
GJC	Generalized James Coolidge
GTG	Gaussian type geminals
GVR	Global vector representation
HECG	Hyperspherical ECG
HYL	Hylleraas basis functions
HYL-LOG	Hylleraas basis functions with logarithmic factors
HF	Hartree-Fock
HH	Hyperspherical harmonic
IT	Integral transform approach for evaluation of singular operators

B. The variational principle

The fundamental result underpinning much work in bound state few-body physics is the variational theorem, which states that the Hamiltonian expectation value of any approximate wave function $|\Psi_0\rangle$ forms an upper bound to the exact energy (Kellner, 1927), i.e.

$$\langle\Psi_0|H|\Psi_0\rangle = E_0 \geq E_{\rm exact}. \tag{4}$$

This results is a widely used strategy to generate accurate wave functions and energies. The trial wave function $|\Psi_0\rangle$ will be written as a linear combination of basis functions,

$$|\Psi_0\rangle = \sum_{i=1}^{\mathcal{N}} c_i |\psi_i(\{\alpha\}_i)\rangle \ . \tag{5}$$

The basis functions $\psi_i(\{\alpha_i\})$ will usually have some dependence on a set of parameters $\{\alpha\}_i$. The c_i coefficients and the parameters $\{\alpha\}_i$ are then adjusted to minimize the energy. Minimizing the c_i coefficients leads to the generalized eigenvalue problem

$$H\mathbf{c} = ES\mathbf{c} \ , \tag{6}$$

where the H and S are $\mathcal{N}\times\mathcal{N}$ Hamiltonian and overlap matrices with the elements

$$H_{ij} = \langle\psi_i|H|\psi_j\rangle, \qquad S_{ij} = \langle\psi_i|\psi_j\rangle \ . \tag{7}$$

and $\mathbf{c}$ is a $\mathcal{N}$-component vector of linear coefficients c_i. Trying to minimize the energy with respect to the $\{\alpha\}$ parameters results in a non-linear optimization problem. In general, Eq. (6) has $\mathcal{N}$ solutions. The Hylleraas-Undheim-McDonald theorem (Hylleraas, 1930b; MacDonald, 1933) states that the n-th lowest eigenvalue of (6) gives an upper bound to the corresponding exact n-th excited energy of the system in question.

C. Center of mass reduction

In the absence of external fields it is natural to separate out the contribution from the center-of-mass motion and focus on the intrinsic motion of the system. The most convenient way of doing this is to introduce some set of relative coordinates. There are two common choices here: one is the Jacobi coordinate set, the other is the set of coordinates where the origin is placed on one of the particles (for example, at particle 1) (Suzuki and Varga, 1998).

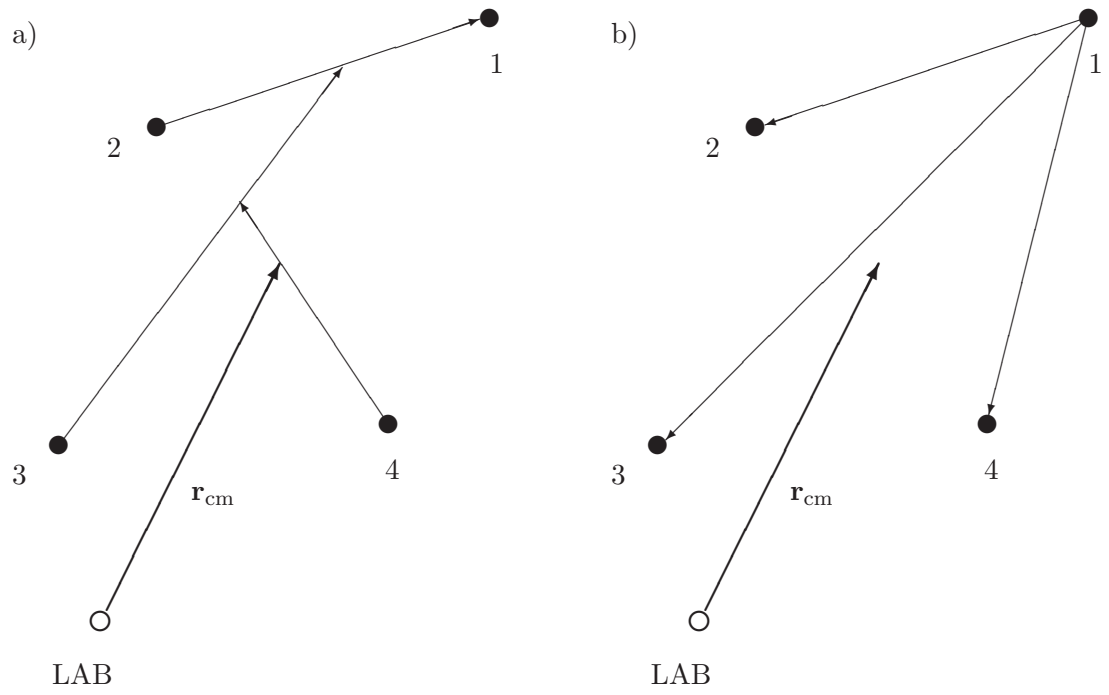

FIG. 2 Possible sets of relative coordinates: (a) the Jacobi coordinates, and (b) the coordinates where one of the particles (in this case the first one) serves as a reference particle.

These choices are schematically illustrated in Fig. 2. The relation between the laboratory frame coordinates $(\mathbf{x}_1, \mathbf{x}_2, \ldots, \mathbf{x}_N)$ and the relative (Jacobi) coordinates $(\mathbf{r}_1, \mathbf{r}_2, \ldots, \mathbf{r}_N)$ (here we assume that $\mathbf{r}_N$ is the position of the center of mass, $\mathbf{r}_{\rm cm}$) is linear and given by

$$\mathbf{r}_i = \sum_{j=1}^{N} \Omega_{ij} \mathbf{x}_j, \qquad \mathbf{x}_i = \sum_{j=1}^{N} (\Omega^{-1})_{ij} \mathbf{r}_j, \qquad i = 1, \ldots, N. \tag{8}$$

The explicit form of the transformation matrix Ω and its inverse for the case of the Jacobi coordinates is the following:

$$\Omega_{\rm Jac} = \begin{pmatrix} 1 & -1 & 0 & \cdots & 0 \\ \frac{m_1}{M_2} & \frac{m_2}{M_2} & -1 & \cdots & 0 \\ \vdots & \vdots & \vdots & \ddots & \vdots \\ \frac{m_1}{M_{N-1}} & \frac{m_2}{M_{N-1}} & \frac{m_3}{M_{N-1}} & \cdots & -1 \\ \frac{m_1}{M_N} & \frac{m_2}{M_N} & \frac{m_3}{M_N} & \cdots & \frac{m_N}{M_N} \end{pmatrix}. \tag{9}$$

For the case of relative coordinates the transformation matrix is:

$$\Omega_{\rm rel} = \begin{pmatrix} -1 & 1 & 0 & \cdots & 0 \\ -1 & 0 & 1 & \cdots & 0 \\ \vdots & \vdots & \vdots & \ddots & \vdots \\ -1 & 0 & 0 & \cdots & 1 \\ \frac{m_1}{M_N} & \frac{m_2}{M_N} & \frac{m_3}{M_N} & \cdots & \frac{m_N}{M_N} \end{pmatrix}, \tag{10}$$

where

$$M_k = \sum_{i=1}^{k} m_i. \tag{11}$$

The inverse transformation matrices can also be written explicitly (Suzuki and Varga, 1998). The choice of a coordinate system where the origin is placed at one of the particles may be natural in many practical situations, for example when that particle is much heavier than the other ones (this situation occurs in an atom with its heavy nucleus and light electrons).

The new linear momenta $\mathbf{p}_i$ conjugated to Jacobi (relative) coordinates $\mathbf{r}_i$ can be obtained by applying the inverse transformation to the linear momentum conjugated to the laboratory frame coordinates:

$$\mathbf{p}_i = \sum_{j=1}^{N} (\Omega^{-1})_{ij} \mathbf{q}_j, \qquad \mathbf{q}_i = \sum_{j=1}^{N} \Omega_{ij} \mathbf{p}_j, \qquad i = 1, \ldots, N. \tag{12}$$

After transforming the coordinates using relation Eq. (9) or (10) the kinetic energy operator,T, of the new Hamiltonian, contains two terms: the kinetic energy of $n = N - 1$ (pseudo)particles moving in the new reference frame and the kinetic energy of the center of mass:

$$T = \frac{1}{2} \sum_{i,j=1}^{n} \Lambda_{ij} \mathbf{p}_i \cdot \mathbf{p}_j + T_{\rm cm}. \tag{13}$$

Here Λ is a $n \times n$ "mass" matrix with the elements

$$\Lambda_{ij} = \sum_{k=1}^{N} \frac{1}{m_k} \Omega_{ik} \Omega_{jk}. \tag{14}$$

The operator of the kinetic energy of the center of mass is given by

$$T_{\rm cm} = \frac{\mathbf{p}_{\rm cm}^2}{2M_{\rm N}}. \tag{15}$$

Since the potential in the absence of external fields depends only on the inter-particle coordinates, the total Hamiltonian of the system in the new coordinates is independent of $\mathbf{r}_{\rm cm}$. Therefore, the total wave function can be represented as a product of the wave function describing the intrinsic motion of the system, ψ, and a plane wave corresponding to the motion of the system as a whole:

$$\psi_{\rm tot} = \exp(i\mathbf{k}_{\rm cm}\cdot\mathbf{r}_{\rm cm})\psi(\mathbf{r}_1,\ldots,\mathbf{r}_n). \tag{16}$$

From now on we will concentrate on finding ways to approximate the intrinsic wave function.

D. Choice of basis functions

In this subsection the ECG functions that are used to expand the system wave function are introduced. The ECGs, which depend on relative coordinates are defined as follows

$$G_A(\mathbf{r}) = \exp(-\mathbf{r}'A\mathbf{r}), \tag{17}$$

where A is an $n\times n$ symmetric positive-definite matrix whose elements are variational parameters and the quadratic form in the exponent is defined as

$$\mathbf{r}'A\mathbf{r} = \sum_{i,j=1}^{n} A_{ij}\mathbf{r}_i\cdot\mathbf{r}_j. \tag{18}$$

Here and below the prime symbol is used to denote the vector or matrix transpose. The ECG function can be rewritten in a more intuitive form:

$$\exp(-\mathbf{r}'A\mathbf{r}) = \exp\left(-\sum_{j>i=1}^{N}\alpha_{ij}(\mathbf{r}_i-\mathbf{r}_j)^2 - \sum_{i=1}^{N}\beta_i\mathbf{r}_i^2\right). \tag{19}$$

The parameters α_{ij} and β_i can be expressed by the elements of matrix A and vice versa. The advantage of this notation is that it explicitly connects the nonlinear parameters α_{ij} to the pair correlation between the particles i and j and thus explains the name "explicitly correlated Gaussians". The second part, $\exp\left(-\sum_{i=1}^{N}\beta_i\mathbf{r}_i^2\right)$, is a product of independent single-particle Gaussians centered at the origin.

A variational trial wave functions can be formed by linear combination of ECGs:

$$\psi_{SM_S}(\mathbf{r},A) = \sum_{k=1}^{\mathcal{N}} c_k\mathcal{A}\{G_{A_k}(\mathbf{r})\chi_{SM_S}\}, \tag{20}$$

where the operator $\mathcal{A}$ is an antisymmetrizer (or symmetrizer in the case of bosons), and χ_{SM_S} is the spin function of the system with the total spin S and its projection M_S. The spin function is defined by coupling the single-particle spin functions $\xi(i)$ (i is the particle label) as

$$\chi_{SM_S} = \Big[\big[[\xi(1)\xi(2)]_{S_{12}}\,\xi(3)\big]_{S_{123}}\ldots\Big]_{SM_S} \tag{21}$$

using the common rules of addition of angular momenta. In this scheme $S_{12\ldots i}$ represents the intermediate total spin at each successive coupling. The accuracy of the trial function depends on the dimension of the expansion, $\mathcal{N}$, and the nonlinear parameters A_k in Eq. (20).

1. *Central potentials and states with small total orbital angular momentum*

The ECGs of Eq. (17) are spherically symmetric (the quadratic form is invariant with respect to 3D rotations) and suitable for describing states with zero total orbital angular momentum. It should be noted that such functions can be used in calculations of systems where one of the particles is infinitely heavy (such as an atom with a clamped nuclei). In this case the origin of the laboratory coordinate system can be placed at the infinitely heavy particle and the positions of other particles in the lab frame will coincide with the relative coordinates with respect to that particle. For example, if the clamped particle is the N-th particle, then $\mathbf{r}_i = \mathbf{x}_i$, $i = 1, \ldots, N-1$.

The formalism has to be extended to describe systems with nonzero angular momentum. It becomes necessary to construct basis functions that are eigenfunctions of the square of the total angular momentum operator with angular momentum L.

A common approach to building basis functions of proper rotational symmetry, i.e. those that correspond to a certain value of quantum numbers L and M, is to multiply $G_A(\mathbf{r})$ by a generalized solid spherical harmonic:

$$\psi_k = \theta_{LM}(\mathbf{r})\exp(-\mathbf{r}'A_k\mathbf{r}). \tag{22}$$

The non-spherical part, $\theta_{LM}(\mathbf{r})$, can be formed by successively coupling solid spherical harmonics,

$$\begin{aligned}\theta_{LM}(\mathbf{r}) \;=\; & r_1^{l_1}\cdots r_n^{l_n}\Big[\big[[Y_{l_1m_1}(\hat{\mathbf{r}}_1)Y_{l_2m_2}(\hat{\mathbf{r}}_2)]_{L_{12}M_{12}}\\ & \times Y_{l_3m_3}(\hat{\mathbf{r}}_3)\big]_{L_{123}M_{123}}\cdots Y_{l_nm_n}(\hat{\mathbf{r}}_n)\Big]_{LM}.\end{aligned} \tag{23}$$

According to the Wigner-Eckardt theorem, the energy of the system described by a spherically symmetric Hamiltonian is independent of M. In most calculations it is advantageous to choose $M = 0$ in $\theta_{LM}(\mathbf{r})$ as such basis functions are real and the calculations do not require the use of complex arithmetic.

Using Eq. (23) it is possible to build basis functions for any value of the total orbital angular momentum and its z-projection. Since the angular momenta of the relative motion (denoted l_1, l_2, L_{12}, L_{123}, ..., $L_{12\cdots(n-1)}$ in Eq. (23)) are not conserved quantities, it is sometimes necessary to include several sets of single-particle and intermediate angular momenta to have an accurate variational expansion. The inclusion of different sets of relative angular momenta is of particular importance in the case of nuclear few-body problems with non-central interaction.

In the following a few special cases are considered. For $L = 1$, $M = 0$ states with negative parity, in which the dominant configuration corresponds to one particle with $l = 1$ and all others with $l = 0$, the ECGs have the following form:

$$\psi_k = z_{i_k} \exp(-\mathbf{r}' A_k \mathbf{r}), \tag{24}$$

where z_{i_k} is the z-component of $\mathbf{r}_{i_k}$ and $i_k = 1, \ldots, n$ is a variational parameter whose value is not necessarily be the same for each basis function ψ_k.

Similarly, for the positive parity $L = 1$, $M = 0$ states, which arise when the dominant configuration is formed by two particles with $l = 1$ and all others with $l = 0$, the basis functions are

$$\psi_k = (x_{i_k} y_{j_k} - x_{j_k} y_{i_k}) \exp(-\mathbf{r}' A_k \mathbf{r}), \quad i_k \neq j_k. \tag{25}$$

Here both integers i_k and j_k are variational parameters.

Finally, the basis functions for the natural parity $L = 2$, $M = 0$ states (D-states):

$$\psi_k = (x_{i_k} x_{j_k} + y_{i_k} y_{j_k} - 2 z_{i_k} z_{j_k}) \exp(-\mathbf{r}' A_k \mathbf{r}). \tag{26}$$

2. Global vector representation for states with arbitrary L

Upon increasing the total L value in Eq. (23), matrix elements with the corresponding $\theta_{LM}(\mathbf{r})$ function become progressively more complicated. Also, as it was mentioned above, it may be necessary to include several different forms of $\theta_{LM}(\mathbf{r})$ simultaneously. As the number

of such forms (which may or may not be relevant in a particular calculation) grows very rapidly, one faces a serious problem. The difficulty can be avoided by adopting a different form for the orbital part in Eq. (22) (Suzuki and Varga, 1998; Varga and Suzuki, 1995; Varga *et al.*, 1998):

$$\theta_{LM}(\mathbf{r}) = v^{2K+L} Y_{LM}(\mathbf{v}), \tag{27}$$

where

$$\mathbf{v} = \sum_{i=1}^{n} u_i \mathbf{r}_i, \tag{28}$$

$v = |\mathbf{v}|$, and Y_{LM} is the usual spherical harmonic. Only the total orbital angular momentum value L appears in Eq. (27). This quantum number is a good quantum number (assuming a central interaction). The vector $\mathbf{v}$, defined as a linear combination of all (pseudo)-particle coordinates, is called a "global vector". The coefficients in the linear combination are treated as real-valued variational parameters. In general case, they are unique for each basis function, just like the Gaussian parameters. One may choose the optimal values of u_i based on the minimization of the energy functional. It is possible to take advantage of efficient optimization algorithms, which assume smoothness of the objective function (energy) with respect to small variations of variables. The integer variational parameter K, which can take any nonnegative value, introduces an additional flexibility that can be used to improve the short range behavior of the basis functions. A remarkable property of the orbital part in Eq. (27) is that all necessary matrix elements can be evaluated analytically in an algebraically compact form (Suzuki and Varga, 1998).

The scheme introduced in Eq. (28) (Varga and Suzuki, 1995) only covers states with natural parity (i.e. the parity $= (-1)^L$). A generalization to handle unnatural parity states was recently proposed (Suzuki *et al.*, 2008).

3. Explicitly correlated Gaussians with shifted centers

Molecular calculations in the Born-Oppenheimer (BO) approximation where the nuclear positions are fixed require the inclusion of coordinate shifts in the ECGs. The electrons are attracted to the nuclei and their densities are expected to peak around the nuclear positions. These shifts can be incorporated by writing

$$G_{A\mathbf{s}}(\mathbf{r}) = \exp\left[-(\mathbf{r}-\mathbf{s}_k)' A_k (\mathbf{r}-\mathbf{s}_k)\right], \tag{29}$$

where the $3n$-component vectors $\mathbf{s}_k$ are variational parameters. In general, each ECG in the basis can have a unique shift $\mathbf{s}_k$. Such basis functions are sometimes called floating Gaussians. Shifted ECGs can also be used in molecular calculations where the BO approximation is relaxed. A more intuitive way to write these functions for a N electron molecule in the BO-approximation would be

$$\psi_k = \exp\left(-\sum_{i=1}^{N} \alpha_{ki}(\mathbf{x}_i - \mathbf{a}_{ki})^2 - \sum_{i>j=1}^{N} \beta_{kij}(\mathbf{x}_i - \mathbf{x}_j)^2\right). \tag{30}$$

The parameters α_{ki}, β_{kij}, and $\mathbf{a}_{ki}$ can be expressed by the elements of matrix A_k and shifts $\mathbf{s}_k$ and vice versa. For diatomic molecules the shifts $\mathbf{a}_{ki}$ are usually placed on the line connecting the two nuclei. A reasonable initial choice for the shifts in the fixed nuclei case is $\mathbf{s} = (\mathbf{R}_i, \mathbf{R}_j, \ldots)$, where $\mathbf{R}_i$ is the position vector of the i-th nucleus. Depending on the choice of indices $i, j, \ldots$ in $(\mathbf{R}_i, \mathbf{R}_j, \ldots)$ the Gaussians may resemble an "ionic" or "covalent" product of atomic orbitals with additional electron–electron correlation factors. In the case of a homo-nuclear diatomic system it is easy to build in the *gerade* or *ungerade* symmetries. For a gerade system, one simply creates a molecular wave function that is symmetric about the inter-nuclear midpoint by adding a term to each ECG by mapping $\mathbf{a}_{ki} \rightarrow -\mathbf{a}_{ki}$ (the coordinate origin is at the internuclear midpoint) and giving the same linear coefficient.

The shifted ECGs of Eq. (29) are not eigenfunctions of the square of the total orbital angular momentum operator, unless the shift is zero. This is not a concern in the fixed nuclei case, where the total orbital angular momentum is not an integral of motion. In non-BO calculations, the shifted ECGs might not have the correct rotational symmetry. However, using a large basis set with sufficient variational flexibility will result in a wave function that approaches the proper symmetry when the energy is optimized because the Hamiltonian and symmetry operators commute.

Alternatively, one can use an angular momentum projector and filter out the desired quantum state. The angular momentum projection operator is defined as (Blanco and Heller, 1983; Peierls and Yoccoz, 1957)

$$P^L_{MK} = \frac{2L+1}{8\pi^2} \int D^{L*}_{MK}(\Omega) R(\Omega) d\Omega, \tag{31}$$

where Ω denotes the Euler angles α, β and θ, $R(\Omega)$ is a rotation operator

$$R(\Omega) = \mathrm{e}^{i\alpha L_z} \mathrm{e}^{i\beta L_y} \mathrm{e}^{i\gamma L_z}, \tag{32}$$

L_x, L_y and L_z are angular momentum operators, and $D^{L*}_{MK}(\Omega)$ are the Wigner functions. Using P^L_{MK}, a matrix element with prescribed quantum numbers can be calculated as

$$\langle \psi_{LMi}|H|\psi_{LKj}\rangle = \langle \psi_i|HP^L_{MK}|\psi_j\rangle. \tag{33}$$

To calculate this matrix element the rotation of the wave function can be evaluated by (Blanco and Heller, 1983)

$$R(\Omega)\psi_j(\mathbf{r}) = \psi_j(\mathbf{R}^{-1}(\Omega)\mathbf{r}), \tag{34}$$

where $\mathbf{R}(\Omega)$ represents the matrix of coordinate rotation by the Euler angles. The integrations over the Euler angles are usually carried out numerically.

4. Basis functions for systems in external fields

In some problems, e.g. in systems subjected to a magnetic field, it is advantageous to use basis functions with cylindrical symmetry. The magnetic field breaks the rotational symmetry and the Hamiltonian no longer commutes with the L^2 operator, while it still commutes with the L_z operator. To adapt the trial functions to this case a deformed ECG (DECG) is used (Suzuki and Varga, 1998):

$$\exp\left(-\sum_{i,j=1}^{n} A_{ij}(x_i x_j + y_i y_j) - \sum_{i,j=1}^{n} B_{ij} z_i z_j\right), \tag{35}$$

where the nonlinear parameters are different (and independent) in the $\boldsymbol{\rho}$ direction and in the z direction ($\boldsymbol{\rho}_i = (x_i, y_i)$). This extension brings a great deal of flexibility by allowing a separate description of the motion on the xy-plane and along the z-axis. Such functions are eigenfunctions of the L_z operator. The above form of the DECG is restricted to $M = 0$. To allow for $M \neq 0$ states, the basis is multiplied by

$$\prod_{i=1}^{n} \xi_{m_i}(\boldsymbol{\rho}_i), \tag{36}$$

where

$$\xi_m(\boldsymbol{\rho}) = \begin{cases} (x+iy)^m & m > 0, \\ (x-iy)^{-m} & m < 0. \end{cases} \tag{37}$$

Thus the variational basis functions for systems in magnetic fields read

$$\psi_k^M(\mathbf{r}) \;=\; \mathcal{A}\left[\left(\prod_{i=1}^{n}\xi_{m_i}(\boldsymbol{\rho}_i)\right)\right. \\ \left.\times\exp\left(-\sum_{i,j=1}^{n}A_{ij}\boldsymbol{\rho}_i\cdot\boldsymbol{\rho}_j-\sum_{i,j=1}^{n}B_{ij}z_iz_j\right)\right], \tag{38}$$

where $M = m_1 + m_2 + \ldots + m_n$.

5. Completeness of Gaussian basis sets

One consideration of importance relates to the completeness of Gaussian basis sets. For all practical purposes, the ECG functions form a complete basis set (Bukowski *et al.*, 1995; Hill, 1998; Jeziorski *et al.*, 1997; King, 1967). Issues of linear dependence can arise during calculations since the Gaussian functions used are not mutually orthogonal. This is discussed later in Sect. III.F.

E. Matrix elements

The success of ECG based methods ultimately relies on the simplicity of the matrix elements of the Hamiltonian and other operators. For example, the overlap of two spherically symmetric ECGs, Eq. (17), is

$$S(A_k, A_l) \;=\; \langle G(A_k)|G(A_l)\rangle = \left(\frac{\pi^n}{\det(A_{kl})}\right)^{\frac{3}{2}}, \tag{39}$$

where $A_{kl} = A_k + A_l$. The matrix element of the kinetic energy has the following form:

$$\langle G(A_k)|T|G(A_l)\rangle = 3\mathrm{tr}\left(A_kA_{kl}^{-1}A_l\Lambda\right)S(A_k, A_l). \tag{40}$$

In the above expressions det(...) and tr(...) denote the determinant and trace, of a matrix, respectively. The matrix elements of any one-body operator based on the spatial coordinate can be written as

$$\langle G(A_k)|V(\mathbf{r}_i)|G(A_l)\rangle = I(\beta_i)S(A_k, A_l). \tag{41}$$

In this equation, $I(\beta)$ is defined

$$I(\beta) = \left(\frac{\beta}{\pi}\right)^{\frac{3}{2}}\int V(\mathbf{a})\,\exp\left(-\beta a^2\right)d\mathbf{a} \tag{42}$$

and

$$\frac{1}{\beta_i} = w_i' A_{kl}^{-1} w_i. \tag{43}$$

where w_i is a vector, $w_i = \delta_{im}$. The expressions for matrix elements of a two body interaction $V(\mathbf{r}_i - \mathbf{r}_j)$ are similar to that in Eq. (41),

$$\langle G(A_k)|V(\mathbf{r}_i - \mathbf{r}_j)|G(A_l)\rangle = I(\beta_{ij})S(A_k, A_l), \tag{44}$$

but now

$$\frac{1}{\beta_{ij}} = w_{ij}' A_{kl}^{-1} w_{ij}, \qquad w_{ij} = \delta_{im} - \delta_{jm}. \tag{45}$$

There is almost no restriction on the functional form of the potential. In particular, for central interactions the integral Eq. (42) is reduced to a one-dimensional integral, which can be easily evaluated either analytically or numerically. This is one of the fundamental reasons for the success of ECG basis sets. For example, for power law potentials, $V(r) = r^k$ ($k > -3$), one finds

$$I(\beta) = \frac{2}{\sqrt{\pi}\beta^{\frac{k}{2}}}\Gamma\left(\frac{k+3}{2}\right), \tag{46}$$

where Γ is the Euler gamma function. Another remarkable property of the ECG basis is that the analytical complexity of the matrix elements does not change when the number of particles is increased. Assuming pairwise interactions, the computational effort associated with the evaluation of the matrix elements increases as $n^3 \times k!$, where k is the number of identical particles in the system (for an atom $k = n$) and the $k!$ factor comes from the need to antisymmetrize the wave function. Another factor is that given the same relative accuracy the length $\mathcal{N}$ of the expansion has to increase when n increases. This increase, however, is slower than than $k!$. The $k!$ dependence has so far limited the application of ECG methods to systems with no more than eight particles.

As a guide through the literature, a non-exhaustive list of works is presented in Table XXIV that give technical details on the derivation of matrix elements for various types of ECGs. Material on the related topic of evaluating multi-center integrals with single-electron Gaussian orbitals can be found in (Brinkmann and Kleindienst, 1991; Head-Gordon and Pople, 1988; Kuang and Lin, 1997; Obara and Saika, 1986; Petersson and Hellsing, 2010) and references therein.

TABLE II List of references describing the analytical calculation of ECG matrix elements.

Interaction/operators	ECG type	Form	Reference
Coulomb	Shifted ECGs	Direct	(Boys, 1960; Singer, 1960)
Coulomb	Shifted ECGs, one pair of electrons correlated	Direct	(Cencek and Rychlewski, 1993)
Coulomb	Shifted ECGs	Recursion	(Saito and Suzuki, 2001)
Coulomb	Spherical ECGs, $L = 0$, Analytic energy gradient	Direct	(Kinghorn, 1996; Kinghorn and Adamowicz, 1999)
Central	Complex ECGs, $L = 0, 1, 2$, Analytic energy gradient	Direct	(Bubin and Adamowicz, 2006) (Bubin and Adamowicz, 2008) (Sharkey *et al.*, 2011a)
J^2, J_z	Shifted ECGs with prefactors	Recursion	(Kozlowski and Adamowicz, 1995)
Coulomb	Shifted ECGs Analytical energy gradient	Direct	(Kozlowski and Adamowicz, 1992)
Coulomb	Shifted Gaussians Analytic energy gradient	Direct	(Cafiero and Adamowicz, 2001)
Various interactions including noncentral	GVR ECGs, arbitrary L	Direct	(Suzuki and Varga, 1998; Varga and Suzuki, 1995)
Central and noncentral, Relativistic kinetic energy	GVR ECGs, arbitrary L	Direct	(Silvestre-Brac and Mathieu, 2007, 2008)
Various interactions	GVR ECGs, for unnatural parity states, arbitrary L	Direct	(Suzuki *et al.*, 2008; **?**)
Coulomb	Spherical ECGs with prefactors	Recursion	(Harris and Monkhorst, 2006)
Atomic core-exchange, OPP, 3-body polarization	Spherical ECGs	Direct	(Ryzhikh *et al.*, 1998b)
General	Infinitesimally shifted ECGs for arbitrary L	Direct	(Hiyama *et al.*, 2003)

F. Relativistic and QED corrections

The relativistic and quantum electrodynamic (QED) effects in light atoms and molecules can be conveniently accounted for using the nonrelativistic QED expansion (Caswell and Lepage, 1986; Pachucki, 1997) of the bound state energy in powers of the fine-structure constant α

$$E = \sum_n \alpha^n E^{(n)} \,. \tag{47}$$

Each term of this expansion can be given a clear physical interpretation. The nonrelativistic energy computed (after center-of-mass motion separation) of the Schrödinger equation is $E^{(0)}$. The next, $\alpha E^{(1)}$ term is absent and the $\alpha^2 E^{(2)}$ represents the leading relativistic correction. The $\alpha^3 E^{(3)}$ term, containing terms depending logarithmically on α, describes

the leading QED effects. The higher order terms of the α-expansion provide all the remaining relativistic and QED corrections proportional to α^n with $n \geq 4$.

The main advantage of this expansion is that its coefficients can be evaluated using the nonrelativistic wave function Ψ. The leading coefficients are known from literature for a long time now. $E^{(2)}$ can be evaluated from an expectation value of the Breit-Pauli Hamiltonian (Bethe and Salpeter, 1977), which in a simplified form (nuclei at rest and $^1\Sigma$ molecular electronic state) reads in atomic units

$$\begin{aligned} \alpha^{-2}\, H_{\rm BP} = &-\frac{1}{8}\sum_i \mathbf{p}_i^4 + \frac{\pi}{2}\sum_{i,A} Z_A \delta(\mathbf{r}_{iA}) + \pi \sum_{i<j} \delta(\mathbf{r}_{ij}) \\ &- \frac{1}{2}\sum_{i<j}\left(\mathbf{p}_i \frac{1}{r_{ij}} \mathbf{p}_j + \mathbf{p}_i \cdot \mathbf{r}_{ij} \frac{1}{r_{ij}^3} \mathbf{r}_{ij} \cdot \mathbf{p}_j\right). \end{aligned} \tag{48}$$

In the above formula, i and j stand for the electrons, A for the nuclei, Z_A is the charge of A-th nucleus, $\mathbf{r}_{ij} = \mathbf{r}_i - \mathbf{r}_j$, $\mathbf{r}_{iA} = \mathbf{r}_i - \mathbf{R}_A$, and δ denotes the three-dimensional Dirac δ-function. The subsequent terms are usually referred to as the mass-velocity, the one- and two-electron Darwin, and the Breit contributions.

The leading QED correction can be expressed as

$$\begin{aligned} E^{(3)} = &\sum_{i<j}\left\{\left[\frac{164}{15} + \frac{14}{3}\,\ln\alpha\right]\,\langle\delta(\mathbf{r}_{ij})\rangle + \langle H_{\rm AS}\rangle\right\} \\ &+ \sum_{i,A}\left[\frac{19}{30} - 2\ln\alpha - \ln K\right]\frac{4Z_A}{3}\,\langle\delta(\mathbf{r}_{iA})\rangle\,. \end{aligned} \tag{49}$$

In the above, two expressions require a special consideration. The first one is the Araki-Sucher operator (Araki, 1958; Sucher, 1958),

$$H_{\rm AS} = -\frac{7}{6\pi}\,\mathcal{P}\left(\frac{1}{r_{ij}^3}\right), \tag{50}$$

defined (in atomic units) through the distribution $\mathcal{P}$, which takes care of the divergence at $r_{ij} = 0$,

$$\left\langle \mathcal{P}\left(\frac{1}{r_{ij}^3}\right)\right\rangle = \lim_{a\to 0}\langle r_{ij}^{-3}\,\theta(r_{ij}-a) + 4\,\pi\,(\gamma + \ln a)\,\delta(\mathbf{r}_{ij})\,\rangle. \tag{51}$$

Here θ is the Heaviside step function and γ is the Euler-Mascheroni constant. The other expression, that is difficult to compute in Eq. (49), is the Bethe logarithm

$$\ln K = \frac{\langle \mathbf{j}\,(H-E^{(0)})\,\ln\left[(H-E^{(0)})/Ry\right]\mathbf{j}\rangle}{\langle \mathbf{j}\,(H-E^{(0)})\,\mathbf{j}\rangle}, \tag{52}$$

where $\mathbf{j}$ is the electric current operator, $\mathbf{j} = -e\sum_i (1/m_e)\mathbf{p}_i$, and Ry is the Rydberg constant (1/2 hartree in atomic units). For a long time this quantity was accurately known only for one- or two-electron atoms and for the one-electron molecular hydrogen cation (Bukowski *et al.*, 1992). Only in recent years was progress made towards determination of the Bethe logarithm for larger atoms (Pachucki and Komasa, 2003, 2004; Yan and Drake, 2003) as well as for molecules (Piszczatowski *et al.*, 2009).

Formulas for the $\alpha^4 E^{(4)}$ term are also known (Pachucki, 2005). Unfortunately, practical difficulties in evaluation of certain divergent terms prevent accurate calculations of this correction for systems with more than two electrons. From the hydrogen and helium atom calculations (Pachucki, 2006a,b, 2007), however, it is known, that the dominant contribution to the higher order QED correction is the so-called one-loop term

$$E^{(4)}_{\rm one-loop} = \pi\left(\frac{427}{96} - \ln 4\right)\sum_{i,A} Z_A \langle\delta(\mathbf{r}_{iA})\rangle, \tag{53}$$

which can be used as an estimation of the $E^{(4)}$.

The relativistic and QED theory outlined above carries along difficulties in evaluating of certain quantities. This concerns not only the above mentioned Bethe logarithm and Araki-Sucher operator but also the expectation values of the singular Dirac delta (δ) operators or the relativistic kinetic energy operator, $\mathbf{p}^4$. The difficulties can be significantly diminished by special regularization techniques discussed in Sec. III.C.

G. Perturbative treatment of the finite mass effects

For molecules it is very common to perform calculations within the framework of the BO approximation. The effects of nuclear motion can be treated perturbatively with the adiabatic BO wave function taken as the unperturbed state. Here a short theory is presented, which gives, in connection with the ECG wave functions highly accurate results for light diatomic molecules.

1. Adiabatic approximation

In non-adiabatic perturbation theory (Pachucki and Komasa, 2008, 2009) the zeroth order approximation to the wave function of a diatomic molecule, with nuclei held at fixed

position, is represented by the adiabatic ansatz

$$\phi_{\rm a}(\mathbf{r},\mathbf{R}) = \phi_{\rm el}(\mathbf{r};\mathbf{R})\;\chi(\mathbf{R})\,, \tag{54}$$

where $\mathbf{r}$ stands for the coordinates of the electrons and $\mathbf{R}$ connects the positions of nuclei A and B. The Hamiltonian of the system is split into electronic and nuclear parts, $H = H_{\rm el} + H_{\rm n}$. The electronic Hamiltonian is

$$H_{\rm el} = \sum_i \frac{\mathbf{p}_i^2}{2m} + V, \tag{55}$$

where V is the Coulomb interaction between the electrons and between the electrons and nuclei at fixed nuclear positions. The perturbation is defined by the nuclear part of the total Hamiltonian

$$\begin{aligned} H_{\rm n} = &-\frac{1}{2\,\mu_{\rm n}}\nabla_R^2 - \frac{1}{8\,\mu_{\rm n}}\left(\sum_i \boldsymbol{\nabla}_{\boldsymbol{i}}\right)^2 \\ &+ \left(\frac{1}{M_A} - \frac{1}{M_B}\right)\boldsymbol{\nabla}_R \cdot \sum_i \boldsymbol{\nabla}_i\,, \end{aligned} \tag{56}$$

where $\mu_{\rm n} = (1/M_A + 1/M_B)^{-1}$ is the nuclear reduced mass.

The adiabatic ansatz enables the separation of the nuclear and electronic variables. The electronic wave function $\phi_{\rm el}$ is a solution to the clamped nuclei Schrödinger equation

$$[H_{\rm el} - \mathcal{E}_{\rm el}(R)]\,\phi_{\rm el} = 0 \tag{57}$$

and parametrically depends on the internuclear distance R. This equation is solved variationally.

The wave function of the nuclear motion is calculated from the nuclear Schrödinger equation. For a given angular momentum J, the nuclear equation becomes one-dimensional

$$\begin{aligned} &\left[-\frac{1}{R^2}\frac{\partial}{\partial R}\frac{R^2}{2\,\mu_{\rm n}}\frac{\partial}{\partial R} + \frac{J\,(J+1)}{2\mu_{\rm n}R^2} + \mathcal{E}_{\rm el}(R) + \mathcal{E}_{\rm a}(R)\right]\,\chi_J(R) \\ &= E_{\rm a}\,\chi_J(R) \end{aligned} \tag{58}$$

with $E_{\rm a}$ being the adiabatic approximation to the total energy. The adiabatic correction $\mathcal{E}_{\rm a}(R)$ is given by the electronic matrix element

$$\mathcal{E}_{\rm a}(R) = \langle H_{\rm n}\rangle_{\rm el}\,. \tag{59}$$

From here and forth, the brackets $\langle\cdots\rangle_{\rm el}$ denote integration over the electronic coordinates only.

2. Nonadiabatic nuclear equation

Non-adiabatic perturbation theory yields a series of successive approximations to the total energy E expressed in progressive powers of the electron-nuclear mass ratio. Up to order $\mu_{\rm n}^{-2}$ they can also be found by solving the following nonadiabatic version of the nuclear equation

$$\left[-\frac{1}{R^2}\,\frac{\partial}{\partial R}\,\frac{R^2}{2\,\mu_{\parallel}(R)}\,\frac{\partial}{\partial R}\,+\frac{J\,(J+1)}{2\,\mu_{\perp}(R)R^2}\,+\mathcal{Y}(R)\right]\,\tilde{\chi}_J(R)$$
$$=E\,\tilde{\chi}_J(R). \tag{60}$$

The finite nuclear mass effects appear in this equation as R-dependent corrections to the nuclear reduced mass and to the interaction potential. The corrections to $\mu_{\rm n}$ are given by the following two R-dependent functions

$$\frac{1}{2\,\mu_{\parallel}(R)}\;=\;\frac{1}{2\,\mu_{\rm n}}+\frac{1}{\mu_{\rm n}^2}$$
$$\times\sum_{i,j}\left\langle\frac{R^i}{R}\nabla_R^i\left|\frac{1}{(\mathcal{E}_{\rm el}-H_{\rm el})'}\right|\frac{R^j}{R}\nabla_R^j\right\rangle_{\rm el}, \tag{61}$$

and

$$\frac{1}{2\,\mu_{\perp}(R)}\;=\;\frac{1}{2\,\mu_{\rm n}}+\frac{1}{2\,\mu_{\rm n}^2}\sum_{i,j}\left(\delta^{ij}-\frac{R^i\,R^j}{R^2}\right)$$
$$\times\left\langle\nabla_R^i\left|\frac{1}{(\mathcal{E}_{\rm el}-H_{\rm el})'}\right|\nabla_R^j\right\rangle_{\rm el}, \tag{62}$$

where the prime symbol in the resolvent indicates the orthogonalization to electronic reference state (Piela, 2007). The interaction potential is also corrected by an R-dependent nonadiabatic correction

$$\mathcal{Y}(R)=\mathcal{E}_{\rm el}(R)+\mathcal{E}_{\rm a}(R)+\mathcal{E}_{\rm na}(R)\,. \tag{63}$$

The internuclear potential can be further augmented by the relativistic and QED potentials. In such a case, the eigenvalue of Eq, (60) accounts for all the leading corrections resulting from the finite nuclear mass and the finite speed of light, and should be directly comparable to the experimental value.

III. COMPUTATIONAL METHODOLOGIES

A. Parameter optimization

Variational calculations employing ECGs can provide very accurate energies and wave functions and numerous examples will be presented later in this review. However, achieving high accuracy is only possible when the non-linear parameters of the basis functions are carefully optimized. This sensitivity gets stronger for larger systems and excited states where the wave function in general has a more complicated structure. The most natural way to optimize the parameters of the basis functions is to minimize the total energy.

Finding the absolute minimum of the energy with respect to the nonlinear parameters for a large (dimension of 100–10 000) ECG expansion of the wave function is very difficult due to the large number of parameters and the very complicated energy hypersurface. However, it is only necessary to find a wave function that is sufficiently low lying in energy. This can be achieved by maintaining the right balance between the amount of effort spent on the optimization of nonlinear parameters and the additional amount of effort required when the dimension of the ECG basis is increased.

The importance of being able to systematically optimize the basis was outlined in the original paper that described the stochastic variation method (Kukulin and Krasnopol'sky, 1977). This paper also described how this optimization could be carried out in a reasonably efficient manner. This work was not widely appreciated in atomic and molecular structure physics and the development of ECG based methods here followed a course of parallel evolution leading to roughly the same outcome. In atomic physics the importance of doing intensive optimization of the individual non-linear parameters of the ECG basis became apparent during a series of calculations on the helium atom performed over a period of a few decades (Alexander *et al.*, 1990; Cencek and Kutzelnigg, 1996; Kinghorn and Adamowicz, 1997; Komasa and Thakkar, 1995; Longstaff and Singer, 1960; Longstaff and Singer, 1964; Poshusta, 1979; Regier and Thakkar, 1985; Rybak *et al.*, 1989).

A similar pattern of events is apparent when one looks at the application of ECG functions to calculations of the H_2 molecule (Alexander *et al.*, 1990; Handy, 1973; Jeziorski and Szalewicz, 1979; Lester, Jr. and Krauss, 1964; Longstaff and Singer, 1960; Longstaff and Singer, 1964, 1965; Salmon and Poshusta, 1973). The potential utility of ECG based

approaches for describing molecular structure became more apparent by 1979, when the best ECG energy of H_2 had an error of 0.05 mhartree (Jeziorski and Szalewicz, 1979), which was unmatched by any other calculation except for those performed using a generalized James-Coolidge (GJC) basis that were accurate to 0.01 mhartree (Kołos and Wolniewicz, 1965). The full advantages of optimized ECG bases for molecular systems were realized when ECG-type wavefunction expansions gave the best variational energies for the H_2, LiH, and linear H_3 molecules (Cencek *et al.*, 1995; Cencek and Rychlewski, 1993; Rychlewski *et al.*, 1994).

ECGs have also been adopted to speed up the convergence of many-electron molecular structure calculations based on perturbation theory and coupled cluster methods. The ECGs used in these calculations are usually restricted to two-electron functions which have been traditionally referred to as Gaussian type geminals (GTGs). Optimization of the GTG parameters resulted in calculations that were able to reproduce the best perturbative results for Be and LiH by other methods (Alexander *et al.*, 1986, 1988).

There are two types of nonlinear optimization that are typically performed. The first occurs when the basis size is increased and new basis functions are included. Here, stochastic optimization is normally used. The second type of optimization occurs when the basis size is kept fixed. Here one can use either a direct or stochastic optimization.

1. Stochastic optimization

Stochastic optimization methods are optimization methods that generate and use random variables. For stochastic problems, the random variables appear in the formulation of the optimization problem itself, which involve random objective functions or random constraints (Spall, 2003). The problem of optimizing the large number of nonlinear parameters of the ECG basis naturally lends itself to an application of a stochastic optimization procedure. The stochastic optimization of the ECG parameters, "the stochastic variational method" (SVM), was first proposed by Kukulin and Kranopol'sky (Kukulin and Krasnopol'sky, 1977).

In the SVM $\mathcal{K}$, different sets of nonlinear parameters A in Eq. (17) are generated randomly. The parameter set which gives the lowest variational energy is selected and the function corresponding to these parameters is retained in the set of ECGs.

The stochastic selection procedure differs slightly depending on whether the basis is being enlarged or the parameters of an existing basis are being refined.

(1) *Set up a new basis* (or enlarging an existing one):
Assuming that the basis set has $\mathcal{N}-1$ elements, one generates $\mathcal{K}$ random basis states and calculates ($i=1,\ldots,\mathcal{K}$) new energies $E_{\mathcal{N}i}$ with the $\mathcal{N}$-dimensional bases. The new $\mathcal{N}$-dimensional bases contain the i-th random element and the previously selected $\mathcal{N}-1$ basis elements. The random state giving the lowest energy is selected as a new basis state and added to the basis. The variational principle ensures that the eigenvalues of the $\mathcal{N}$-dimensional basis are always lower than the corresponding eigenvalues of the $\mathcal{N}-1$ dimensional basis. This procedure is guaranteed to give a better new upper bound of the ground state energy. The rate of convergence can be determined by examination of the $\epsilon_{\mathcal{N}}=E_{\mathcal{N}}-E_{\mathcal{N}-1}$ energy differences.

(2) *Refinement:*
In the refinement process the dimension of the basis is kept fixed while $\mathcal{K}$ new ECGs are generated randomly with a view to replacing the k-th element of the basis. If the best energy obtained by substituting the k-th basis state with the random candidate is lower than that of the original basis, then the k-th basis state is discarded and the new random state is included in the basis. This procedure is repeated for $k=1,\ldots,\mathcal{N}$. As the dimension of the model space is fixed, this step does not necessarily give a lower energy, but in practice it usually does. In fact, if one cannot find better basis elements, it is an indication of a well-converged energy/basis.

While the SVM described above is part of a fully variational calculation, the selection of the optimal parameters of the GTGs used in perturbative calculations is done in a process that has many features common with the approaches described above (Alexander *et al.*, 1986, 1988; Bukowski *et al.*, 1994)

2. Why extensive optimization is feasible

The optimization process of the nonlinear parameters is performed at an individual level for each basis function. When this is done, the Hamiltonian matrix has a particularly simple structure. Since there exists an $(\mathcal{N}-1)\times(\mathcal{N}-1)$ block that is already diagonalized, the full diagonalization of an $\mathcal{N}\times\mathcal{N}$ matrix is not needed. It is only necessary to calculate a new row of the Hamiltonian and overlap matrices. The simplicity of expressions for the ECG matrix elements ensures that this can be done quickly.

Furthermore, the determination of the energy eigenvalues is quick since the off-diagonal elements are confined to one row and one column of the Hamiltonian matrix. The diagonalization of this almost diagonal Hamiltonian can be completed by a process similar to Schmidt orthogonalization (Varga and Suzuki, 1995) or by an iterative approach such as the one outlined in (Bubin *et al.*, 2005c).

3. Direct optimization

One of the advantages of stochastic optimization is that it is easy and quick to implement. A disadvantage is that it does not utilize any information about the continuity, smoothness, and the gradient of the energy with respect to the non-linear parameters. Knowledge of the energy gradient can greatly speedup any optimization process (Fletcher, 1987; Press *et al.*, 1992) and so a direct optimization strategy can improve the convergence of the energy for a given basis dimension.

Direct optimization methods require multiple evaluations of both the total energy of the system and the gradient of the energy. Once the number of nonlinear parameters, $\mathcal{M}$, being optimized simultaneously gets large, the evaluation of the gradient based on the finite difference approximation becomes very expensive since the evaluation of the gradient at a single point using finite differences requires at least $2\mathcal{M}$ energy evaluations. This problem can be avoided if the analytic gradient of the energy can be computed. The amount of computation needed to evaluate of the analytic gradient is typically proportional to and a few times larger than the effort needed to form the Hamiltonian and overlap matrices and compute the energy.

The energy derivative with respect to a non-linear parameter, α_i, can be written as

$$\begin{aligned}\frac{\partial E}{\partial \alpha_i} &= 2\Re\left[c_i^* \sum_{j=1}^{\mathcal{N}} c_j \left(\frac{\partial H_{ij}}{\partial \alpha_i} - E\frac{\partial S_{ij}}{\partial \alpha_i}\right)\right] \\ &\quad -c_i c_i^* \left(\frac{\partial H_{ii}}{\partial \alpha_i} - E\frac{\partial S_{ii}}{\partial \alpha_i}\right). \end{aligned} \tag{64}$$

By calculating such a derivative for each α_i ($i = 1 \ldots \mathcal{N}$) one can obtain the entire energy gradient. It is computationally advantageous to evaluate the derivatives of E with respect to the entire set of nonlinear parameters of a particular ECG since there are many identical operations for each individual parameter α_i that do not have to be repeated. The derivatives

of H_{ij} and S_{ij} with respect to the nonlinear parameters can usually be evaluated in closed form when dealing with the ECG basis functions.

There are a variety of optimization algorithms that can be adopted when energy gradients are available, such as the Broyden-Fletcher-Goldfarb-Shanno (this is sometimes known as BFGS) algorithm (Fletcher, 1987) or the conjugate gradient algorithm (Powell, 1964).

B. Computational requirements

While calculations using optimized ECGs can be time-consuming, they actually do not require much in the way of computational resources. The basis dimension, $\mathcal{N}$, of a large calculation would typically not exceed 10,000. Storage of the overlap and Hamiltonian matrix elements requires two dense $\mathcal{N}\times\mathcal{N}$ matrices. The amount of available random access memory (RAM) is almost never an issue in ECG calculations. The only conceivable circumstance when memory may become a bottleneck would be if it was decided to optimize the nonlinear parameters of all basis functions simultaneously, something that is rarely done in practice for large basis dimensions. Even here, the memory requirements of the optimization algorithm such as limited memory Broyden-Fletcher-Goldfarb-Shanno or conjugated gradient grow sufficiently slowly (the memory requirements for conjugate gradient scale as $\mathcal{O}(n_p\mathcal{N})$, where n_p is the number of nonlinear parameters per basis function) to become a problem. Many of the calculations described in this manuscript have literally been done using single processors on personal computers tucked under a desk.

The amount of CPU time required is dictated primarily by such factors as the number of particles in the system, functional form of the interaction, complexity of the wave function for a particular state, maximum number of basis functions, and thoroughness of the optimization. Some of the calculations reported here involved more than one year of optimization. Others can be done in a matter of minutes on a desktop computer. Human intervention can normally be kept minimal. Typically an initial analysis based on wave functions obtained in a (relatively) small basis set calculations would be made. Once that is done, a favorable strategy of growing the basis and optimizing nonlinear parameters of basis function can be deduced.

To speed up calculations and/or make it possible to consider systems with a larger number of particles, one can parallelize the computer code. The two major tasks that consume

most of the computational time are the evaluation of the Hamiltonian and overlap matrix elements and the solution of the generalized eigenvalue problem Eq. (6). The first task can be effectively parallelized in a straightforward manner with nearly perfect scalability. The second one also allows for a certain degree of parallelization (although the scalability may be somewhat worse).

C. Improving the convergence of the expectation values of singular operators

As mentioned in the introduction ECGs have incorrect asymptotics with respect to what is expected on the basis of some theoretical considerations, e.g. the Kato cusp conditions at the inter-particle coalescence points (Kato, 1957). This deficiency slows the convergence of the energy and other properties, but has a particularly severe effect on the expectation values of operators that are singular at coalescence points. The slow convergence of expectation values of singular operators also occurs for variational calculations that employ distinctly different basis sets (Puchalski *et al.*, 2011). Calculations of relativistic and QED effects have required the development of methods to accelerate the convergence of the expectation values of singular operators. These methods are described below.

1. Expectation value identities

One acceleration technique replaces the expectation value of the singular Dirac delta function, $\langle\delta(\mathbf{r}_{ij})\rangle$, by the expectation value of a global operator which yields the same result if the wave function is exact (Challacombe and Cioslowski, 1994; Cioslowski and Lopez-Boada, 1998; Drachman, 1981; Hiller *et al.*, 1978; Rassolov and Chipman, 1996; Sundholm, 1995). It can be shown that

$$4\pi\langle\delta(\mathbf{r}_{jk})\rangle \;=\; 2\left\langle\frac{1}{r_{jk}}(E-V)\right\rangle - \sum_i \left\langle\nabla_i\left|\frac{1}{r_{jk}}\right|\nabla_i\right\rangle, \tag{65}$$

where V is the potential energy operator. Atomic units ($\hbar = e = m_e = 1$) are assumed in all expressions. For an approximate function, the right hand side converges faster towards the exact value than the original expression. A similar regularization method can be applied to the mass-velocity term of the relativistic correction, e.g.

$$\left\langle\sum_i \nabla_i^4\right\rangle = 4\langle(E-V)^2\rangle - 2\sum_{i>j}\left\langle\nabla_i^2|\nabla_j^2\right\rangle. \tag{66}$$

An analogous identity has been found for the singular Araki-Sucher term present in the QED correction (Pachucki *et al.*, 2005).

The identities above hold independently of the basis functions employed to expand the wave function. The penalty associated with the faster convergence is that the matrix elements become more complicated. Fortunately, in the atomic case, all the integrals can be evaluated analytically. This is generally not true for the molecular case.

Table III illustrates the convergence of some operators involved in the relativistic and QED calculations of the beryllium atom ground state using increasingly larger ECG bases. In all cases, the expectation value identities (EVI) with 200 ECGs are superior to the direct evaluation with 1600 ECGs. This is particularly visible in the case of the Araki-Sucher distribution $\mathcal{P}\left(1/r_{ij}^3\right)$, for which the direct evaluation of the integral only gives the leading digit correctly.

TABLE III Convergence of the expectation values computed directly and using the technique of the expectation value identities (EVI). Results are shown for the ground state of the beryllium atom (Pachucki *et al.*, 2005). $\mathcal{N}$ is the dimension of the ECG basis. All values are in atomic units.

$\mathcal{N}$	Direct	EVI	Direct	EVI
	$\langle\delta(\mathbf{r}_i)\rangle$		$\langle\delta(\mathbf{r}_{ij})\rangle$	
100	33.379 145	35.174 770	1.627 741	1.604 558
200	34.897 648	35.339 657	1.618 229	1.605 055
400	35.029 311	35.340 791	1.610 911	1.605 253
800	35.297 307	35.368 099	1.608 106	1.605 293
1600	35.317 352	35.368 900	1.606 742	1.605 303
	$\langle p_i^4\rangle$		$\left\langle\mathcal{P}\left(1/r_{ij}^3\right)\right\rangle$	
100	2137.407	2164.851	−8.552 39	−7.304 29
200	2153.618	2165.594	−8.123 10	−7.318 37
400	2155.764	2165.567	−7.730 23	−7.324 54
800	2161.966	2165.644	−7.552 88	−7.326 22
1600	2162.989	2165.637	−7.455 34	−7.326 63

2. Integral transform technique

Another regularization technique utilizes integral representations of the singular operators. The great advantage of the integral transform (IT) methodology (Pachucki *et al.*, 2005), in contrast to EVI, is its possible application to both atoms and molecules.

For instance, the expectation value of the Dirac delta can be represented as

$$\langle \delta(\mathbf{r}) \rangle = \frac{1}{2\pi^{3/2}} \int_0^\infty \left\langle 2t^2 \left(3 - 2t^2 r^2\right) e^{-t^2 r^2} \right\rangle dt \,. \tag{67}$$

The expectation value within the integral can be evaluated with high accuracy by an ECG basis provided that the value of t is not excessively large. For large values of t, this integrand can be replaced by its asymptotic form with the prefactor known from the Kato's cusp condition (Kato, 1957)

$$\frac{4Z}{\sqrt{\pi}\, t^2} \langle \delta(\mathbf{r}) \rangle \left(1 + \sum_i \frac{A_i}{t^i}\right). \tag{68}$$

The first few leading coefficients A_i are then determined by fitting to the integrand evaluated on a large grid.

An analogous expansion has been found for the expectation value of the Araki-Sucher distribution

$$\left\langle \mathcal{P}\left(\frac{1}{r_{ij}^3}\right) \right\rangle \;=\; \int_0^\infty (2\,\ln t - \gamma)\, f(t)\, dt \,, \tag{69}$$

where

$$f(t) = \left\langle 2t \left(t^2 r_{ij} - \frac{1}{r_{ij}} \right) e^{-t^2 r_{ij}^2} \right\rangle \,, \tag{70}$$

having the following asymptotic form

$$f(t) = \frac{\pi^{3/2}}{t^2} \left\langle \delta(\mathbf{r}_{ij}) \right\rangle \left(1 + \sum_i \frac{A_i}{t^i}\right). \tag{71}$$

The IT regularization of the mass-velocity operator is more involved. Its expectation value is first expressed by an integral over the radial momentum density $I(p)$, which can be safely evaluated for not too large arguments. For large electronic momentum p, it is expressed by its asymptotic form

$$I(p) = \frac{s_6}{p^6} + \frac{s_7 \sin(p\,R)}{p^7} + \mathcal{O}(p^{-8}) \,. \tag{72}$$

The leading coefficients s_6 and s_7 are given by

$$s_6 \;=\; 32 \sum_{i=1}^{N} \left(Z^2 \left\langle \delta(\mathbf{r}_i) \right\rangle + \frac{1}{2} \sum_{i>j}^{N} \langle \delta(\mathbf{r}_{ij}) \rangle \right) \tag{73}$$

and

$$s_7 \;=\; 0 \tag{74}$$

for atoms. For diatomic molecules with internuclear separation of R one writes

$$s_6 \;=\; 32 \sum_{i=1}^{N} \Bigg(Z_A^2 \,\langle \delta(\mathbf{r}_i - \mathbf{r}_A) \rangle + Z_B^2 \,\langle \delta(\mathbf{r}_i - \mathbf{r}_B) \rangle + \frac{1}{2} \sum_{i>j}^{N} \langle \delta(\mathbf{r}_{ij}) \rangle \Bigg) \tag{75}$$

and

$$s_7 \;=\; 64\, N\, Z_A\, Z_B\, R^{-1}\, \rho(R)\,. \tag{76}$$

The quantity ρ, appearing in the last equation, is the one-electron density matrix evaluated at the positions $\mathbf{R}_A$ and $\mathbf{R}_B$ of the two nuclei

$$\int \Psi^*(\mathbf{R}_A, \mathbf{r}_2, \ldots, \mathbf{r}_N) \Psi(\mathbf{R}_B, \mathbf{r}_2, \ldots, \mathbf{r}_N) \prod_{i=2}^{N} d\mathbf{r}_i\,. \tag{77}$$

For atoms, the convergence speedup is similar to that observed for the EVI method. Tests on molecules, in particular the helium dimer (Table IV), show that the IT regularization gives expectation values that are one to three orders of magnitude more accurate than the direct evaluation for a given basis.

TABLE IV Convergence of the relativistic correction expectation values for the helium dimer when computed with the integral transform technique (IT) (Pachucki *et al.*, 2005). All values are in atomic units.

$\mathcal{N}$	Direct	IT	Direct	IT
	$\langle \delta(\mathbf{r}_{iI}) \rangle$		$\langle \delta(\mathbf{r}_{ij}) \rangle$	
600	7.22913	7.241464	0.213116	0.2127378
1200	7.23567	7.241585	0.212907	0.2126987
2400	7.23650	7.241603	0.212824	0.2126893
4800	7.23758	7.241606	0.212783	0.2126877
	$\langle p_i^4 \rangle$		$\langle \mathcal{P}(1/r_{12}^3) \rangle$	
600	216.029	216.34890	0.32416	0.333518
1200	216.196	216.34893	0.32658	0.333797
2400	216.218	216.34881	0.32763	0.333882
4800	216.246	216.34874	0.32820	0.333898

3. ECG basis functions with linear prefactors

Another approach modifies the ECG functional form by multiplying them by linear prefactors in the interparticle distance (Pachucki and Komasa, 2004). This enhances the convergence of the singular relativistic correction operators. Furthermore, such a modification makes it possible to satisfy the Kato cusp conditions (Kato, 1957) involving the ratio of expectation values at the coalescence points, e.g. $\mathrm{cusp}(\mathbf{r}) = \frac{\langle \delta(\mathbf{r}) \partial/\partial r \rangle}{\langle \delta(\mathbf{r}) \rangle}$. The Kato cusp conditions can never be exactly fulfilled with an ECG basis.

While explicit expressions for the matrix elements for systems involving three electrons do exist (Pachucki and Komasa, 2004), the method has only been applied to the helium atom (Pachucki and Komasa, 2004). The use of a linearized ECG basis resulted in helium atom cusp conditions that were accurate to better than 0.05% for a basis dimension of 600. The convergence of δ-function operators was significantly improved.

To some extent the use of ECGs with linear prefactors runs counter to the philosophy underpinning the success of ECGs. One reason behind the extraordinary success of ECGs has been the ease with which most matrix elements can be evaluated. The additional complications resulting from adding linear multiplying factors to ECGs have prevented their widespread application and there have been almost no applications of these modified ECGs since their initial usage.

D. Strongly repulsive interactions

Strongly repulsive interactions pose a particular problem in variational calculations. Consider the Schrödinger equation for two particles interacting through the central potential $V(r)$,

$$\left(-\frac{\hbar^2}{2\mu} \nabla^2 + V(r) \right) \Psi(\mathbf{r}) = E \Psi(\mathbf{r}). \tag{78}$$

In the classically forbidden region, where $E < V(r)$ as $r \to 0$, the s-wave relative wave function should decay according to the rule

$$\Psi(\mathbf{r}) \approx A \exp[-k(r) r], \tag{79}$$

where

$$k(r) = \sqrt{\frac{2\mu[V(r) - E]}{\hbar^2}}. \tag{80}$$

When the product $r^2 2\mu V(r)/\hbar^2$ is large as $r \to 0$, the wave function has to have an extremely rapid decay for $r \to 0$. It is very difficult to describe such systems using global basis functions such as $\exp(-\lambda r)$ or $\exp(-\lambda r^2)$. The finite size of any ECG close to the origin leads to large positive matrix elements. Attempting to construct a linear superposition of basis functions for $\Psi(r)$ by optimizing nonlinear parameters would result in a set of basis functions with similar exponents with linear coefficients that have alternate signs. This leads to a loss of numerical significance before linear dependence effects would cause the calculation to fail.

The nucleon-nucleon interaction is well known to possess a strongly repulsive short-range core (Epelbaum *et al.*, 2009). Similarly, the interaction between two atoms, e.g. the two hydrogen atoms in the H_2 molecule, also has a strongly repulsive core. To some extent, the strongly repulsive core problem is a computational problem as opposed to a physics problem. For example, it is difficult to calculate the vibrational states using a Gaussian basis directly, but one can easily find the vibrational states by numerical integration of the Schrödinger equation with a H-H interatomic potential.

One solution to the hard-core problem is to simply modify the potential to effectively soften the repulsive hard-core. Effective field theory provides one framework by which this can be done (Epelbaum *et al.*, 2009; Lepage, 1997). When the two-body interaction is modified, it is sometimes necessary to add a compensating three-body interaction. In effect, one modifies the interaction to solve a computational problem.

An alternative approach is to modify the basis functions so that they are able to better represent the very small amplitude for the inter-particle wave functions. One solution is to add basis functions that are obtained by multiplying the exponential parts of the ECG by prefactors r_{ij}^{2m} with some large m integers. This naturally leads to a decreased probability amplitude for the wave function when the two particles are close together. Using even powers as the prefactor leads to simpler matrix elements. In the case of a diatomic molecule, where the two nuclei are treated on the same footing as the electrons, the ECGs in Eq. (17) become (Kinghorn and Adamowicz, 1999)

$$\psi_k = r_1^{2m_k} \exp(-\mathbf{r}' A_k \mathbf{r}), \tag{81}$$

where r_1 is the distance between the two nuclei. The values m_k can be treated as variational parameters. Typically, they are chosen from the range 0–100. Prefactors have also been used in calculations of the H_2^+ molecular ion using the Hylleraas basis (Yan *et al.*, 2003).

The matrix elements with ECGs containing r_{ij}^{2m} prefactors can be derived by parametric differentiation of the exponents in the standard formulae. They become quite involved for the case when more than one prefactor with a large power is used.

E. Highly excited states

Highly excited states with a number of oscillations and nodes are difficult to reproduce with a Gaussian basis set. The problems can be alleviated to a great extent by choosing ECGs with complex exponential parameters (Bubin *et al.*, 2007; Hiyama *et al.*, 2003):

$$\psi_k = \exp(-\mathbf{r}'[A_k + iB_k]\mathbf{r}). \tag{82}$$

Such basis functions have a sinususoidal component, e.g. $\sin(kr^2)$, as well as an exponentially decaying component. Numerical tests have shown that ECGs with a complex component give orders of magnitude better estimates of the highly excited states of the harmonic oscillator (Hiyama *et al.*, 2003).

A practical disadvantage of complex ECGs is that the optimization of nonlinear parameters, A_k and B_k of Eq. (82), is much more time consuming. However, the analytic complexity of the matrix elements is comparable to that for the normal ECGs with real exponents.

ECGs with complex exponents can also be used to treat systems with strongly repulsive interactions, although generally they exhibit significantly worse performance than functions with prefactors given by Eq. (81).

F. Linear dependence issues

Since the ECGs are not mutually orthogonal, it is possible that the ECG basis could become linearly dependent as the basis is increased in size during the optimization. Linear dependencies sometimes occur when the ECGs are not well adapted to describing aspects of the wave function of the system/state under investigation.

One common problem arises when trying to approximate a wave function that vanishes abnormally quickly, e.g. as in the case of the relative wave function for two particles interacting via a strongly repulsive potential. The relative wave function can be described with Gaussians with roughly equal exponents and linear coefficients. For example, at small x and

δ the wave function $\phi(x) = \exp(-ax^2) + \exp(-(a+\delta)x^2)$ will reduce to $\phi(x) \propto x^2 \exp(-ax^2)$. The relative wave function is now small, but the basis functions have a higher degree of linear dependence.

Linear dependencies between basis functions do have the potential to cause numerical instabilities in the calculation of the energy eigenvalue. Some linear dependencies may cause no harm at all, provided a proper algorithm is chosen for solving the generalized eigenvalue problem. However, when two (or more) basis functions with near unity overlaps acquire large linear coefficients that add up to nearly zero total magnitude, it almost always leads to a problem.

Consider two basis functions ψ_i and ψ_j that have $S_{ij} \approx 1$. Each eigenvalue of Eq. (6), as well as the expectation value of any operator, can be represented as a simple Rayleigh quotient. The contribution of these terms to the expectation value of any operator, O

$$\langle\psi_i|O|\psi_i\rangle + \langle\psi_j|O|\psi_j\rangle - \langle\psi_i|O|\psi_j\rangle - \langle\psi_j|O|\psi_i\rangle, \tag{83}$$

will lead to loss of numerical significance due to cancellation of leading digits arising from the subtraction. The contribution to the final result from the near linearly dependent basis functions will be of reduced precision and this can impact the overall accuracy. A loss of precision in the energy will degrade the optimization of non-linear parameters of the basis. In the worst case scenario the energy eigenvalue may become completely unreliable.

There are a variety of ways to keep the linear dependency problem under control. One straightforward approach is to eliminate linearly dependent basis functions as they appear. For example, the value of the overlap functions between any pair of basis functions, i.e. S_{ij} of Eq. (7), can be monitored. ECGs functions with overlaps too close to unity with any other element in the basis are simply excluded. Typical values of the critical overlap range from 0.95 to 0.99.

The situation becomes somewhat more complicated when optimizing the nonlinear parameters of an existing ECG basis that has become linearly dependent. Discarding one (or several) of ECGs which contribute to a linear dependency may significantly worsen the total energy.

A possible solution is to introduce a penalty function to the total energy during optimization. This function would add something to the energy whenever S_{ij} was larger than a given threshold. The penalty function, $\mathcal{P}$, should be constructed to be smooth so as not to

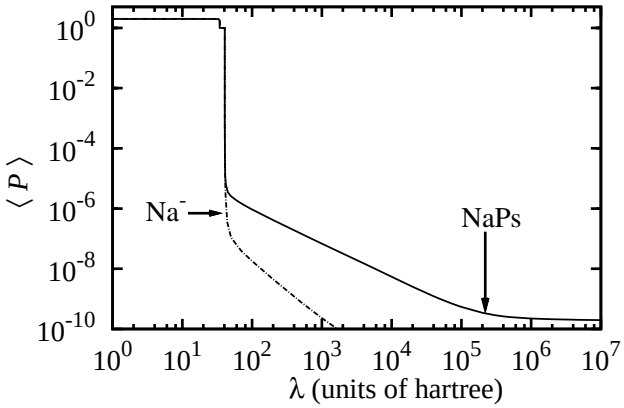

FIG. 3 The expectation value of the projection operator $\langle \hat{P} \rangle$ for the Na^- ion and the sodium plus positronium (NaPs) ground state as a function of λ. Adapted from Fig. 5 of (Mitroy and Ryzhikh, 1999c)

interfere with the optimization algorithm. One such function is

$$\mathcal{P} = \sum_{ij} \mathcal{P}_{ij}, \tag{84}$$

where the sum is over all pairs of basis functions and

$$\mathcal{P}_{ij} = \begin{cases} \beta \frac{|S_{ij}|^2 - t^2}{1 - t^2}, & |S_{ij}| > t \\ 0, & |S_{ij}| \leq t \end{cases} . \tag{85}$$

In the above expression, t is the value of the overlap threshold, and β controls the weight of the penalty term for each overlap. The choice of parameters t and β would be based on experience. Typical values might be $t = 0.99$ and β be chosen so the energy would be affected at the 0.001-0.00001% level. The value of β might be decreased as the energy gets closer to convergence.

G. Fixed core methods

The range of fermionic systems for which ECG methods can be usefully applied can be extended by the use of frozen core approximations. The tendency for fermionic systems to form closed shells naturally leads to approximations with the particles separated into inert particles in the core and active valence particles.

Two modifications to the Hamiltonian need to be made for fixed core calculations. First an effective interaction between the core and the active particles needs to be constructed.

The effective interaction can be based on a microscopic model of the core wave function, or a more empirical model potential approach can be adopted. An example of the microscopic approach is the series of calculations demonstrating positron binding to a variety of atoms (Ryzhikh *et al.*, 1998b). The core wave function was represented by a HF wave function. The direct interaction with the core was straightforward to compute since this was effectively a single particle potential. The exchange interaction with the core could also be computed provided the core single electron orbitals were expanded as a linear combination of Gaussians (Ryzhikh *et al.*, 1998b). Model potentials used to describe interactions with closed shell systems tend to be more phenomenological in nature.

When fixed core potentials are used, the Pauli principle requires that the valence particles be prevented from occupying the already occupied core states. The orthogonalising pseudo-projector (OPP) (Kukulin and Pomerantsev, 1978; **?**) and the orthogonality condition model of Saito (Saito, 1969) can be used to enforce the requirements of the Pauli principle. In the area of quantum chemistry, Bonifacic and co-workers have developed a model potential method (Bonifacic and Huzinga, 1974) that is related to the OPP. The full projection operator of the $\hat{Q}\hat{H}\hat{Q}$ form (where $Q = 1 - P$, and P is the projector to the occupied states) is not used due to the computational expense of evaluating its matrix elements.

The basic philosophy of the OPP as put forward by Krasnopol'sky and Kukulin is to add a penalty function, $\lambda\hat{P}$, to the Hamiltonian to enforce orthogonality with those orbitals to be excluded from the active space. The penalty function is an operator of the type,

$$\lambda\hat{P} = \sum_i \lambda|\varphi_i\rangle\langle\varphi_i|, \tag{86}$$

where $\lambda\hat{P}$ is constructed by summing over the single particle orbitals to be excluded from the calculation (typically the orbitals occupied by the core electrons). Provided λ is positive, the expectation value of this operator is always positive. When λ is chosen to be a sufficiently large number, any component of the wave function which is not orthogonal to the core will tend to increase the energy. The wave functions $|\varphi_i\rangle$ in Eq. (86) have Gaussian form.

Therefore, any variational method which seeks to minimize the energy will attempt to construct a wave function with a minimum overlap with the core orbitals. This can be seen in Fig. 3, which depicts the expectation value $\langle\hat{P}\rangle$ as a function of λ. Application of the pseudo-projection operator causes an abrupt change in the structure of the valence wave

function once λ becomes large enough (Mitroy and Ryzhikh, 1999c).

The OPP is most effective when the number of excluded states is relatively small. When the core complexity increases, the complexity of the nodal surfaces increases, requiring a larger ECG expansion for the valence particles. In addition, the projector results in some of the basis functions having large positive energy expectation values. The overall numerical precision of the calculation is degraded by the cancellation of the large positive matrix elements inherent to the eigenvalue calculation. The evaluation of the $\lambda\hat{P}$ matrix elements and any exchange matrix elements involving the core also becomes more time consuming as the complexity of the the core increases.

H. The Gaussian expansion method

The Gaussian expansion method (GEM), also known as the coupled-rearrangement-channel Gaussian basis, was first developed in 1988 (Hiyama *et al.*, 2003; Kameyama *et al.*, 1989; Kamimura, 1988) to determine the structure of muonic molecules, specifically the $dt\mu$ three body system. The wave function was written as

$$\Psi = \psi_{t\mu}(\mathbf{r}_1)\psi_d(\mathbf{R}_1) + \psi_{d\mu}(\mathbf{r}_2)\psi_t(\mathbf{R}_2) + \psi_{dt}(\mathbf{r}_3)\psi_\mu(\mathbf{R}_3) \ . \tag{87}$$

The channel wave function $\psi_{t\mu}(\mathbf{r}_1)$ describes the structure of the $t\mu$ cluster while $\psi_d(\mathbf{R}_1)$ describes the motion of d about the $t\mu$ cluster. All the channel functions are written as linear combinations of Gaussians, which allows for an easy evaluation of the matrix elements. Fig. 4 shows the different sets of Jacobi coordinates that would be used in the construction of the three-body wave function. The GEM method is essentially an ECG based approach but based on a physically motivated coupled channels expansion of the total wave function.

The Gaussian basis functions used to represent the radial dependence for a particular channel in the GEM often have their exponents chosen to be a geometric progression

$$\alpha_n = \alpha_1/A^{n-1}. \tag{88}$$

This basis is sometimes called an even-tempered basis. The value of A depends on the shape and range of the interaction. It is typically between 1.15 and 1.5. The overlap between adjacent basis functions is constant in this basis. Such a basis is characterized by three parameters, α_1, A and N, the number of Gaussians. It is relatively simple to optimize

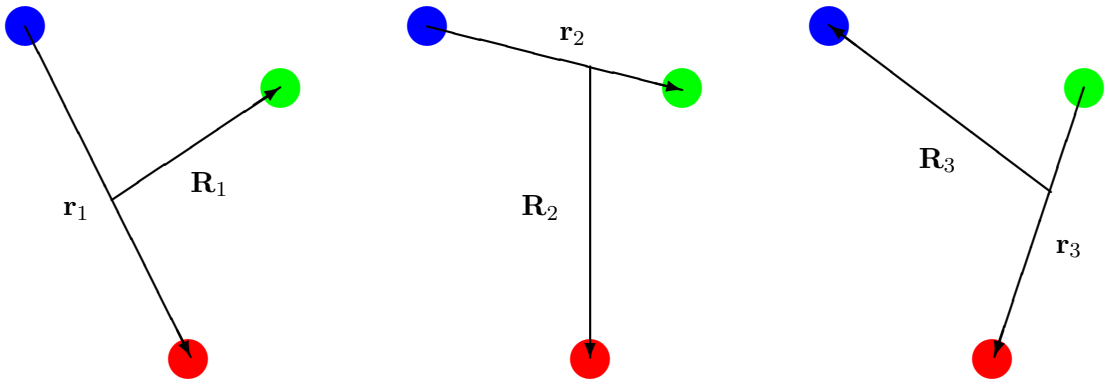

FIG. 4 (Color online) Schematic diagram showing the three different sets of Jacobi coordinates that are used in the GEM representation of a three-body system.

such a basis. To some extent, the GEM substitutes the time-consuming optimizations of the SVM by using a larger basis that does not need an intensive optimization of the nonlinear parameters. The extension of the GEM to four and five body systems results in a significant increase in the basis set dimension as the number of different sets of Jacobi recouplings increases rapidly (Hiyama *et al.*, 2005, 2003).

I. Other types of basis functions

1. Hylleraas and related functions

Hylleraas and related basis function have been used to get very accurate energies for small atoms with no more than three electrons. In particular, extremely high accuracy (more than 40 digits for the energy) has been achieved for helium (Nakashima and Nakatsuji, 2007; Schwartz, 2006a,b). Not all approaches to the determination of the helium ground state wave function are equally useful. Comparison with experiment requires the determination of relativistic corrections to the energy through the use of perturbation theory. This becomes difficult if the mathematical structure of the basis functions is excessively complex. For example, the calculations of Schwartz include logarithmic factors in the basis functions. Hylleraas basis functions satisfy the dual criteria of being able to generate very accurate energies as well as permit the evaluation of relativistic corrections (Drake, 1987). Recently, a novel method of solving the Schrodinger equation, the iterative-complement-interaction

method has been developed and been used with correlated basis functions to generate very accurate energies for the He and H_2 ground states (Nakashima and Nakatsuji, 2007; Nakatsuji *et al.*, 2007).

The Hylleraas basis functions for a three-electron system are written

$$r_1^{j_1} r_2^{j_2} r_3^{j_3} r_{12}^{j_{12}} r_{23}^{j_{23}} r_{31}^{j_{31}} e^{-\alpha_t r_1 - \beta_t r_2 - \gamma_t r_3} \mathcal{Y}^{LM}_{(\ell_1\ell_2)\ell_{12},\ell_3}(\hat{\mathbf{r}}_1, \hat{\mathbf{r}}_2, \hat{\mathbf{r}}_3) \ , \tag{89}$$

where the $\mathcal{Y}^{LM}_{(\ell_1\ell_2)\ell_{12},\ell_3}$ is a vector coupled product of one-electron spherical harmonics. The index t labels different sets of nonlinear parameters α_t, β_t and γ_t. Except for some truncations to avoid linear dependence, all terms are included such that

$$j_1 + j_2 + j_3 + j_{12} + j_{23} + j_{31} \leq \Omega \, . \tag{90}$$

where Ω is some integer. Calculations using these basis sets are typically performed using multiple precision arithmetic and often use double or multiple sets with different exponential parameters (Puchalski and Pachucki, 2006; Puchalski and Pachucki, 2008; Wang *et al.*, 2011a; Yan *et al.*, 1996).

A variation on the Hylleraas basis is the correlated Slater basis (Frolov and Smith, 1995; Korobov, 2000; Puchalski *et al.*, 2009). The radial function here is written

$$\psi = \exp(-\alpha_1 r_1 - \alpha_2 r_{22} - \alpha_3 r_3 - \alpha_{12} r_{12} - \alpha_{13} r_{13} - \alpha_{22} r_{23}). \tag{91}$$

No distinction is made between the correlated Slater basis and the Hylleraas basis in this review. The most accurate energies (including relativistic corrections) for Li and Li-like ions have been computed with Hylleraas basis functions (Wang *et al.*, 2011a).

2. James-Coolidge type functions for H_2

Generalizations of the James and Coolidge functions (James and Coolidge, 1934) have been used for calculations of the hydrogen molecule. The generalized GJC functions have the form

$$\begin{aligned} \phi(1,2) \ = \ & \exp(-\alpha_1\xi_1 - \alpha_2\xi_2)\xi_1^{n_a}\eta_1^{n_b}\xi_2^{n_c}\eta_2^{n_d}(r_{12}/R)^{n_e} \\ & \times \exp(\beta_1\xi_1 + \beta_2\xi_2)\big[\exp(\beta_1\eta_1 + \beta_2\eta_2) \\ & + (-1)^P \exp(-\beta_1\eta_1 - \beta_2\eta_2)\big], \end{aligned} \tag{92}$$

where r_{12} is the inter-electronic distance, $\xi_i = (r_{iA} + r_{iB})/R$ and $\eta_i = (r_{iA} - r_{iB})/R$, $r_{iA(B)}$ is the distance between electron i and nucleus $A(B)$, and P is a factor that equals 0 and 1 for gerade and ungerade symmetry, respectively (Kolos and Rychlewski, 1993; Kołos and Wolniewicz, 1965). The GJC functions can only be used to treat the H_2 in the BO (fixed nuclear positions) approximation. However, relativistic corrections to the energy can be evaluated (Kołos and Wolniewicz, 1964a,b, 1965).

3. Single center basis functions

Most atomic structure calculations use atom centered basis functions. The basic building block is the state function constructed from antisymmetric products of single particle orbitals with a common point as origin (Hibbert, 1975). The limitations of this approach for high precision work are exposed by considering the helium atom.

The general properties of the single-center configuration-interaction (CI) expansion have been known since the work of Schwartz (Schwartz, 1962), which provided the underlying foundation for later investigations (Bromley and Mitroy, 2007a; Carroll *et al.*, 1979; Hill, 1985; Ottschofski and Kutzelnigg, 1997). The CI expansion using single center orbitals is slowly convergent with respect to $L_{\max}$, the maximum angular momentum of any orbital included in the CI expansion. In particular, the leading term to the energy increment is expected to behave at high L as:

$$\Delta E_L = \langle E \rangle_L - \langle E \rangle_{L-1} \approx \frac{A_E}{(L + \frac{1}{2})^4} \, . \tag{93}$$

The most recent numerical investigation of this issue was carried out in 2007 (Bromley and Mitroy, 2007a). A large CI calculation, consisting of 465 single particles states, including orbitals up to $L_{\max} = 12$ gave an energy of $-2.903\,712\,786$ hartree for the helium atom to be compared with $-2.903\,724\,377\,034$ hartree (Drake, 1996). The expectation value for the coalescence matrix element, $\langle \delta(\mathbf{r}_1 - \mathbf{r}_2) \rangle$ was 0.109 744 a.u. which is 3% larger than the exact value of 0.106 345 371 (Drake, 1996).

Extrapolation techniques need to be applied for CI calculations to produce results even remotely close to the precision achievable by correlated basis sets. Extrapolations need to be applied to both the radial and angular basis sets. When this is done, the energy is $-2.903\,724\,38$ hartree (Bromley and Mitroy, 2007a).

The helium atom to some extent represents the best case scenario for the convergence of a single center expansion. The convergence is much slower if the system exhibits any degree of clustering. Extreme examples of the slow convergence of the CI method occur for exotic positron binding atoms. The maximum L in a (fixed core) CI calculation of the e^+Li ground state was $L_{max} = 30$ and even then the binding energy after extrapolation was grossly underestimated (Bromley and Mitroy, 2002b).

The analogue of the CI method in nuclear structure physics is the no core shell model (Navrátil *et al.*, 2009). These calculations are based on realistic two-nucleon, or two- plus three-nucleon interactions. The strongly repulsive nature of the interaction can slow down the convergence unless various techniques such as modifying the interaction are used to circumvent the problem.

Besides the CI approach, there is another popular method based on single particle orbitals. This is the non-variational coupled cluster method, which is widely used in quantum chemistry (Bartlett and Musiał, 2007; Cizek, 1966). The coupled cluster method with single, double, and non-iterative triple excitations [CCSD(T)] is particularly popular.

One way to improve convergence of single center calculations is to include terms where the wave function is multiplied by r_{ij} correlation factors (Kutzelnigg, 1985; Sims and Hagstrom, 1971, 2011). Such calculations are sometimes referred to as R12 calculations.

J. Many body perturbation theories and coupled cluster methods

The slow $O(L^{-4})$ convergence of the energy for single center CI type calculations involving the Coulomb interaction also manifests itself in calculations based on many body perturbation theory (MBPT). Generating precise estimates of perturbation theory energies requires a large number of partial waves typically followed by an extrapolation to the $L \to \infty$ limit.

In atomic and molecular physics, MBPT is most often associated with the Möller-Plesset partition of the Hamiltonian (Möller and Plesset, 1934), i.e., the zeroth-order Hamiltonian is the Fock operator. The nth-order energy correction in such approach is usually denoted as MPn.

The convergence of MP2 theory can be accelerated by writing the two electron virtual excitations as ECG type functions as opposed to the product of two single electron states (Szalewicz and Jeziorski, 2010). Such two electron functions have in the context of

MP2 calculations been typically referred to as Gaussian type geminals (GTGs) (note, it is also common in quantum chemistry calculations of two electron systems to refer to GTGs as opposed to ECGs).

In the first-quantized formulation of the coupled-cluster theory with single and double excitations (CCSD), the correlation energy of a closed-shell N-electron system can be expressed as

$$E_{\rm corr} = \langle \Phi | H T_2 \Phi \rangle + \frac{1}{2} \langle \Phi | H T_1^2 \Phi \rangle, \tag{94}$$

where H is the Hamiltonian, $\Phi(1,2,\ldots,N)$ is the HF function, and T_1 and T_2 are the one- and two-electron cluster operators

$$T_1 = \sum_{i=1}^{N} \hat{t}_1(i), \qquad \hat{t}_1 = \sum_{\alpha=1}^{N/2} |\tau_\alpha\rangle\langle\phi_\alpha|, \tag{95}$$

$$T_2 = \sum_{j>i=1}^{N} \hat{t}_2(i,j), \qquad \hat{t}_2 = \sum_{\alpha,\beta=1}^{N/2} |\tau^1_{\alpha\beta}\rangle\langle\phi^1_{\alpha\beta}| + |\tau^3_{\alpha\beta}\rangle\langle\phi^3_{\alpha\beta}|. \tag{96}$$

In the equations above, ϕ_α are the canonical HF orbitals, $\phi^s_{\alpha\beta}$ are their (anti)symmetrized products

$$\phi^s_{\alpha\beta} = [1 + (2-s)P_{12}]\ \phi_\alpha(1)\phi_\beta(2), \tag{97}$$

τ_α are one-electron *cluster functions*, and $\tau^s_{\alpha\beta}$ are (anti)symmetrized two-electron cluster functions, fulfilling the orthogonality and strong orthogonality (SO) conditions, respectively, relative to the occupied space. The cluster functions are solutions of the equations

$$[f - \varepsilon_\alpha]\,\tau_\alpha = S_\alpha, \tag{98}$$

$$[f(1) + f(2) - \varepsilon_\alpha - \varepsilon_\beta]\,\tau^s_{\alpha\beta} = R^s_{\alpha\beta}, \tag{99}$$

where f and ε_α are the one-electron Fock operators and orbital energies, respectively, and the right-hand sides are defined in (Bukowski *et al.*, 1999, 2003).

Each of the terms S_α ($R^s_{\alpha\beta}$) depends, in general, on *all* functions τ_α ($\tau_\alpha, \tau^s_{\alpha\beta}$). Therefore, except for the second-order MBPT approach based on the Møller-Plesset partition of electronic Hamiltonian (MP2), Eqs. (98–99) define coupled sets of equations that must be solved iteratively. Eq. (99) is solved by a minimization of the Hylleraas functional

$$\mathcal{J}^s_{\alpha\beta}[\tilde{\tau}] = \langle \tilde{\tau} | \hat{f}(1) + \hat{f}(2) - \varepsilon_\alpha - \varepsilon_\beta | \hat{q}_2 \tilde{\tau} \rangle - 2\Re\langle \tilde{\tau} | R^s_{\alpha\beta} \rangle, \tag{100}$$

where the trial functions $\tilde{\tau}$ approximating $\tau^s_{\alpha\beta}$ are expanded in a GTG basis and $\hat{q}_2$ is the SO projector. Since, in a coupled cluster theory, the term involving $R^s_{\alpha\beta}$ is expensive to calculate, the functional is usually minimized only with respect to the linear parameters of the GTG expansion. This involves solving a linear system of equations. The nonlinear GTG parameters can be optimized in advance at the MP2 level. In most cases, the MP2-optimized bases lead to satisfactory convergence of the coupled cluster energies. Recently, a new, infinite-order functional was presented (Przybytek *et al.*, 2009), which can be used in cases where post-MP2 contributions to the CCD or CCSD energies are large.

Even at the MP2 level, the straightforward variational solution of Eq. (100) (Adamowicz and Sadlej, 1978; Pan and King, 1970, 1972) leads to serious complications, because the presence of both the SO projector $\hat{q}_2$ and the Fock operators $\hat{f}(i)$ results in a large number of three- and four-electron integrals. This problem has been remedied by adding a penalty term which vanishes for orthogonal pair functions. This approach is called the weak-orthogonality method (Szalewicz *et al.*, 1982; Wenzel *et al.*, 1986), and somewhat similar to the OPP projection discussed in Subsec. III.G.

Additional approximations are necessary in coupled cluster calculations since the $\hat{q}_2$ projector contained in the $R^s_{\alpha\beta}$ term still renders the calculations very time-consuming. The most efficient approach currently used in practical calculations is called "superweak orthogonality plus projection" (Szalewicz *et al.*, 1984). In this method, $\hat{q}_2$ is replaced by the much simpler operator $1-\hat{p}(1)\hat{p}(2)$, where $\hat{p}(i)$ ensures orthogonality to the occupied orbital space. The cluster functions obtained as solutions of Eq. (99) contain then some SO violating components, which can be, however, projected out before using these functions in the next iteration. In this projection, instead of the original SO operator $\hat{q}_2$, one uses an approximate SO operator defined as $\hat{q}_B = \hat{P}_B\hat{q}_2$, where $\hat{P}_B$ is the orthogonal projector on the geminal basis set used. Since the superweak plus projection approach becomes equivalent to the exact SO projection in the limit of the complete GTG basis, all practical calculations converge to the correct result as the basis goes to completeness. The superweak plus projection method leads to a dramatic reduction of the computational cost. In particular, no integrals more complicated than three-electron ones appear at the factorizable coupled cluster with double excitations level. This is of considerable practical importance, because the contributions beyond factorizable coupled cluster are less sensitive to electron correlations and are relatively easy to saturate with orbital methods (Cencek *et al.*, 2004; Patkowski *et al.*, 2007).

Another group of methods using explicitly correlated functions in MBPT/CC calculations are the so-called R12 and F12 approaches. The convergence of a CI expansion can be dramatically improved by multiplying only the leading configuration by the factor r_{12} (Kutzelnigg, 1985). The resulting many-electron integrals can be reduced to two-electron ones by inserting an approximate resolution of the identity and this has been done at various levels of MBPT/CC theory (Helgaker *et al.*, 2008; Klopper and Noga, 2003; Kutzelnigg and Klopper, 1991). One consequence of this is that the R12-MP2 energies are no longer upper bounds to the exact MP2 values (May *et al.*, 2005).

A weakness of the linear-r_{12} factor is that at large interelectronic separations it is difficult to damp it by exponential terms. This obvious observation led to a family of the so-called F12 methods where r_{12} is replaced by a function $f(r_{12})$ which behaves similarly to r_{12} at small separations but does not diverge at large ones. This function can be written as a linear combination of GTGs (Bukowski *et al.*, 1994; Dahle *et al.*, 2007; Persson and Taylor, 1996). After the inclusion of the resolution of identity technique (May and Manby, 2004), the F12 method was implemented in standard quantum chemistry packages (Adler *et al.*, 2007; Shiozaki *et al.*, 2009). A way of including such factors in the triple-excitation functions at the CCSD(T) level has recently been proposed by Kohn (Kohn, 2009).

Whereas the most effective implementations of F12-MBPT/CC methods use only modestly larger computer resources than calculations in the same orbital-only basis and at the same level of theory, this effectiveness has been achieved applying a series of approximations. As a result F12-MBPT/CC approaches may not be competitive with orbital calculations in very large basis sets followed by extrapolations to the complete basis set limit if one aims at benchmark accuracies (Patkowski and Szalewicz, 2010).

K. Hyperspherical methods

The hyperspherical and the hyperspherical harmonic methods constitute general approaches to the solution of the 3-body and N-body systems (Fabre de La Ripelle, 1983; Krivec, 1998; Lin, 1995; Rittenhouse *et al.*, 2011; Viviani *et al.*, 1995). One typically refers to hyperspherical calculations for the 3-body calculation and hyperspherical harmonics (HH) for systems with $N > 3$. The HH wave function expands the relative wave function Ψ in terms of a complete set of channel functions $\Phi_\nu(\mathbf{\Omega}; R)$, which depend parametrically on the

hyperradius R, and weight functions $F_{\nu q}(R)$,

$$\Psi = \sum_{\nu q} R^{-(3N-4)/2} F_{\nu q}(R) \Phi_\nu(\mathbf{\Omega}; R). \tag{101}$$

Here, $\mathbf{\Omega}$ collectively denotes the $3N-4$ hyperangular coordinates and R is the hyperradius, $\mu R^2 = \sum_{j=1}^{N} m_j \mathbf{r}_j^2$; μ denotes the hyperradial mass, which can be viewed as a conveniently chosen scaling parameter (Rittenhouse *et al.*, 2011). The hyperradius R can be interpreted as a measure of the overall size of the system and plays a role analogous to the radial distance coordinate in the reduced mass two-body problem. By construction, in the adiabatic hyperspherical representation the channel functions Φ_ν are solutions to the hyperangular Schrödinger equation

$$H_{\rm ad} \Phi_\nu(\mathbf{\Omega}; R) = U_\nu(R) \Phi_\nu(\mathbf{\Omega}; R), \tag{102}$$

where

$$H_{\rm ad} = \frac{\hbar^2 \Lambda^2}{2\mu R^2} + \frac{\hbar^2 (3N-4)(3N-6)}{8\mu R^2} + V_{\rm int}. \tag{103}$$

The grand angular momentum operator Λ contains derivatives with respect to the $(3N-4)$ hyperangles and can be formally viewed as a generalized angular momentum operator. Plugging Eq. (101) into the relative Schrödinger equation $(T_{\rm rel} + V_{\rm int})\Psi = E_{\rm rel}\Psi$, where $T_{\rm rel}$ denotes the kinetic energy operator associated with the relative degrees of freedom, results in an infinite set of coupled ordinary radial differential equations that depend on the hyperangular eigenvalues $U_{\nu'}(R)$ and the hyperangular coupling matrix elements $P_{\nu'\nu}(R)$ and $Q_{\nu'\nu}(R)$, which involve the first and second derivative of the channel functions Φ_ν with respect to R (Rittenhouse *et al.*, 2011).

L. Monte Carlo techniques

Monte Carlo approaches (Ceperley and Alder, 1986; Hammond *et al.*, 1994), exhibit a more favorable scaling with respect to the computational effort associated with increasing number of degrees of freedom than the ECG approach. A key advantage of Monte Carlo methods is that they can be applied to few-body systems as well as large systems with as many as a few thousand particles (Lester Jr. *et al.*, 2002). Commonly employed Monte Carlo approaches are the variational Monte Carlo (VMC) approach and the diffusion Monte Carlo

(DMC) or Green's function Monte Carlo (GFMC) approach (Hammond *et al.*, 1994; Kosztin *et al.*, 1996; Reynolds *et al.*, 1982b), the path integral Monte Carlo (Boninsegni *et al.*, 2006; Ceperley, 1995) approach, and the auxiliary field Monte Carlo approach (Blankenbecler *et al.*, 1981; Zhang and Krakauer, 2003). For the purpose of this review, the VMC and DMC techniques are the most relevant.

The VMC approach is built on the Ritz variational principle. As in the ECG approach, the wave function of the state of interest is parameterized in terms of a set of variational parameters. However, in contrast to the ECG approach, the Hamiltonian matrix elements are generally not known analytically but instead evaluated stochastically. The stochastic nature of the algorithm introduces a statistical uncertainty of the energy expectation value, which can be decreased systematically by increasing the sampling. The variational parameters are typically optimized by minimizing some combination of the energy expectation value and its variance, and the treatment of excited states is possible through application of the Gram-Schmidt orthogonalization scheme. Expectation values such as structural properties can be calculated fairly straightforwardly. The accuracy of the VMC results crucially depends on the quality of the variational wave function employed. In certain cases, the resulting variational description is sufficient for the task at hand. More often, though, the variational wave function serves as an input for the DMC approach.

In the DMC approach, the ground state energy and structural ground state properties are obtained by starting with an initial "walker distribution", which can be thought of as a stochastic representation of the many-body wave function, and by then projecting out the lowest stationary eigenstate using a time propagation. The time propagation in the DMC algorithm is similar to that of the "standard" propagation scheme in imaginary time (Press *et al.*, 1992). However, to allow for efficient treatment of systems with many degrees of freedom, a stochastic realization of the short-time Green's function propagator is used. In most applications, importance sampling is employed so that the walker distribution represents the product of the true wave function and the so-called guiding function (which is, in most cases, obtained by the VMC approach). If the eigenstate of interest and the guiding function employed are nodeless, as is the case for the ground state of bosonic systems, the DMC method results in the exact ground state eigenenergy, within statistical uncertainties.

The fermionic wave functions exhibit nodal surfaces which cannot be crossed by the walkers. Therefore, for fermionic systems, the fixed-node DMC method is used (Reynolds *et al.*,

1982b). In the fixed-node DMC method, the nodal surface of the many-body wave function coincides with that of the guiding function and is, in general, only known approximately. The fixed-node DMC method results in an upper bound to the ground state of fermionic systems (Reynolds *et al.*, 1982a). The exact eigenenergy of states with nodes can be obtained by releasing the nodal constraint (Ceperley and Alder, 1984). In the DMC and fixed-node DMC approaches, the determination of expectation values that do not commute with the Hamiltonian can be done using the so-called mixed or pure estimators. The former results in expectation values that are calculated with respect to the mixed density, i.e., the product of the exact eigenstate and the guiding function, while the latter is exact within statistical uncertainties.

IV. ATOMIC STRUCTURE APPLICATIONS

One successful application of the ECG methodology is in solving the Schrödinger equation for light few electron atomic systems. Such systems can consist of ordinary atomic systems, but there are also exotic systems where the other coulombic particles such as positrons, muons and antiprotons can be bound to the atom.

One area of activity is simply an aim to determine the energies and wave functions of ordinary atoms with less than six electrons to increasingly higher precision. These serve to benchmark the theoertical methods used to calculate atomic properties for larger atoms. In addition, highly precise calculations coupled with highly precise experiments provide a stringent testbed for the fundamental principles of quantum mechanics and QED that underly modern physics. Another area of activity is the investigation of eoxtic atoms which can be very difficult to describe with the more generic methods usually applied to atomic structure calculations.

A. Benchmark calculations of non-relativistic atoms

The most accurate energies for two-, and three-electron atoms have been obtained with Hylleraas type wave functions. For four- and five-electron atomic systems the most accurate energies and wavefunctions have been obtained using the ECGs. In this section, we first report on the nonrelativistic calculations obtained with infinite nuclear mass. Table V gives

TABLE V Total nonrelativistic energies (assuming infinite nuclear mass) for the ground and excited states of some few-electron atoms and ions. All values are given in hartrees. The values in parentheses for DMC calculations give the statistical uncertainty while those for other calculations give an estimate of the energy uncertainty arising from a finite basis set.

System	Method	Basis size	Energy
He($1s^2$)	CI (Bromley and Mitroy, 2007a)	8586	−2.903 712 786
	ECG (Rybak *et al.*, 1989)	100	−2.903 723 818 0
	ECG (Cencek and Kutzelnigg, 1996)	1200	−2.903 724 377 030 1
	ECG (Komasa, 2002)	600	−2.903 724 377 022
	HYL (Drake *et al.*, 2002)	2358	−2.903 724 377 034 119 598 305
	HYL (Korobov, 2002)	5200	−2.903 724 377 034 119 598 311 1587
	ICI (Nakashima and Nakatsuji, 2007)		−2.903 724 377 034 119 598 311 159 245 194 404 446 696 905 37
	HYL-LOG (Schwartz, 2006a,b)	24099	−2.903 724 377 034 119 598 311 159 245 194 404 446 696 925 309 838
Li($1s^2 2s$)	CI (Jitrik and Bunge, 1997)		−7.478 025 4
	ECG (Komasa, 2002)	1536	−7.478 060 314 3
	ECG (Stanke *et al.*, 2008)	10000	−7.478 060 323 81
	HYL (Wang *et al.*, 2011a)	26520	−7.478 060 323 910 134 843
Li($1s^2 2p$)	ECG (Komasa, 2002)	3700	−7.410 156 22
	HYL (Wang *et al.*, 2011a)	30224	−7.410 156 532 650 66
Li($1s^2 3d$)	ECG (Sharkey *et al.*, 2011c)	4000	−7.335 523 542 97(60)
	HYL (Yan and Drake, 1995)	1673	−7.335 523 540 35
Be^+ ($1s^2 2s$)	ECG (Stanke *et al.*, 2008)	8000	−14.324 763 176 4
	HYL (Puchalski *et al.*, 2009)	13944	−14.324 763 176 790 150
Li^-($1s^2 2s^2$)	ECG (Bubin *et al.*, 2009a)	10000	−7.500 776 613 4(200)
Be($1s^2 2s^2$)	CI (Bunge, 2010)	2,614,689	−14.667 347 30
	ECG (Komasa *et al.*, 1995)	1200	−14.667 355 0
	SVM (Mitroy, 2011)	1800	−14.667 354 0
	ECG (Komasa *et al.*, 2002)	1600	−14.667 355 5
	ECG (Stanke *et al.*, 2009b)	10000	−14.667 356 486(15)
	CI-R12 (Sims and Hagstrom, 2011)	41871	−14.667 356 411
Be($1s^2 2s2p$)	ECG (Bubin and Adamowicz, 2009)	5000	−14.472 543 683(70)
Be($1s^2 2s3s$)	ECG (Stanke *et al.*, 2009b)	10000	−14.418 240 328(30)

energies for atoms and ions with two to five electrons. All energies in this section are given in hartree (1.0 hartree = 27.21138505 eV). Sometimes high precision *ab initio* calculations include extrapolations to the estimated nonrelativistic limit. No such estimated variational limits are included in Table V. Corrections due to finite nuclear mass, relativistic and QED effects are discussed later.

1. The hydrogen atom

The energy (−0.50 hartree) of the hydrogen atom is known exactly. Gaussian basis sets can do a reasonable job of reproducing the hydrogen energy. An optimized basis of dimension 20 is accurate to 10^{-10} hartree while a basis of dimension 40 is accurate to 10^{-15} hartree (Cencek and Kutzelnigg, 1996).

2. Two-electron atoms

Table V shows a sampling of energies for a variety of calculations based on ECGs and compares the results with other methods. The slow convergence of the CI energy is very apparent. The best ECG based wave function, namely the 1200 term function (Cencek and Kutzelnigg, 1996) is accurate to 4×10^{-12} hartree. This is still much less accurate than calculations based on Hylleraas type wave functions with logarithmic factors which are converged to more than 40 significant digits. (Nakashima and Nakatsuji, 2007; Schwartz, 2006a,b).

Helium atom calculations using ECGs have to a certain extent been motivated by a desire to test ECG methods as opposed to a desire to obtain the most accurate energies. The results of some of the earlier calculations which did not extensively optimize the non-linear parameters of the ECG basis are listed in Table V.

3. Three-electron atoms

The best three-electron atom energies are obtained with Hylleraas type wave functions. Although the accuracy reached with such functions for lithium is far from that achievable for helium, it is sufficient to extract very subtle QED effects by comparison of the theoretical

results with the most sophisticated contemporary experiments (Puchalski and Pachucki, 2008; Yan *et al.*, 2008). The first ECG calculations for Li were reported in 1993 (Kinghorn and Poshusta, 1993). Since then much progress has been made in obtaining accurate ground and excited state wave functions (Komasa, 2002; Rychlewski, 2003; Sharkey *et al.*, 2011c; Stanke *et al.*, 2008), as seen by the energies in Table V. The best ECG energies are accurate to about 10^{-10} hartree. The most important ECG results for the ground state lithium atom are collected in Table V in comparison with the state-of-the-art results from Hylleraas type (Puchalski and Pachucki, 2010; Wang *et al.*, 2011a) wave functions.

There have been applications of ECG functions to the three-electron Be^+ ion (Pachucki and Komasa, 2004; Puchalski *et al.*, 2009; Stanke *et al.*, 2008). The ground state energy obtained with an 8000-term ECG basis (Stanke *et al.*, 2008) is only 0.4 nano-hartree different from the best Hylleraas energy (Puchalski *et al.*, 2009).

4. Four-electron atoms

The first and rather preliminary ECG calculations for the total energy of the beryllium atom achieved near millihartree accuracy (Schwegler *et al.*, 1993). Since then, there have been numerous treatments reporting precisions of close to or better than 10^{-6} hartree (Komasa, 2002; Komasa *et al.*, 1995, 2002; Pachucki and Komasa, 2006b; Stanke *et al.*, 2007a; Stanke *et al.*, 2009b) with the best ECG wave functions having energies precise to 10 nano-hartree (Stanke *et al.*, 2007a; Stanke *et al.*, 2009b). All these calculations have achieved a lower energy than the most recent CI calculation employing 2,614,489 configurations (Bunge, 2010). Most recently a CI-R12 calculation achieved a comparable accuracy (Sims and Hagstrom, 2011) but its upper bound is still inferior to the most recent ECG energy (Stanke *et al.*, 2009b).

Calculations have been extended to treat members of the Be iso-electronic series (Komasa *et al.*, 2002). They include the low lying excited states, and encompass states with non-zero angular momentum (Komasa and Rychlewski, 2001; Sharkey *et al.*, 2011b; Stanke *et al.*, 2007b; Stanke *et al.*, 2009b).

The advantages of applying a direct versus a stochastic optimization can be seen in the Table. The best SVM energy for Be equals to $-14.667\,354$ hartree with 1800 ECGs is 10^{-6} hartree higher than the energy of Komasa et. al. (Komasa *et al.*, 1995) obtained with only

1200 ECGs. However, the SVM energy is still superior to all other variational approaches with the exception of the CI-R12 calculation (Sims and Hagstrom, 2011).

The B^+ ECG binding energy is 4×10^{-5} hartree smaller than the best semi-empirical estimate of the exact non-relativistic energy, namely -24.34892 hartree (Chakravorty *et al.*, 1993). The semi-empirical estimates were derived by performing the relativistic CI calculations to estimate the relativistic contribution to experimental ionization energies. A similar disagreement occurs with C^{2+} where the semi-empirical binding energy, namely -36.53499 hartree (Chakravorty *et al.*, 1993) is more than 10^{-4} hartree larger than the best ECG energy. There have been independent calculations of 4-electron atoms using ECGs that give energies in agreement at the level of 10^{-6} hartree. The conclusion to be drawn is that explicit calculations using ECG basis sets give better estimates of the exact non-relativistic energies of 4-electron atoms and ions than those derived from experiment. This is of wider significance since the semi-empirical energies (Chakravorty *et al.*, 1993) are often used as fundamental reference data to test atomic structure calculations for atoms and ions up to a nuclear charge of 28. An update of the recommended Table of non-relativistic energies is probably desirable with the ECG energies being adopted to give the reference for four-electron ions.

5. Five-electron atoms

Recently ECG based methods were applied to determine the wave functions of five-electron atoms. Table V gives the energies of the ground $^2P^o$ and the excited $^2S^e$ state of the B atom. The latest ECG energies are estimated to have better than 10^{-5} hartree accuracy (Bubin and Adamowicz, 2011). The ECG based wave functions give better energies than the CI calculations (Almora-Diaz and Bunge, 2010) and a DMC calculation (Seth *et al.*, 2011). The level of accuracy achieved for five-electron atoms is about four orders of magnitude worse than that achieved for four-electron atoms due to additional wave function complexity and the additional computational intensity of dealing with an extra electron.

The B $^2P^o$ ECG binding energy is 4×10^{-5} hartree smaller than the best semi-emprical estimate of the exact non-relativistic energy, namely -24.65391 hartree (Chakravorty *et al.*, 1993). The difference between the ECG and semi-empirical energies is about the same size as the difference for B^+ and the ECG energy is likely to be more reliable.

6. Inclusion of relativistic effects

Comparison of high precision calculations with experiment requires inclusion of relativistic effects using Eq. (47). This has been accomplished for several lithium- and beryllium-like ions (Bubin and Adamowicz, 2008; Bubin *et al.*, 2009a, 2010a; Pachucki and Komasa, 2004, 2006a,b; Stanke *et al.*, 2009b; Stanke *et al.*, 2008; Stanke *et al.*, 2008). Table VI shows the importance of relativistic effects in the determination of the energy of the $\Delta E(2^1S \rightarrow 3^1S)$ transition of beryllium. The relativistically corrected energy agrees with the experimental value to 0.1 cm^{-1} which is equal to the experimental uncertainty.

TABLE VI Contributions from subsequent terms of the expansion (47) to the Be$(2^1S \rightarrow 3^1S)$ excitation energy (Stanke *et al.*, 2009b).

Contribution	$\Delta E/\mathrm{cm}^{-1}$
$^{\infty}$Be $E^{(0)}$	54 674.677(2)
^{9}Be $E^{(0)}$	54 671.219(2)
$\alpha^2 E^{(2)}$	6.688(18)
$\alpha^3 E^{(3)}$	-0.506(4)
$\alpha^4 E^{(4)}$	-0.023(6)
E	54 677.378(30)
E_{exp} (Kramida and Martin, 1997)	54 677.26(10)
difference	0.12(13)

The ability to achieve this level of accuracy rests on two factors. First, the accuracy of the underlying non-relativistic calculations is about 10^{-8} hartree. Second, the techniques described in Sec. III.C to evaluate the expectation values of the Breit-Pauli Hamiltonian greatly improve the accuracy of the relativistic and QED corrections.

B. Atoms in magnetic fields

The theoretical interest in the studies of atomic and molecular systems in magnetic field is motivated by the discovery of the strong magnetic field on white dwarfs (Angel *et al.*, 1981; Kemp *et al.*, 1970) ($\approx 10^7$ G) and on the surface of neutron stars (Truemper *et al.*,

1978) ($\approx 10^{12}$ G). The strongest magnetic fields available in the laboratory are about 10^6 G.

In a magnetic field the spherical symmetry of the Coulomb interaction is broken. The geometry of the highly anisotropic charge distribution is very challenging for conventional theoretical approaches and high accuracy solutions are only available for the H and He atoms. Precise calculation of the spectra of light elements in magnetic field would assist in the interpretation of the optical absorption spectra and therefore the understanding of the composition of the atmosphere of stars.

Various approaches have been used to calculate the energies of atoms in magnetic fields including variational (Nakashima and Nakatsuji, 2010; Vincke and Baye, 1989), HF (Jones *et al.*, 1996; Proschel *et al.*, 1982), QMC (Jones *et al.*, 1997) and CI (Al-Hujaj and Schmelcher, 2003) calculations.

The Hamiltonian of the few-body system in magnetic field is

$$H = \sum_{i=1}^{N} \frac{1}{2m_i}(\mathbf{p}_i + \frac{e_i}{c}\mathbf{A}_i)^2 + \sum_{i<j} \frac{e_i e_j}{\kappa r_{ij}} \tag{104}$$

where $\mathbf{A}_i = \frac{1}{2}\mathbf{r}_i \times \mathbf{B}$, the magnetic field is $\mathbf{B} = (0, 0, B)$, m_i and e_i are the masses and charges, and $\kappa = 4\pi\epsilon$ (ϵ is the dielectric constant of the medium).

The energies of the He and Li atoms (Tables VII and VIII) have been computed with the SVM using modified ECGs defined in Eq. (38) (Varga, 2011). The magnetic field is characterized by the parameter $\beta = B/2B_0$, with $B_0 = 2.35 \times 10^{15}$ T. The calculated results are in good agreement with other calculations, in most cases improving the accuracy compared to previous results.

C. Atomic polarizability calculations

While the best non-relativistic calculations of the $^{\infty}$He dipole polarizability have been performed using Hylleraas basis functions and gave the value of 1.383 192 174 455(1) a.u. (Pachucki and Sapirstein, 2001), this cannot serve as a comparison with experiment since finite mass, relativistic and QED effects need to be taken into account.

At present the most accurate computed value of ^{4}He polarizability is the result of a hybrid calculation. The finite mass and relativistic corrections up to order α^2 were computed with the ECG basis (Cencek *et al.*, 2001). The set of α^3 QED corrections, including the electric

TABLE VII Energies (in hartree) of the singlet state of helium with M=0, −1 and −2 as calculated with SVM and Hylleraas-like basis. The SVM calculations used 200 basis states.

	SVM	HYL	CI (HYL-Gaussian)
β	(Varga, 2011)	(Scrinzi, 1998)	(Wang and Qiao, 2008)
		$M = 0$	
0.0	−2.903 723 37		−2.903 71
0.1	−2.895 834 45	−2.895 83	−2.895 81
0.2	−2.872 870 76	−2.872 87	
0.4	−2.788 424 46	−2.788 42	
		$M = -1$	
0.0	−2.123 840 89		−2.123 83
0.1	−2.145 275 02	−2.145 27	−2.145 25
0.2	−2.106 157 55	−2.106 18	
0.4	−1.969 856 31	−1.970 11	
		$M = -2$	
0.0	−2.055 615 73		−2.055 619
0.1	−2.079 373 21	−2.07949	−2.079 374
0.2	−2.032 415 90	−2.033 08	
0.4	−1.886 524 46	−1.890 21	

TABLE VIII Energies (in hartree) of the $1s^2 2s$ $M = 0$ state of Li in a magnetic field as calculated with SVM and Hylleraas-like functions.

β	SVM	HYL
	(Varga, 2011)	(Guan and Li, 2001)
0.000	−7.478 058	−7.477 796
0.009	−7.527 529	−7.527 505
0.25	−7.523 784	−7.523 595
0.4	−7.486 518	−7.486 436

field correction to the Bethe logarithm were computed with the correlated Slater basis (Łach *et al.*, 2004). The final value of 1.383 760 79(23) a.u. is accurate to about 0.2 ppm.

A microwave cavity has been used to measure the refractive index of helium to an accuracy of 9 ppm and yielded the value of 1.383 759(13) a.u. (Schmidt *et al.*, 2007). If the ^{4}He polarizability is taken as a known quantity from theory, then this experiment admits another interpretation. Taking the polarizability and diamagnetic susceptibility as known quantities, the refractive index experiment yields a value for the universal gas constant, $R = 8.314\,487(76)$, which in terms of the error is not far from the recommended value of 8.314 2(15) (Mohr and Taylor, 2005). Boltzmann's constant, the definition of the mol and the universal gas constant are all inter-related through the identity, $R = k_B N_A$. Further improvement in the precision of experiments measuring either the refractive index or the dielectric constant of helium could lead to a redefinition of these quantities in terms of a standard which is based on the calculated helium polarizability (Fellmuth *et al.*, 2006; Stone and Stejskal, 2004).

Another atomic polarizability calculation with potential applications is that for the Be atom. ECG type calculations have given the dipole polarizability of 37.755 a.u. for $^\infty$Be (Komasa, 2002). The result has implications for the new generation of atomic frequency standards based on highly forbidden optical transitions (Margolis, 2009; Mitroy *et al.*, 2010). Frequency shifts due to temperature dependent blackbody radiation (BBR) loom as one of the sources of uncertainty in these standards (Mitroy *et al.*, 2010). The significance of this result lies in the coincidence that the $^1S^e \rightarrow {}^3P^o$ clock transition of neutral beryllium has the smallest BBR shift of any of the atoms that could potentially serve as frequency standards (Mitroy, 2010). Besides having the smallest BBR shift, its small size means that first principles calculations using ECGs could permit an accurate estimate of the temperature dependent correction due to the BBR shift. The use of ^{9}Be for an optical frequency standard is currently a theoretical curiosity since the cooling and trapping of this atom is not possible with the existing technology.

D. Positronic complexes

Apart from positronium, the first mixed electron-psoitron system was the positronium ion (Ps^- or e^-Ps) which was predicted to exist in a variational calculation by Wheeler (Wheeler,

1946). Subsequently, positronium hydride (Ore, 1951) and the positronium molecule (or di-positronium) (Hylleraas and Ore, 1947) were also shown to be electronically stable. Positron binding systems are not absolutely stable due to the propensity of the positron to annihilate with the electrons.

Table IX lists the latest energies for a number of small positron binding systems. The calculations based on ECGs give the best energies for all the systems with one exception, namely Ps^-. The positronium negative (positive) ion is a three-body system and is accessible to calculation using Hylleraas or Slater-type basis sets. The PsH system is a four body system and is amenable to calculations using both ECG and Hylleraas basis functions. The ECG energy is clearly superior in this case. The PsH system has a Ps+H structure and the Ps cluster is not well described with a Hylleraas function with the electron-positron correlations solely represented by r_{ij}^k factors (Yan and Ho, 1999). The DMC energies (Mella *et al.*, 2002, 1999) have not achieved the same level of precision as the best ECG and HYL calculations but is in agreement when the statistical uncertainty is taken into consideration.

One class of exotic atomic systems are those atoms or negative ions with an attached positron. The salient feature of these systems is the attractive coulomb interaction between the positron and atomic electrons. This leads to the wave function have a component that is best characterised as a positronium cluster. As mentioned in Section III.I.3, it is difficult to describe such a cluster with a CI wave-function and consequently there had been no conclusive calculation demonstrating positron binding to neutral atoms until 1997 (indicative calculations did exist (Danby and Tennyson, 1988; Dzuba *et al.*, 1995)). when two calculations using ECGs established that e^+Li was electronically stable (Ryzhikh and Mitroy, 1997; Strasburger and Chojnacki, 1998) and has a structure best described as a Ps atom weakly bound to a Li^+ core. The existence of positron binding to electrically neutral atoms and molecules had long been suspected from the results of gas phase positron annihilation spectroscopy. In these experiments, high-energy positrons from a positron source are injected into a gas. After thermalization the annihilation cross section is measured. Very large annihilation cross sections had been measured for a variety of gases. It is now believed that positrons trapped in vibrational Feshbach resonances (i.e. positrons bound to vibrationally excited states of the molecule) provide the mechansism responsible for the huge annihilation cross sections (Gribakin *et al.*, 2010). This mechanism did not gain widespread acceptance until the ability of positrons to form bound states with a variety of atoms (and by implication

moleculaes) was established by variation calculations using ECG basis sets (Reich, 2004; Ryzhikh *et al.*, 1998b)).

This stability of e^+Li was independently verified by a hyperspherical calculation (Yuan *et al.*, 1998). Subsequently positron binding to Na (Ryzhikh *et al.*, 1998a,b; Yuan *et al.*, 1998), Be (Ryzhikh *et al.*, 1998b), Mg (Ryzhikh *et al.*, 1998b), Cu (Ryzhikh and Mitroy, 1998a), Zn (Mitroy and Ryzhikh, 1999a), and Ag (Ryzhikh and Mitroy, 1998b) was quickly established. Crucial to these results was the development of a fixed core variant of the SVM (FCSVM). The FCSVM was validated by performing calculations for light atoms for which both SVM and FCSVM calculations are possible. The differences between the SVM and FCSVM binding energies for the atoms listed in Table IX are about 1%. While DMC calculations have used to estimate the binding energies of some of these systems, e^+Li, e^+Be and LiPs, the DMC energies do not agree with the ECG energies within the DMC statistical uncertainty. A possible cause are imperfectly known nodal surfaces which are needed as input to DMC calculations involving fermions.

Inclusion of various core terms in the FCSVM Hamiltonian increases the amount of time required to calculate the matrix elements by at least one order of magnitude. In addition to the slower matrix element evaluation, the larger systems have core structures that lead to more complicated nodal structures for the valence electrons. Larger ECG expansions are needed to generate an accurate wave function. Furthermore, the strongly repulsive OPP potential leads to a loss in numerical precision making it more difficult for the stochastic search to establish binding.

For these reasons, CI methods were also adapted to study these systems. The CI calculations were all done using a fixed core approximation (FCCI). They demonstrated the electronic stability of e^+Sr (Bromley and Mitroy, 2006b) and e^+Cd (Bromley and Mitroy, 2002a), the stability of a $^2S^e$ ground state and a $^2P^o$ excited state of e^+Ca (Bromley and Mitroy, 2006a,b, 2007b). The FCCI calculations were computationally demanding with very large orbital basis sets, e.g. with more than 100 single electron and 100 single positron orbitals.

Due to the importance of the positronium cluster it has been suggested (Mitroy *et al.*, 1999, 2002) that the structure of any atom binding a positron atom can be written schematically as

$$\Psi = \alpha\Phi(\text{Atom})\phi(e^+) + \beta\Omega(\text{Atom}^+)\omega(\text{Ps}) \ . \tag{105}$$

TABLE IX Total energies of some exotic positron binding systems. Only the latest calculations of a given type by a particular group are listed in this table. In all cases the nuclear masses are set to ∞. The uncertainty associated with the DMC calculations is purely statistical and does not take into consideration uncertainties in the definition of the nodal surfaces.

System	Method	Basis size	Energy (hartree)	Binding Energy (hartree)
Ps^-	SVM (Krivec *et al.*, 2000)	800	−0.262 005 070 226	0.012 005 070 226
	HYL (Korobov, 2000)	2200	−0.262 005 070 232 980 1077(3)	0.012 005 070 232 980 1077(3)
	HH (Krivec *et al.*, 2000)	676	−0.262 005 0695	0.012 005 0695
PsH	ECG (Bubin and Varga, 2011)	4000	−0.789 196 766 900(200)	0.039 196 766 900(200)
	HYL (Yan and Ho, 1999)	5741	−0.789 196 7051	0.039 196 7051
	DMC (**?**)		−0.789 196 7051	0.039 15(4)
e^+PsH	SVM (Zhang and Mitroy, 2007)	1500	−0.810254	0.021 057
Ps_2	ECG (Bubin *et al.*, 2007)	6000	−0.516 003 790 455(50)	0.016 003 790455(50)
	HYL (Ho, 1986)	400	−0.515 105	0.015 105
$(p^+,2e^+,4e^-)$	SVM (Varga, 1999)	800	−1.05542	0.00423
e^+He($^3S^e$)	SVM (Mitroy, 2005a)	1500	−2.250 5951	0.000 5951
e^+Li	SVM (Mitroy, 2004)	1200	−7.532 396	0.002 482
	DMC (Mella *et al.*, 1999)		−7.532 29(2)	0.002 38(2)
	FCSVM (Mitroy, 2004)	240		0.002 479
LiPs	SVM (Mitroy, 2010)	2200	−7.740 4316	0.012 371
	DMC (Mella *et al.*, 2002)		−7.7396(1)	0.0116(1)
	FCSVM (Mitroy, 2010)	1000		0.012 365
e^+LiPs	ECG (Varga, 1999)	800	−7.805 10	0.009 18
e^+Be	SVM (Mitroy, 2010)	2200	−14.670 519	0.003 163
	DMC (Mella *et al.*, 2002)		−14.6688(4)	0.0014(4)
	FCSVM (Mitroy, 2010)	1023		0.003 181
e^+Na	FCSVM (Mitroy, 2005b)	488		0.000 474
e^+Mg	FCSVM (Bromley and Mitroy, 2006b)	1200		0.016 930
	FCCI (Bromley and Mitroy, 2006b)	≈500000		0.017 040
e^+Ca	FCCI (Bromley and Mitroy, 2006b)	≈500000		0.018 930

The first of these terms represents a positron moving in the field of a polarized atom while the second term represents a Ps cluster attached to the residual ion (or atom). The relative strength of these two configurations is determined by the ionization potential of the atomic parent. When the ionization potential is less than 0.250 hartree (the Ps binding energy), the most loosely bound electron is attached to the positron forming a Ps cluster. However, when the ionization potential is greater than 0.250 hartree, the tendency to form a Ps cluster is disrupted by the stronger attraction of the electron to the parent atom. The electron is more strongly attracted to the nucleus and the repulsive positron-nucleus interaction breaks up the cluster.

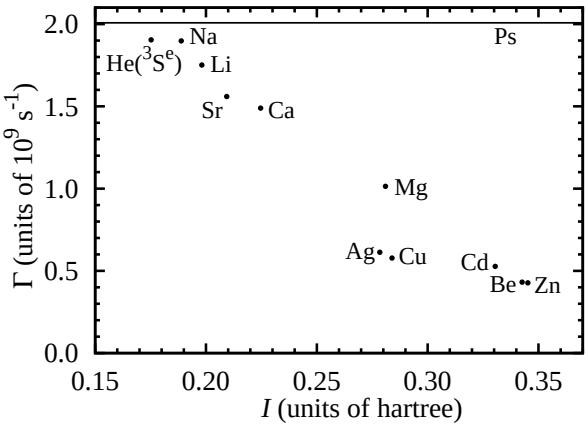

FIG. 5 The spin-averaged 2γ annihilation rate, Γ (in units of 10^9 s^{-1}) as a function of the ionization potential, I for a number of positronic atoms. Source of annihilation rate for each system is as follows; He($^3S^e$) (Mitroy, 2005a), Li (Mitroy, 2004), Be (Mitroy, 2010), Na (Ryzhikh *et al.*, 1998b), Mg (Bromley and Mitroy, 2006b), Ca (Bromley and Mitroy, 2006b), Cu (Mitroy *et al.*, 2001), Zn (Mitroy *et al.*, 2008a), Sr (Bromley and Mitroy, 2006b), Ag (Mitroy *et al.*, 2001) and Cd (Bromley and Mitroy, 2010). The annihilation rates for Ca, Sr, Zn and Cd come from FCCI calculations which have large corrections from an extrapolation procedure.

This tendency is clearly seen in Fig. 5 where the spin-averaged annihilation rate for electron-positron annihilation is plotted as a function of I. The annihilation rate is very close to the spin-averaged Ps annihilation rate of 2.0081×10^9 s^{-1} (Mitroy *et al.*, 2002) for e^-He($^3S^e$) and e^+Na. The annihilation rate steadily decreases as I increases.

The value of I also influences the feasibility of doing CI calculations on these systems. The e^+Li, e^+Na and e^+He(^{3}S^e) systems (with small values of I) all consist of a bound Ps-cluster bound in the field of the residual ion and the partial wave expansion is very slowly convergent. No CI calculations giving an estimate of the binding energy even remotely close to the FCSVM energies have been reported.

The ionization potential also has an influence on the likelihood of positron binding. The binding energy is largest when the parent atom ionization potential is closest to 0.250 hartree (the binding energy of Ps) (Mitroy *et al.*, 1999, 2002). The atoms with the largest positron binding energies in Table IX are e^+Mg and e^+Ca with ionization potentials of 0.28099 and 0.22465 hartree (Ralchenko *et al.*, 2008), respectively.

Bound states of systems containing more than one positron have also been predicted

(Varga, 1999) by SVM calculations. Some examples are listed in Table IX. The H^- ion can bind not only one but two positrons. The binding energy of e^+PsH (0.021057 a.u.) is comparable to that of PsH (0.039 197 a.u.).

While the e^+PsH system can be viewed as Ps^+ bound to the hydrogen atom, there are also exotic systems more akin to a charged particle bound to the Ps_2 molecule. The Ps_2 molecule cannot bind an extra electron or positron because of restrictions imposed by the Pauli principle. However, a distinguishable singly charged particle can bind to Ps_2. For example, the five-body system $Ps_2+x^+=(2e^+,\ 2e^-,\ x^+)$, containing a hypothetical "x" particle is bound for any $0 \leq m_e/m_x \leq 1$ mass ratio. An atomic example from Table IX is the seven-body e^+LiPs system (Mezei *et al.*, 2001; Mitroy and Ryzhikh, 1999b; Varga, 1999). The structure is best described as Li^++Ps_2. The FCSVM has also been used to describe e^+LiPs and also demonstrates the electronic stability of e^+NaPs (Mitroy and Ryzhikh, 1999b).

Another seven-body bi-positron system from Table IX is the H^-Ps_2 system. This system consisting of a proton, four electrons and two positrons has an estimated binding energy of 0.00423 hartree (Varga, 1999). It is not clear whether this system would be best described as H^-+Ps_2 or as the H^- analogue, p+2Ps^-.

Another significant achievement of the SVM was the identification of a second bound state of the Ps_2 molecule with an orbital angular momentum $L = 1$ and a total energy of $-0.334\,408\,317\,34(81)$ a.u. (Puchalski and Czarnecki, 2008; Usukura *et al.*, 1998; Varga *et al.*, 1998). The lowest energy dissociation threshold is at -0.31250 a.u. The electronic dipole transition between this state and the Ps_2 ground state would be an unambiguous signature of the experimental formation of Ps_2.

E. Coulomb few-body systems

There are numerous Coulombic systems that can be formed from combinations of charged mesons, baryons and leptons. The determination of which four (Varga *et al.*, 1997) and five-body (Mezei *et al.*, 2001) systems are bound is reduced by application of the SVM to a largely mechanical exercise.

Coulomb few-body systems do admit the possibility of Borromean binding. A N-body Borromean state is one which has no bound $(N-1)$-body subsystems (Zhukov *et al.*, 1993). The existence of Coulombic four-body Borromean systems was established (Richard, 2003)

by combining results from different 4-body DMC calculations (Bressanini *et al.*, 1997) and 3-body SVM calculations (Mitroy, 2000). The $(p, \bar{p}, d, \bar{d})$ system is an example of a Borromean system.

F. Outlook

The $n!$ growth in computational intensity is the one reason limiting the precision achieved by ECG methods to atoms with five (or six) electrons. Another reason that the wave function itself becomes more complex and difficult to describe with high accuracy. The energies for the B $^2P^o$ ground state took about one year of continuous calculation on a machine wtth six processors and four cores per processor.

An important unresolved problem in atomic structure physics is to diagonalize the Dirac-Coulomb Hamiltonian for few electron systems with correlated basis functions. The problems in generating very precise energies are fundamental to the Dirac-Coulomb Hamiltonian and are not merely a matter of choosing the best basis functions.

V. MOLECULAR STRUCTURE APPLICATIONS

One of the core goals of quantum chemistry is simply the first principles prediction of the structure of molecules from the Schrodinger or Dirac equations. The systems of interest range from light diatomics to systems with hundreds of atoms. Very light molecules such as H_2 and LiH allow very accurate solutions of the Schrodinger equation by using ECGs and consequently can be used a laboratory to test the computational approaches used to determine the electronic structure of large systems. In addition, calculations on light systems can be used to test a fundamental approximation that underpins practically all molecular calculations, namely the Born-Oppenheimer separation.

A. Geminals and perturbation theory

GTG functions in the framework of MBPT (see Sect. III.J for theoretical details) were pioneered for atoms at the MP2 level (Pan and King, 1970). The approach was extended to the H_2, LiH, and BH molecules (Adamowicz, 1978; Adamowicz and Sadlej, 1978). Early

applications were restricted to small basis sets because of the computationally expensive direct treatment of the strong orthogonality problem. The introduction of the more efficient weak-orthogonality second-order energy functional (Szalewicz *et al.*, 1982) resulted in MP2 (Szalewicz *et al.*, 1983a) and MP3 energies (Szalewicz *et al.*, 1983b) of He, Be, H_2, and LiH that were the most accurate ones at that time. This approach was also applied to ten-electron systems: the Ne atom (Wenzel *et al.*, 1986) and the water molecule (Bukowski *et al.*, 1995).

Considerable effort was invested over the years to find efficient techniques to optimize GTG parameters. The current method of choice is a stochastic optimization approach similar to those described in Sec. III.A.1. The computational overhead associated with the optimization means that calculations using GTGs can only surpass those utilizing single particle orbitals for relatively small systems (Bukowski *et al.*, 2003).

The first coupled cluster applications utilizing the GTG functions were performed in 1984 when this approach was applied at the coupled cluster double excitations (CCD) level to He, Be, H_2, and LiH (Jeziorski *et al.*, 1984). Later the formalism was extended to the coupled cluster with single and double excitations (CCSD) level of theory with benchmark results reported for some two-electron (He, Li^+, H_2) and four-electron (Be, Li^-, LiH) systems (Bukowski *et al.*, 1999).

The most significant application of coupled cluster approaches has been to the calculation of a helium dimer potential accurate at the millikelvin level (Cencek *et al.*, 2004; Jeziorska *et al.*, 2007; Patkowski *et al.*, 2007) (1 K = 3.1668153×10^{-6} Hartree). The most accurate values from these calculations are listed in Table X. To calculate the dominant contribution, the CCD correlation energy, the pair functions τ^1_{11}, τ^1_{12}, τ^3_{12}, and τ^1_{22} in Eq. (99) were expanded in large GTG basis sets (up to $\mathcal{N} = 800$ terms). It was possible to eliminate basis set superposition errors in the interaction energy (the difference in energy with respect to two non-interacting He atoms) by using the same basis set for each pair at a given $\mathcal{N}$ (Bukowski *et al.*, 1996). The GTG parameters were carefully optimized in an MP2 calculation. Corrections going beyond the coupled-cluster with double excitations (i.e. including single excitations as well), $E_{\mathrm{CCSD}} - E_{\mathrm{CCD}}$ were obtained from calculations using single particle orbital basis sets. At some selected distances (due to computational expense), GTG-based CCSD calculations were performed, yielding results consistent with those using orbitals. The post-CCSD contributions, were calculated as $E_{\mathrm{CCSD(T)}} - E_{\mathrm{CCSD}}$

and $E_{\mathrm{CI}} - E_{\mathrm{CCSD(T)}}$ using large single particle orbital basis sets. The energy differences between any two levels of theory were computed using identical basis sets. At 5.6 a_0, the obtained interaction energy amounts to −11.0037(31) K.

GTG functions have been used also in another perturbative approach, namely symmetry-adapted perturbation theory (SAPT) (Jeziorski *et al.*, 1994; Szalewicz, 2011; Szalewicz *et al.*, 2005). SAPT is a perturbation theory using as the zeroth-order approximation monomers at infinite separation, i.e., it is designed to treat weak (van der Waals) intermolecular (interatomic) interactions. In SAPT, the interaction energy is expanded in a double perturbation series with respect to the intermonomer (interatomic) interaction operator and to the intramonomer correlation operators. The dominant (in the helium dimer) attractive component, the second-order dispersion energy, can be obtained by minimization of an appropriate Hylleraas-type functional (Chalasinski *et al.*, 1977; Rybak *et al.*, 1987; Szalewicz and Jeziorski, 1979) with a two-electron dispersion pair function. The main repulsive component, the first-order energy, can be obtained from the accurate wave functions of the monomers. Some additional second-order components can be computed from a standard (single orbital-based) SAPT code (Bukowski *et al.*, 2011). The residual parts of the interaction energy can be computed with a large basis FCI calculation method, where FCI denoted the full CI methods, i.e., with up to n-electron excitations. Using this strategy, a complete SAPT-based helium dimer potential was obtained (Korona *et al.*, 1997; Williams *et al.*, 1996), with the interaction energy of −11.059(30) K at $R = 5.6$ a_0. This potential was used extensively in the next decade to predict various properties of helium (Janzen and Aziz, 1997). Recently, the SAPT calculations for the helium dimer were repeated (Jeziorska *et al.*, 2007) with much larger basis sets. The new SAPT results are fully consistent with the coupled cluster results discussed above but have smaller uncertainties at large distances. The current recommended helium dimer potential combines coupled cluster and SAPT results and includes adiabatic, relativistic, and QED corrections (see Section V.B).

B. Ab-initio Born-Oppenheimer calculations

For almost 30 years after the pioneering work of James and Coolidge (James and Coolidge, 1934), the GJC functions were still the only explicitly correlated basis set applied to molecular systems, but such applications were limited to H_2 and isoelectronic diatomic species like

TABLE X Interaction energy $E_{\rm int}$ (in kelvin) of He_2 at R=5.6 a_0 as a function of the number of expansion terms, K. The interaction energy values were calculated using the exact monomer energy and are strict upper bounds to the exact value. ϕ_0 in Eq. (106) contained 56953 terms resulting from a product of two helium atom functions with L=337 terms. During the optimization, a shorter expansion of ϕ_0 was used (40186 terms, L=283). The conversion factor is 315 774.65 K/hartree.

		without ϕ_0	with ϕ_0	
K	$E_{\rm int}$	Reference	$E_{\rm int}$	Reference
1200	−10.9582	(Cencek *et al.*, 2005)	−10.998 53	(Cencek and Szalewicz, 2008)
2400	−10.9900	(Cencek *et al.*, 2005)	−11.000 12	(Cencek and Szalewicz, 2008)
4800	−10.9953	(Cencek *et al.*, 2005)	−11.000 35	(Cencek and Szalewicz, 2008)
extrap.			−11.000 6(2)	(Cencek and Szalewicz, 2008)
CCSD using ECGs, CCSD(T) + FCI using orbitals.			−11.0037(31)	(Patkowski *et al.*, 2007)
SAPT using GTGs to second order (higher-order contributions using orbitals)			−10.999 6(105)	(Jeziorska *et al.*, 2007)
GFMC			−10.998(5)	(Anderson, 2004)

HeH^+. One well known milestone of the GJC approach was the prediction of the ground state dissociation energy, D_0 (Kolos and Wolniewicz, 1968) that later proved to be more accurate than the concurrent experimental data (Herzberg, 1970). Generalizations of the GJC approach to systems with more than two electrons resulted in prohibitively complicated integrals, although one should mention the calculations for He_2^+ and He_2 by Clary and Handy (Clary and Handy, 1977). Going beyond diatomic molecules for a GJC basis seems almost impossible because of intractable many-center integrals.

The introduction of the ECG basis has resulted in succession of very accurate calculations on a variety of diatomic and triatomic molecules. Calculations on the H_2 molecule using GJC and ECG have been leap-frogging each other in accuracy for a number of years (Cencek and Szalewicz, 2008; Rychlewski and Komasa, 2003). The current best estimate of the BO energy of H_2 at the equilibrium distance of 1.4011 a_0, equal to 1.174 475 931 400 216 7(3) hartree, results from extrapolated GJC expansions with up to 22363 terms (Pachucki, 2010). The current best ECG energy of 1.174 475 931 400 21(6) hartree was obtained with shorter expansions of only 4800 terms (Cencek and Szalewicz, 2008).

The first applications of ECG functions with $N > 2$ were limited LiH studies by Karunakaran and Christoffersen (Karunakaran and Christoffersen, 1977, 1982). This pioneering work was resumed only 15 years later with applications to He_2^+ (Cencek and Rychlewski, 1995, 2000), LiH (Cencek and Rychlewski, 1993, 2000; Tung *et al.*, 2011), H_3 (Cencek

TABLE XI The total electronic energy (in hartree) of the LiH molecule at R=3.015 a_0.

Method	E	Reference
CI [$9s8p6d1f$] basis set	−8.069 336	(Bendazzoli and Monari, 2004)
GFMC	−8.070 21(5)	(Chen and Anderson, 1995)
DMC	−8.070 1(4)	(Ospadov *et al.*, 2011)
CCSD[T]-R12 Coupled-cluster method with linear r_{12} terms.	−8.070 491	(Noga *et al.*, 1995)
Iterative-Complement-Interaction.	−8.070 516	(Nakatsuji *et al.*, 2007)
ECG, 200 terms	−8.069 221	(Cencek and Rychlewski, 1993)
ECG, 2400 terms	−8.070 538	(Cencek and Rychlewski, 2000)
ECG, 2400 terms	−8.070 547 3	(Tung *et al.*, 2011)
ECG, extrapolated	−8.070 553(5)	(Cencek and Rychlewski, 2000)

and Rychlewski, 1993; Pavanello *et al.*, 2009), H_4 (Patkowski *et al.*, 2008; Tung *et al.*, 2010), and H_5^+ (Müller and Kutzelnigg, 2000). These calculations invariably yielded variational energies lower than those obtained by other methods.

Table XI gives a comparison of ECG energies with the best results from other methods for the LiH molecule. Table XI shows that only ECG based approaches have achieved μhartree-level accuracy for this system. There have been some some very large CI calculations of LiH reported recently (Gadéa and Leininger, 2006; Holka *et al.*, 2011). However, these calculations only give vibrational energies so direct comparison with ECG potential energies is not possible. The two independent ECG calculations (Cencek and Rychlewski, 2000; Tung *et al.*, 2011) give energies that agree to within 10 μhartree. Both of the ECG energies are more than 20 μhartree lower than the energy from the iterative complement interaction approach (Nakatsuji *et al.*, 2007). An estimate of the variational limit has been made from a series of ECG calculations (Cencek and Szalewicz, 2008) and it is 8 μhartree lower than the best explicit calculation (Tung *et al.*, 2011). Comparisons with the best ECG energies of the four-electron Be atom suggest it is likely that explicit ECG calculations could give explicit energies converged to better than 1 μhartree.

The two-electron three-center H_3^+ molecular ion is a system particularly suitable for ECG applications. The H_3^+ ion has been the subject of numerous *ab initio* calculations (Kutzelnigg and Jaquet, 2006), but had eluded the efforts to achieve spectroscopic accuracy until 1998, when a potential energy surface (PES) based on roughly optimized 1300-term ECG expansions was obtained (Cencek *et al.*, 1998). The wave functions were used to evaluate the lowest-order relativistic corrections and the diagonal adiabatic (post-BO) corrections.

In a follow-up paper (Jaquet *et al.*, 1998), the total energies were fitted to a functional form and used to calculate the rovibrational frequencies in H_3^+ and D_3^+, resulting in a close agreement with experiment (on average, about 0.3 and 0.1 cm^{-1}, respectively). This PES has remained the basis for most *ab initio* investigations of the low-energy (up to about 10000 cm^{-1}) spectrum of H_3^+ for over 10 years and was recently extended (Bachorz *et al.*, 2009). In 2009, a new nonrelativistic BO PES in the low-energy region was published (Pavanello *et al.*, 2009). The authors used only a 900-term ECG expansion, but performed a very thorough parameter optimization which resulted in energies 0.01 to 0.02 cm^{-1} lower than those in the 1998 PES.

The helium dimer plays an important role in many areas of physics, including establishing new standards of temperature and pressure (Fischer and Fellmuth, 2005; Mehl, 2009; Pitre *et al.*, 2006). The best current BO potential (Jeziorska *et al.*, 2007) is based on coupled-cluster GTG and SAPT GTG calculations (see Sect. V.A). However, the most accurate value of the interaction energy at the potential minimum (R=5.6 a_0) was obtained using the direct variational optimization of the full four-electron ECG function (Cencek and Szalewicz, 2008). For He_2, the linear combination of ECGs is supplemented by an additional contraction term leading to the following expansion

$$\Psi = c_0\phi_0 + \sum_{k=1}^{K} c_k\phi_k(1,2,\ldots N) \ . \tag{106}$$

The term ϕ_0 in Eq. (106) is a linear combination of ECGs that are designed to represent two non-interacting helium atoms separated by a distance of $R = 5.6\ a_0$. The helium atom basis consisted of 337 terms and had an energy of $-2.903\,724\,377\,002$ hartree. With ϕ_0, the whole optimization effort could then be directed towards the interaction energy, which in this case constitutes only 0.0006% of the total energy of the dimer. Since the inclusion of ϕ_0 is computationally expensive, it is advisable to use a moderate size monomer contraction in the optimization and replace it with a more accurate one for the final energy evaluation. It is also possible to obtain ϕ_0 by a separate optimization of a four-electron ECG expansion. In this approach, one minimizes the expectation value of the four-electron Hamiltonian with the intermonomer terms switched off (Patkowski *et al.*, 2008). This leads to much shorter ϕ_0 expansions (compared to monomer products) without any loss of accuracy.

Table X presents the interaction energies obtained both without and with the use of the monomer contraction method. The inclusion of ϕ_0 results in a dramatic improvement of

the accuracy and the extrapolated value, −11.0006(2) mK, has 15 times smaller uncertainty than the next best literature result, where the dominant contributions were also obtained using ECG functions.

Both for metrological purposes and for the investigation of the sole vibrational state of He_2, it is of critical importance to account for post-BO contributions to the interaction energy. The adiabatic corrections, the lowest-order relativistic contributions (of the order α^2), and the QED contributions (of the order α^3) were recently evaluated for a broad range of intermonomer distances (Przybytek *et al.*, 2010). The nonrelativistic ECG wave functions with up to K=2400 terms (and orbital CCSD(T)/CI wave functions at large distances) were used to calculate the appropriate expectation values. The total energies [including the BO potential of Ref. (Jeziorska *et al.*, 2007)] were fitted to an asymptotically correct functional form and an appropriate component of the Casimir-Polder potential was added to account for the long-range retardation damping. The resulting dissociation energy and average separation of the helium dimer are 1.62±0.03 mK and 47.1±0.5 Å, respectively. The latter value has an order of magnitude tighter error bar than the current best experimental result (Grisenti *et al.*, 2000) of 52 ± 4 Å.

Apart from the interaction potential, the proposed helium based temperature and pressure standards assume accurate knowledge of the helium atom polarizability and helium dimer collision-induced polarizabilities. The critical components of the former were discussed in Section IV.C. The benchmark values of the latter were recently obtained using four-electron ECG expansions (Cencek *et al.*, 2011).

1. Relativistic and QED corrections for light molecules

One of the most spectacular applications of ECG functions is in predicting energy levels of light molecules to an accuracy competitive with the experiment. The precision of the measurements has reached the level at which not only nonadiabatic and relativistic but also QED effects become important (Salumbides *et al.*, 2011). This challenge has been taken up by ECG calculations on the hydrogen molecule and its isotopomers in the framework of the relativistic and QED theory described in Sec. II.F, II.G, and III.C. At the present time the current best theoretical value of $D_0 = 36\,118.0695(10)$ cm^{-1} (Piszczatowski *et al.*, 2009) of the H_2 molecule dissociation energy was obtained with a basis that used a GJC potential

TABLE XII Comparison between the measured (Druin, 2010; Liu *et al.*, 2009, 2010; Salumbides *et al.*, 2011; Sprecher *et al.*, 2010) and theoretically predicted (Komasa *et al.*, 2011; Pachucki and Komasa, 2010; Piszczatowski *et al.*, 2009) dissociation energy D_0 and the lowest rotational energy spacing ($J = 1 \leftarrow 0$) for H_2 and its isotopomers (all entries in cm^{-1}).

	H_2	HD	D_2
		D_0/cm^{-1}	
Exp.	36 118.069 62(4)	36 405.783 66(4)	36 748.362 86(7)
Theo.	36 118.069 6(11)	36 405.782 8(10)	36 748.363 4(9)
Diff.	0.000 0(12)	0.000 9(11)	0.000 5(11)
		$J = 1 \leftarrow 0/cm^{-1}$	
Exp.	118.486 84(10)	89.227 932 6(3)	59.781 30(95)
Theo.	118.486 812(9)	89.227 933(8)	59.780 615(3)
Diff.	0.000 03(10)	0.000 000(8)	0.000 68(95)

curve for $R \leq 6.0\ a_0$ and a ECG potential curve for $R > 6.0\ a_0$.

The very good agreement between the measured and calculated values of the dissociation energy D_0 and lowest rotational energy spacing ($J = 1 \leftarrow 0$) is illustrated by the sample data in Table XII. The accuracy of both the experiment and theory is sufficiently high to enable extraction of the QED contribution from the measurements (Komasa *et al.*, 2011). Dissociation energy of all the bound levels as well as the allowed transition intensities have been computed, leading to a purely theoretical absorption spectrum of Fig. 6. The accuracy of such a model spectrum for HD has been assessed by Campargue (Kassi and Campargue, 2011) on the basis of the first overtone band (2-0): the average line position deviation is $1.1(8.7) \times 10^{-4}$ cm^{-1} and the line intensity deviation is about 1%. It has been recommended that the calculated ro-vibrational spectrum can be used as reference frequencies with uncertainties that range from 0.001 cm^{-1} in the near infrared to 0.005 cm^{-1} at 35000 cm^{-1} (Campargue *et al.*, 2011).

ECG wave functions were also employed to evaluate a state-of-the-art interaction potential for helium dimer (Przybytek *et al.*, 2010). This potential included relativistic, QED,

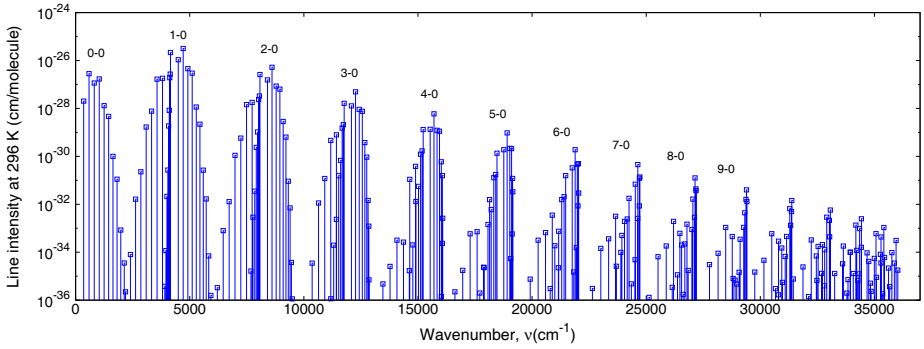

FIG. 6 (Color online) Theoretical rovibrational absorption spectrum of the ground electronic ($X\,^1\Sigma_g^+$) state of H_2 obtained in the framework of QED. The notation v-0 stands for a band of transitions from the $(0, J)$ states to states $(v, J \pm 2)$. The estimated accuracy of the line positions is of the order of 0.001 cm^{-1}, whereas the line intensities are accurate to about 0.1% (Campargue *et al.*, 2011).

and retardation correction, which has already been described in Sec. V.B.

C. Going beyond the Born-Oppenheimer approximation

Recently it became possible to perform *ab-initio* calculations for small molecular systems without making the BO approximation (Kinghorn and Adamowicz, 1999). Both the nuclear and electronic motion are treated on an equal footing. The large nuclear mass of the nucleus makes the nuclear–nuclear interaction strongly repulsive and very difficult to describe with a basis set expansion. As discussed in Subsec. III.D the use of ECGs with r^{2m} prefactors solves this problem.

Calculations without the BO approximation can provide an independent test of the validity of the more usual BO calculations. One regime where one can expect the BO approximation perturbative treatments to be unreliable occurs when the energy spacings between the rovibrational energy levels are comparable to the electronic energy spacings. Another possible regime would be when the energy shifts arising from different nuclear isotopes are comparable to the rovibrational binding energies.

HD^+ and other heteronuclear isotopologues of H_2^+ represent a simple system that, due to the difference in nuclear masses, lacks the center of symmetry. For highly excited vibrational

TABLE XIII Expectation values showing charge asymmetry in highly excited (near the dissociation threshold) rovibrational states of HD^+ vs the ground state ($v = 0$) and a moderately excited state ($v = 10$) (Bubin *et al.*, 2005b). All values are in atomic units.

v	$\langle r_{d-p} \rangle$	$\langle r_{d-e} \rangle$	$\langle r_{p-e} \rangle$	$\left\langle r_{d-p}^2 \right\rangle$	$\langle r_{d-e}^2 \rangle$	$\langle r_{p-e}^2 \rangle$
0	2.055	1.688	1.688	4.268	3.534	3.537
10	3.489	2.445	2.448	13.48	8.250	8.272
21	12.95	2.306	12.19	176.0	12.94	168.2
22	28.62	1.600	28.55	910.0	4.266	911.4
D atom		1.500			3.002	

states that lie close to the dissociation threshold, the electron can be found near the deuteron with noticeably higher probability than near the proton. The D+p^+ configuration is energetically preferred over the H+d^+ configuration, since deuterium's ground state energy is slightly lower than that of the hydrogen. To adequately describe the charge asymmetry in those states near the dissociation threshold, an approach that treats all particles on equal footing is needed.

The asymmetry of the HD^+ wave function has been investigated experimentally (Ben-Itzhak *et al.*, 2000; Carrington *et al.*, 1991). In particular, Ben-Itzhak *et al.* studied the dissociation of the electronic ground state following ionization by fast proton impact and found the H^++D($1s$) dissociation channel is more likely than the H($1s$)+D^+ dissociation channel by about 7%. This asymmetry breakdown was attributed to the finite nuclear mass correction to the BO approximation, which makes the $1s\sigma$ state 3.7 meV lower than the $2p\sigma$ state at the dissociation limit.

In Table XIII a catastrophic breakdown of the BO approximation is seen to occur above the $v = 20$ vibrational level. The calculations were performed with ECGs and up to 4000 basis functions were used (Bubin *et al.*, 2005b). As shown, in the ground vibrational state ($v = 0$) and a moderately excited state ($v = 10$) there is practically no charge asymmetry present. For the highest two states with zero total angular momentum ($v = 21, 22$), the electron is essentially localized around the deuteron.

Similar to the case of atomic calculations and molecular BO calculations, a major advantage of the ECG method in the non-BO case is the possibility to perform accurate

TABLE XIV Total non-BO ground state energies (in hartree) of some small diatomic molecules. In parentheses we show the estimated difference between the variational upper bound and the exact nonrelativistic energy.

System	Basis size	Energy	Reference
H_2	10 000	−1.164 025 030 84(21)	(Bubin *et al.*, 2009b)
HD	10 000	−1.165 471 922 0(20)	(Bubin *et al.*, 2011b)
HeH^+	8 000	−2.971 078 465 9(5)	(Stanke *et al.*, 2008)
LiH	7 200	−8.066 437 1(15)	(Bubin *et al.*, 2005a)
LiH^-	3 600	−8.067 382 5(50)	(Bubin and Adamowicz, 2004)
BeH	4 000	−15.242 03(10)	(Bubin and Adamowicz, 2007)
BH	2 000	−25.287 4(10)	(Bubin *et al.*, 2009c)

calculations of systems containing more than just two electrons. Table XIV lists the energies of several diatomic molecules and molecular ions computed without assuming the Born–Oppenheimer approximation. The largest molecule in the table, boron hydride, is an 8-body system (two nuclei and six electrons). While the size of the basis and the accuracy for such relatively large systems are currently limited by available computational resources, the results can be easily improved when more powerful hardware becomes available.

Results obtained with the variational non-BO approach can be compared directly with those calculated within the BO approximation with the finite nuclear mass effects determined perturbatively by means of the methodology described in Sec. II.G. Inspection of Table XV, which contains such a comparison for a dissociation energy of molecular hydrogen and its isotopomers, allows a conclusion that at present stage of the accuracy both ECG methods yield equivalent results.

Nonrelativistic non-BO calculations calculations can be complemented with evaluation of relativistic corrections (Stanke *et al.*, 2006) as demonstrated in Table XVI for some three electron systems. The theoretical $v = 0 \rightarrow 1$ transition energy for $^3He^4He^+$ agrees with experiment when the theoretical and experimental uncertainties are taken into consideration. Table XVI also shows that the relativistic corrections tend to cancel for the $v = 0$ and $v = 1$ vibrational states.

TABLE XV An equivalence of the nonrelativistic dissociation energy D_0 obtained from the non-BO approach (Bubin *et al.*, 2009b, 2011a; Stanke *et al.*, 2009a) and the results based on the BO approximation augmented by perturbative treatment of the finite nuclear mass effects (Pachucki and Komasa, 2009, 2010; Piszczatowski *et al.*, 2009).

	D_0/cm^{-1}		
	H_2	HD	D_2
BO	36 118.7978(2)	36 406.5108(2)	36 749.0910(2)
non-BO	36 118.79774(1)	36 406.5105(4)	36 749.0910(0)
Diff.	0.00006(20)	0.0003(4)	0.0000(2)

TABLE XVI Nonrelativistic and relativistically corrected non-BO energies and transition frequencies for the lowest vibrational states of three-electron molecular ions: $^3\mathrm{He}^4\mathrm{He}^+$ and LiH^+ (Bubin *et al.*, 2010c, 2011c; Stanke *et al.*, 2007).

System	State/Transition	Nonrelativistic	Relativistic	Experiment
$^3\mathrm{He}^4\mathrm{He}^+$	$v=0$ (hartree)	−4.989719657(30)	−4.989926676(30)	
	$v=1$ (hartree)	−4.981743256(80)	−4.981950301(80)	
	$1\rightarrow 0$ (cm^{-1})	1750.618(60)	1750.612(60)	1750.55687(98)
LiH^+	$v=0$ (hartree)	−7.783247013(40)	−7.783882745(40)	
	$v=1$ (hartree)	−7.781629462(500)	−7.782265092(500)	
	$1\rightarrow 0$ (cm^{-1})	355.011(50)	355.034(50)	

D. Outlook

The last decade has seen two different strands of calculations on small molecules, conventional calculations within the BO approximations, and completely *ab-initio* calculations where all particles are free to move. These non-BO calculations provide a superb tool for testing the validity of the BO method at levels of precision comparable to the best experiment. However, it is doubtful whether the non-BO calculations will become more widespread. For example, all the calculations that have so far been carried out have been done for the rotational ground state.

1. Contractions of ECGs

The best description so far of the He_2 molecule potential curve resorted to a basis function consisting of a linear combination of ECGs. Similar composite basis functions made up of linear combinations of ordinary gaussians have had a long history in quantum chemistry where they are called contracted gaussians. Sets of contracted ECGs can be very usefully employed to describe systems which contain clearly delineated fragments.

VI. APPLICATION TO NUCLEAR STRUCTURE CALCULATIONS

A. Nuclear Hamiltonian and wave function

The solution of the nuclear few-body problem is crucial to generating a complete description of the nucleon-nucleon interaction. The nucleon-nucleon (NN) interaction is not a fundamental interaction but is a consequence of Quantum Chromodynamics (QCD). At present, our knowledge of the short-range behaviour of the (NN) interaction could be improved. In addition, the (NN) interaction also contains three-body and four-body terms that could be better characterized. Consequently, it is not guaranteed that high accuracy calculations of the binding energies of light nuclei will agree precisely with experiment. There are even larger uncertainties in defining the hyperon-nucleon interactions. High accuracy calculations of light nuclei which are close to convergence can be compared with experiment and consequently constitue a bridge to refine existing NN interactions.

The accuracy of ECG calculations in nuclear structure physics is remarkable when the complexity of the nuclear interaction is considered. In nuclear physics the Hamiltonian includes the kinetic energy, K_i, hard core and non-central two-nucleon NN potentials, v_{ij}, as well as three-nucleon interactions, v_{ijk}:

$$H = \sum_i K_i + \sum_{i<j} v_{ij} + \sum_{i<j<k} v_{ijk} \ . \tag{107}$$

Various phenomenological or field theory motivated (NN) potentials have been proposed (Epelbaum *et al.*, 2009). The most widely used and tested NN potential is the AV18 potential (Wiringa *et al.*, 1995). The AV18 is one of a class of highly accurate NN potentials that fit both pp and np scattering data up to 350 MeV with a χ^2/datum ≈ 1. In the calculations presented in this section the AV8′ NN potential (Pudliner *et al.*, 1997) was

used, which is a simplified, re-projected version of the fully realistic AV18 model, but still has most of its complexity, e.g., the tensor force is built in. The AV8′ potential consists of 8 parts:

$$\begin{aligned} v(r) &= V_c(r) + V_\tau(r)(\tau\cdot\tau) + V_\sigma(r)(\sigma\cdot\sigma) \\ &\quad + V_{\sigma\tau}(r)(\sigma\cdot\sigma)(\tau\cdot\tau) + V_t(r)S_{12} + V_{t\tau}(r)S_{12}\ (\tau\cdot\tau) \\ &\quad + V_b(r)(L\cdot S) + V_{b\tau}(r)(L\cdot S)\ (\tau\cdot\tau) \\ &= \sum_{i=1}^{8} V_i(r)\mathcal{O}_i, \end{aligned} \tag{108}$$

where $(\sigma\cdot\sigma)$, $(\tau\cdot\tau)$, S_{12} and $(L\cdot S)$ stand for spin-spin, isospin-isospin, tensor, and spin-orbit interactions (Wiringa *et al.*, 1995), respectively, $V_i(r)$ are radial functions of Yukawa- and Wood-Saxon types, and

$$S_{12} = \sqrt{24\pi}[Y_2(\widehat{\boldsymbol{r}_1-\boldsymbol{r}_2})\times[\boldsymbol{\sigma}_1\times\boldsymbol{\sigma}_2]_2]_{00}. \tag{109}$$

A phenomenological interaction that reproduces the ground state energies of ^{3}H and ^{4}He was used as a three-nucleon potential (3NF) (Hiyama *et al.*, 2004).

A total wave function with the isospin TM_T is expressed in an LS-coupled scheme as

$$\Psi^\pi_{JM_JTM_T} = \sum_{iLS} C^i_{LS}\Psi^\pi_{i(LS)JM_JTM_T}, \tag{110}$$

where the basis function is defined as

$$\Psi^\pi_{i(LS)JM_JTM_T} = \mathcal{A}\left\{\left[\theta^i_L(\hat{\mathbf{x}})\xi^i_S\right]_{JM}\xi^i_{TM_T}\exp\left(-\mathbf{x}A_i\mathbf{x}\right)\right\}, \tag{111}$$

where $\mathcal{A}$ is the antisymmetrizer, $\mathbf{x}$ stands for a set of $N-1$ intrinsic coordinates $(\mathbf{x}_1,\mathbf{x}_2,\ldots,\mathbf{x}_{N-1})$ and $\xi^i_{SM_S}$ $(\xi^i_{TM_T})$ is the spin (isospin) function of the N-particle system. The non-spherical (orbital) part, $\theta^i_L(\hat{\mathbf{x}})$, of the trial function is represented either by a successively coupled product of spherical harmonics or by the global vector representation (see Sec. II.D.2). Equally good results have been obtained in both representations (Suzuki *et al.*, 2008).

B. Alpha particle

The nuclear structure calculation will be exemplified by a complex four fermion system, ^{4}He. Accurate calculations for the ground state of ^{4}He, the alpha particle, were performed

TABLE XVII Comparison of the binding energies E_b (in MeV) and the root-mean-square radius (in fm) of the alpha particle calculated by different methods (Kamada *et al.*, 2001). The Coulomb and 3N interactions were turned off.

Method	Reference	E_b	$\sqrt{\langle r^2 \rangle}$
FY	(Glöckle and Kamada, 1993)	−25.94(5)	1.485
GEM	(Kamimura, 1988)	−25.90	1.482
SVM		−25.92	1.486
HH	(Viviani *et al.*, 1995)	−25.90(1)	1.483
GFMC	(Wiringa *et al.*, 2000)	−25.93(2)	1.490
NCSM	(Navrátil and Barrett, 1999)	−25.80(20)	1.485
EIHH	(Barnea *et al.*, 2000)	−25.944(10)	1.486

with various sophisticated methods (Kamada *et al.*, 2001) including the SVM. Table XVII compares the binding energy and radius of the alpha particle calculated by different methods.

^{4}He has many excited (resonance) states, and some of them have the same spin and parity. The width of some of these states is relatively small and in the calculation they are treated as bound states. The wave functions of states with identical spin and parity are optimized simultaneously by SVM. Fig. 7 compares the calculated energy spectrum with experiment (Horiuchi and Suzuki, 2008) (note, the original calculation in (Horiuchi and Suzuki, 2008) did not include a three-body force). The SVM calculation reproduces a sequence of all the excited levels.

Besides the energy, other properties can also be accurately calculated by ECGs. One example is the coordinate-space correlation function

$$C(r) = \frac{1}{4\pi r^2} \frac{1}{2J+1} \sum_M \langle \Psi^\pi_{JM} | \delta(|\boldsymbol{r}_1 - \boldsymbol{r}_2| - r) | \Psi^\pi_{JM} \rangle, \tag{112}$$

which describes the short-range behavior of the NN relative motion. As displayed in Fig. 8, the $C(r)$ calculated for ^{2}H, ^{3}H, and ^{4}He indeed show near vanishing amplitudes at short distances. The function $C(r)$ does not incorporate the $4\pi r^2$ volume element so the small amplitude as $r \to 0$ is a manifestation of the strong repulsion found in the NN interaction at short-range. This can be accommodated to some extent by the SVM since ECGs explicitly include inter-particle distances.

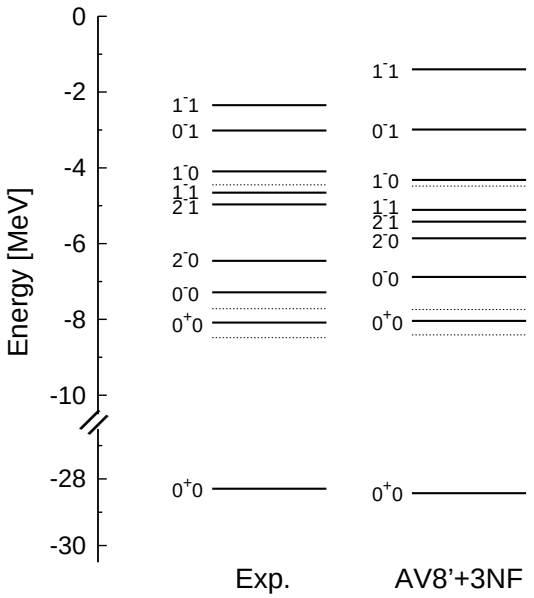

FIG. 7 Energy levels of ^{4}He labeled with $J^\pi T$. Dotted lines indicate the thresholds of ^{3}H+p, ^{3}He+n, and d+d from below. The energy is given from the p+p+n+n threshold and the figure is based on Fig. 2 from (Horiuchi and Suzuki, 2008).

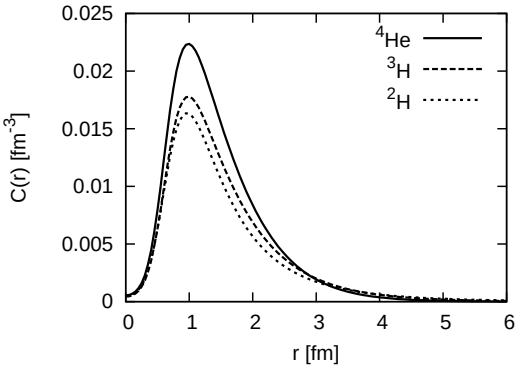

FIG. 8 Coordinate-space correlation functions for the ground states of ^{2}H, ^{3}H and ^{4}He calculated with the AV8′ potential (Pudliner *et al.*, 1997).

The peak position of $C(r)$ is about 1 fm, independent of the system. In fact, the $C(r)$ functions for $r \leq 1$ fm are found to show universal behavior (Feldmeier *et al.*, 2011; Forest *et al.*, 1996). The significance of various correlation functions for the operators $\mathcal{O}_i$ as well as the momentum-space correlation function is discussed in (Suzuki and Horiuchi, 2009).

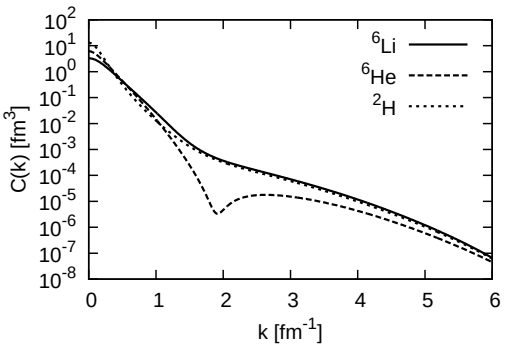

FIG. 9 Momentum distributions of the relative motion between the valence nucleons in ^{6}He and ^{6}Li. The momentum distribution of d is also shown.

C. Application to multi-cluster systems

Extensive applications of the ECG+SVM approach to light nuclei including halo nuclei started in the 1990s (Arai *et al.*, 2001; Suzuki *et al.*, 2003). The first careful test of SVM was actually performed in a microscopic $\alpha(^4\mathrm{He})+n+n$ three-cluster model for a two-neutron halo nucleus ^{6}He (Varga *et al.*, 1994). Here the cluster indicates a subsystem in nuclei, that is, ^{6}He is considered to be composed of α and two neutrons. Though the cluster model is useful and physically sound for extending a few-body approach to light nuclei, a fully microscopic cluster-model calculation that takes into account the correlations among the particles accurately is fairly involved because of the antisymmetry requirement on the wave function of the system. A simpler macroscopic version has often been employed by treating the cluster as a structureless particle but instead by considering the Pauli principle into account through the elimination of particular states. Such an $\alpha+N+N$ model has in fact been carefully worked out for ^{6}He and ^{6}Li to describe the correlated motion of the two nucleons outside the α core (Baye *et al.*, 2009; Horiuchi and Suzuki, 2007). The α-N interaction is phenomenological in nature and constructed to fit to low energy N-α scattering data (Kanada *et al.*, 1979). This potential supported a low lying s-wave bound state, which was eliminated by the inclusion of an OPP potential. Fig. 9 compares the momentum distribution of the two-nucleon relative motion, a momentum-space analog of $C(r)$. The distribution of ^{6}Li is similar to that of d reflecting the effect of the tensor force, while the two neutrons in ^{6}He exhibit quite a different pattern due to the dominant s-wave motion.

A macroscopic $^{20}\mathrm{C}+n+n$ model has been applied to look into two-neutron halo structure

in ^{22}C (Horiuchi and Suzuki, 2006). The size of this fragile nucleus is predicted to be as large as that of a nucleus with mass number 60. The information on the structure of unstable nuclei is obtained through the analysis of interaction and breakup cross sections (Suzuki *et al.*, 2003).

It should be noted that a subtle and intricate problem appears in different versions of the cluster model calculation. This problem is explained in a 3α model for ^{12}C. The soundness of this model is confirmed in a fermionic molecular dynamics calculation (Chernykh *et al.*, 2007) that does not assume the existence of α clusters *a priori*. The first excited 0^+ state at the excitation energy of 7.65 MeV, called the Hoyle state, plays a significant role in producing ^{12}C element in a star through triple-α reactions. It is well-known that both the ground and first excited 0^+ states of ^{12}C are well reproduced by a microscopic 3α calculation (Kamimura, 1981; Matsumura and Suzuki, 2004). However, an unexpected thing happens in macroscopic model calculations (Suzuki *et al.*, 2007). Even a local α-α potential, that reproduces the phase shifts and produces no bound states consistently with experiment, leads to a ground state energy of the 3α system that is far above the experimental value (Suzuki *et al.*, 2008), as seen from the result with the ABd potential of Table XVIII. In contrast to this model one often uses a deep α-α potential and excludes some bound states as Pauli-forbidden states. The results of this model denoted as BFW in Table XVIII depend on the definition of the forbidden states. When they are chosen to be harmonic-oscillator states based on the nuclear shell model, the ground state turns out to be deeply bound and the first excited state appears slightly below the 3α threshold. If the forbidden states are chosen to be bound states of the BFW potential, the result is quite different from the harmonic-oscillator case but is similar to the ABd case. This enigmatic result has been resolved by analyzing the Pauli-forbidden states carefully (Matsumura *et al.*, 2006). Semi-microscopic calculation in the table uses a nonlocal α-α potential $V^{\rm RGM}$ derived from a microscopic 2α calculation (Suzuki *et al.*, 2008), and reproduces both the ground and first excited 0^+ states reasonably well. The usefulness of this type of nonlocal potential is confirmed in other multi-cluster systems as well (Theeten *et al.*, 2007). The accuracy of the ECG calculation for this nonlocal potential has been tested by comparing to the result of the HH method (Suzuki *et al.*, 2008).

The GEM has also been applied to the study of hypernuclei which consist of one hyperon (e.g. a Λ particle) in addition to the nucleons. For example it has been applied to determine the energy levels of ${}^{7}_{\Lambda\Lambda}$He, ${}^{7}_{\Lambda\Lambda}$Li, ${}^{8}_{\Lambda\Lambda}$Li, ${}^{9}_{\Lambda\Lambda}$Li, ${}^{9}_{\Lambda\Lambda}$Be, and ${}^{10}_{\Lambda\Lambda}$Be in a four-body α+x+Λ+Λ

TABLE XVIII The energy E (MeV) from the 3α threshold and the root-mean-square radius $\sqrt{\langle r^2 \rangle}$ (fm) of the point α particle distribution for the ground state and the first excited 0^+ state of the 3α system calculated with different models and potentials. The results with BFW depend on the definition of the Pauli-forbidden states: (i) Harmonic-oscillator states, (ii) Bound states of the BFW potential. Experimental energies are -7.27 and 0.38 MeV for the 0^+_1 and 0^+_2 states, respectively.

Potential	J^π	E	$\sqrt{\langle r^2 \rangle}$
ABd (Ali, 1966)	0^+_1	-1.52	2.34
BFW (Buck *et al.*, 1977)(i)	0^+_1	-20.62	1.29
	0^+_2	-1.25	2.34
(ii)	0^+_1	-0.66	2.31
$V^{\rm RGM}$	0^+_1	-9.44	1.62
	0^+_2	0.597	–

cluster model (Hiyama *et al.*, 2002). Most recently a five-body model was applied to ${}^{11}_{\Lambda\Lambda}$Be (Hiyama *et al.*, 2010). The ${}^{10}_{\Lambda\Lambda}$Be calculations predicted binding energies of 11.88 MeV for a $J^P = 2^+$ state and 14.74 MeV for a $J^P = 0^+$ state. The Demachi-Yanagi event, which was identified as ${}^{10}_{\Lambda\Lambda}$Be with a binding energy of 11.90±0.13 MeV (Ahn, 2001; Ichikawa, 2001), was interpreted as an observation of the 2^+ state but the angular momentum parity cannot be definitely determined from the experimental data.

D. Baryon spectroscopy

The ECG basis, due to its accuracy, is also a useful tool in baryon spectroscopy. In a seminal work proposing a chiral constituent quark model the ECG with SVM has been used to predict the correct level ordering of low lying baryons (Glozman *et al.*, 1998) (see Fig. 10). ECGs have also been employed in semirelativistic potential models for three-gluon glueballs (Mathieu *et al.*, 2008) and to calculate the mass of a charmonium hybrid meson with a magnetic gluon (Mathieu, 2009). There are calculations going beyond the three-body problems as well. Pentaquark states in a full five-body model are explored (Hiyama *et al.*, 2006; Matsumura and Suzuki, 2006; Nemura and Nakamoto, 2007).

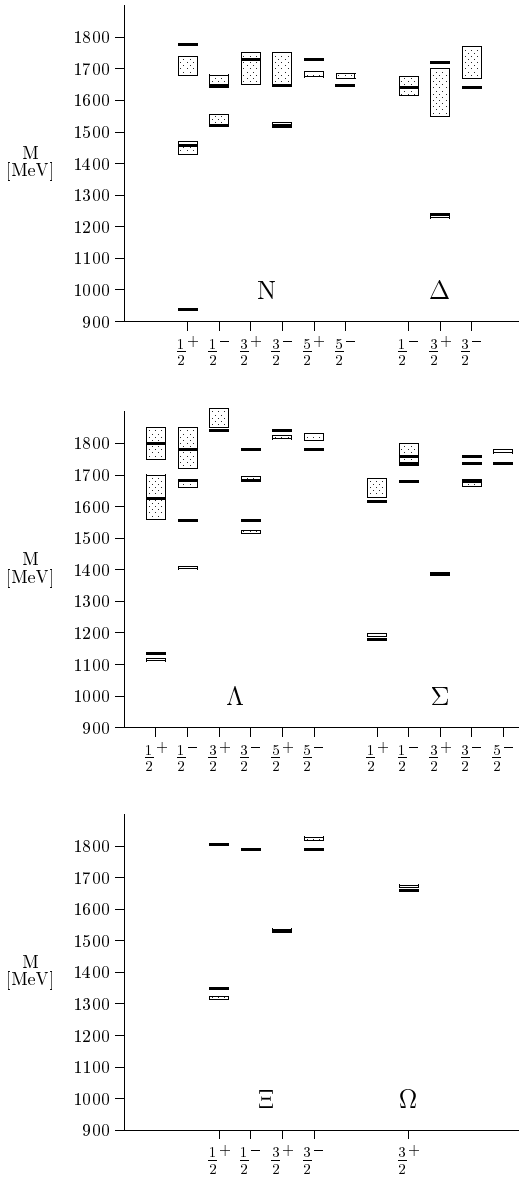

FIG. 10 Energy levels of the lowest light- and strange-baryon states with total angular momentum and parity J^P. The nucleon ground state is 939 MeV. The shadowed boxes represent the experimental values with their uncertainties. The Δ, Σ^*, and Ξ^* ground-state levels practically fall into their rather tight experimental boxes.

E. Outlook

One of the major features of light nucleii is the tendency for the neutrons and protons to colaesce into ^{4}He clusters. It is relatively easy for ECG basis sets to represent wave functions with cluster components. So *ab-intio* descriptions of systems such as ^{6}Li (= ^{4}He+n+p) or the He halo nucleii should not pose insuperable computational difficulties. It is somewhat

surprising that the SVM has not already been applied to nucleii with $5 < A < 8$. One inhibiting factor is the complexity of the (NN) interaction which slows down the formation of the Hamiltonian matrix and the opimization process itself.

VII. FEW-BODY SYSTEMS IN CONDENSED MATTER

The main applications of ECGs in condensed matter systems has been to fermionic systems such as excitonic complexes and quantum dots.

A. Excitonic complexes

Electrons and holes in semiconductors can combine to form hydrogen-like bound states called excitons. These excitons can also form hydrogen molecule like bound states with each other, or charged excitons by binding electrons or holes.

The constituents of these systems are electrons and holes with effective masses m_e^* and m_h^* interacting via the Coulomb potential. The properties of the systems strongly depend on the mass ratio $\sigma = m_e^*/m_h^*$. Previous calculations of the binding energy of biexcitons include Quantum Monte Carlo (Bressanini *et al.*, 1998; Lee *et al.*, 2009), boson representation (Okumura and Ogawa, 2001), and variational (Kleinman, 1983; Riva *et al.*, 2002; Usukura *et al.*, 1999) approaches.

The binding energies in two and three dimensional excitonic complexes have been studied using SVM in Ref. (Usukura *et al.*, 1999). The results of these calculations for the energies $E(\sigma)$ and at the two limiting cases ($\sigma = 0$ and $\sigma = 1$) are collected in Table XIX for 2D and 3D systems. The energies are in perfect agreement with other theoretical results in 3D for H_2^+, H^-, H_2 ($\sigma = 0$) and Ps^-, Ps_2 ($\sigma = 1$). In both 2D and 3D cases the charged excitons, *eeh* and *ehh* and the biexciton *eehh* are bound for any mass ratio. The *eeehh* complex is not bound for any σ while *eehhh*, a semiconductor analog of H_3^+, is bound for small σ values. The behavior of the energies as a function of σ is quite similar in 2D and 3D except that the energies are much larger in 2D due to the reduced dimensionality.

Fig. 11 displays the Haynes factor $f_H = B_{X_2}/B_X$, where B_X and B_{X_2} are the binding energies of the exciton and the biexciton, respectively. The SVM values for f_H are significantly larger than those of a variational calculation using exponential basis functions (Kleinman,

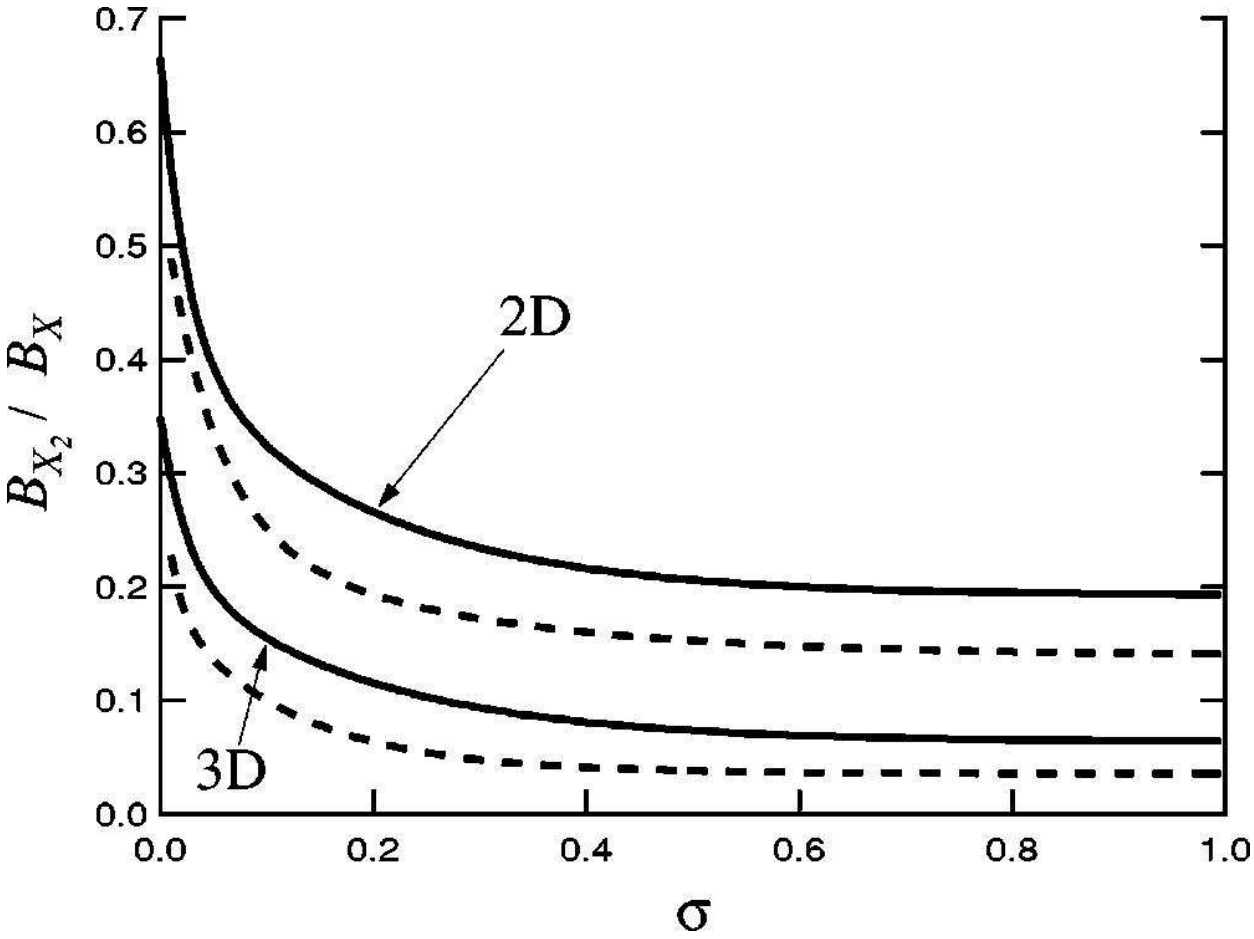

FIG. 11 The SVM binding energy of the biexciton X_2 (eehh) compared to the binding energy of the exciton X as a function of the mass ratio σ. The dashed curves show the result of an earlier variational calculation (Kleinman, 1983).

1983). The Haynes factor predicted in the SVM 2D calculation is 0.20 at $\sigma = 0.68$ GaAs, which is in good agreement with the experimental value f_H=0.2 (Birkedal *et al.*, 1996).

B. 2D and 3D quantum dots and quantum wells

Quantum dots (Fasth *et al.*, 2007; Hanson *et al.*, 2007; Kouwenhoven *et al.*, 2001; Zumbühl *et al.*, 2004) are small man-made structures in a solid, typically with the size ranging from nanometers to a few microns. In semiconductors all electrons are tightly bound to the nuclei except for a small fraction of free electrons. This small number can be anything from a single, free electron to a puddle of several thousands. Current nanofabrication technology allows for precise control over the size and shape of these dots. The electronic properties of dots

TABLE XIX SVM energies of 2D and 3D excitonic complexes in hartree (Usukura *et al.*, 1999).

System	2D		3D	
	$E(\sigma=0)$	$E(\sigma=1)$	$E(\sigma=0)$	$E(\sigma=1)$
eh	-2.000	-1.000	-0.500	-0.250
eeh	-2.240	-1.121	-0.527	-0.262
ehh	-2.818	-1.121	-0.602	-0.262
$eehh$	-5.33	-4.385	-1.174	-0.516
$eeehh$	unbound	unbound	unbound	unbound
$eehhh$	-6.82	unbound	-1.343	unbound

TABLE XX SVM energies of a three-electron system. The electrons are harmonically confined in 2D, the oscillator parameter is $\omega = 0.2841$ H* (in atomic units which corresponds to $\hbar\omega = 3.37$ meV (Varga *et al.*, 2001)). All values are in meV except those in square brackets, which are in effective hartree (1.0 H* = 11.86 meV for the GaAs system). Results from the "exact" diagonalization, DIAG (Hawrylak and Pfannkuche, 1993) and three DMC calculations, DMC1 (Bolton, 1996), DMC2 (Pederiva *et al.*, 2000), and DMC3 (Harju *et al.*, 1999) are shown for comparison.

(M,S)	SVM	DIAG	DMC1	DMC2	DMC3
(1,1/2)	26.7827 [2.2582]	26.82	26.77	26.8214(36)	26.88
(2,1/2)	28.2443 [2.3814]	28.27	28.30		28.35
(3,3/2)	30.0101 [2.5304]	30.02	30.04		30.03

show many parallels with those of atoms. Most notably, the localization of the electrons in all three spatial directions results in a quantized energy spectrum. Quantum dots are therefore regarded as artificial atoms. Quantum dots can be fabricated between source and drain electrical contacts allowing current–voltage measurements to observe the atom-like properties. It is possible to vary the exact number of electrons on the dot by changing the voltage and one can scan through the entire periodic table of artificial elements.

Theoretical calculations of quantum dot systems are based on the effective mass approximation: the electrons move in an external confining potential $V_{\rm conf}$, and interact via the

Coulomb interaction,

$$H = \sum_{i=1}^{N_e} \left(-\frac{\hbar^2}{2m_i} \nabla_i^2 + V_{\rm conf}(\mathbf{r}_i) \right) + \frac{1}{\epsilon} \sum_{i<j}^{N_e} \frac{q_i q_j}{|\mathbf{r}_i - \mathbf{r}_j|} \quad , \tag{113}$$

where m_i is the mass, q_i is the charge of the ith particle, N_e is the number of electrons, and ϵ is the dielectric constant. The confining potential is often modeled by a harmonic oscillator potential,

$$V_{\rm conf}(\mathbf{r}_i) = \frac{1}{2} m^* \omega^2 r_i^2. \tag{114}$$

The apparent similarity of "natural" atoms and quantum dots have motivated the application of sophisticated theoretical methods borrowed from atomic physics and quantum chemistry to calculate the properties of quantum dots, such as exact diagonalization (Hawrylak and Pfannkuche, 1993; Maksym and Chakraborty, 1990), HF approximations (Fujito *et al.*, 1996; Müller and Koonin, 1996; Yannouleas and Landman, 1999), and density functional approaches (Hirose and Wingreen, 1999; Koskinen *et al.*, 1997). QMC techniques have also been used for 2D (Bolton, 1996; Egger *et al.*, 1999; Harju *et al.*, 1999; Pederiva *et al.*, 2000) as well as 3D structures.

The SVM naturally lends itself as a powerful approach to study N_e-particle quantum dots (Varga *et al.*, 2001). In Table XX the SVM energies are compared with the energies of the "exact diagonalization" (Hawrylak and Pfannkuche, 1993; Wojs and Hawrylak, 1996) and the QMC methods (Bolton, 1996; Harju *et al.*, 1999; Pederiva *et al.*, 2000) for $N_e = 3$ electron systems. The different methods give energies for both the ground and excited states that typically agree to about 0.1%. The SVM energy is lower than the "exact diagonalization" indicating that it is probably more reliable.

In Table XXI a similar comparison is presented for $N_e = 2 - 6$ electron systems. The SVM result is in excellent agreement with the DMC predictions (Pederiva *et al.*, 2000).

To explore the spatial structure of the wave function, a pair correlation function is defined

$$P(\mathbf{r}, \mathbf{r}_0) = \frac{2}{N_e(N_e-1)} \langle \Psi | \sum_{i<j} \delta(\mathbf{r}_i - \mathbf{R} - \mathbf{r}) \delta(\mathbf{r}_j - \mathbf{R} - \mathbf{r}_0) | \Psi \rangle. \tag{115}$$

Here $\mathbf{r}_0$ is a fixed vector and its magnitude is chosen to be equal to $\langle \Psi | \sum_i |\mathbf{r}_i - \mathbf{R}| | \Psi \rangle / N_e$ and $\mathbf{R}$ is the position of the center of mass. This correlation function defines the probability of finding an electron at position $\mathbf{r}$ provided that an electron is at position $\mathbf{r}_0$. Fig. 12 shows the pair correlation functions for the ground state $(M, S) = (1, 1/2)$ of the $N_e = 5$

TABLE XXI Comparison of the energies (in units of effective hartree = 11.86 meV) of harmonically confined 2D electron systems ($\omega = 0.28$ $\hbar\omega = 3.32$ meV).

N_e	(M, S)	DMC (Pederiva *et al.*, 2000)	SVM (Varga *et al.*, 2001)
2	(0,0)	1.02162(7)	1.02164
3	(1,1/2)	2.2339(3)	2.2320
4	(0,1)	3.7157(4)	3.7130
4	(2,0)	3.7545(1)	3.7525
4	(0,0)	3.7135(6)	3.7783
5	(1,1/2)	5.5336(3)	5.5310
6	(0,0)	7.5996(8)	7.6020

electron system. For $\omega = 1$, the confinement potential is strong and the contribution of the single-particle energies to the total energy is larger than that of the Coulomb potential. The electrons are confined in a rather compact region so that the contour map does not show four peaks clearly. On the contrary, for $\omega = 0.1$ (in atomic units) the effect of the confinement becomes weak and the contribution of the Coulomb potential is larger than that of the harmonic-oscillator part. The spatial extent of the system increases and a well-separated pentagon-like structure is seen. The Wigner molecule-like structures formed in this case are in a good qualitative agreement with the results from a HF calculation (Yannouleas and Landman, 1999). The SVM calculation is expected to be more accurate.

VIII. ULTRACOLD BOSONIC AND FERMIONIC FEW-BODY SYSTEMS

The study of dilute ultracold atomic and molecular systems is presently at the forefront of modern physics (Bloch *et al.*, 2008; Braaten and Hammer, 2006; Chin *et al.*, 2010; Dalfovo *et al.*, 1999; Giorgini *et al.*, 2008). In the ultracold regime, the thermal de Broglie wave length $\lambda_{\rm dB}$ (Chin *et al.*, 2010), $\lambda_{\rm dB} = h/\sqrt{2mk_BT}$, becomes comparable to the average interparticle distance (here, m denotes the atom mass, T the temperature and k_B Boltzmann's constant). Imagine that two atoms collide at room temperature. In this case, $\lambda_{\rm dB}$ is small and the collision outcome depends on the details of the underlying interaction potential, i.e., a proper

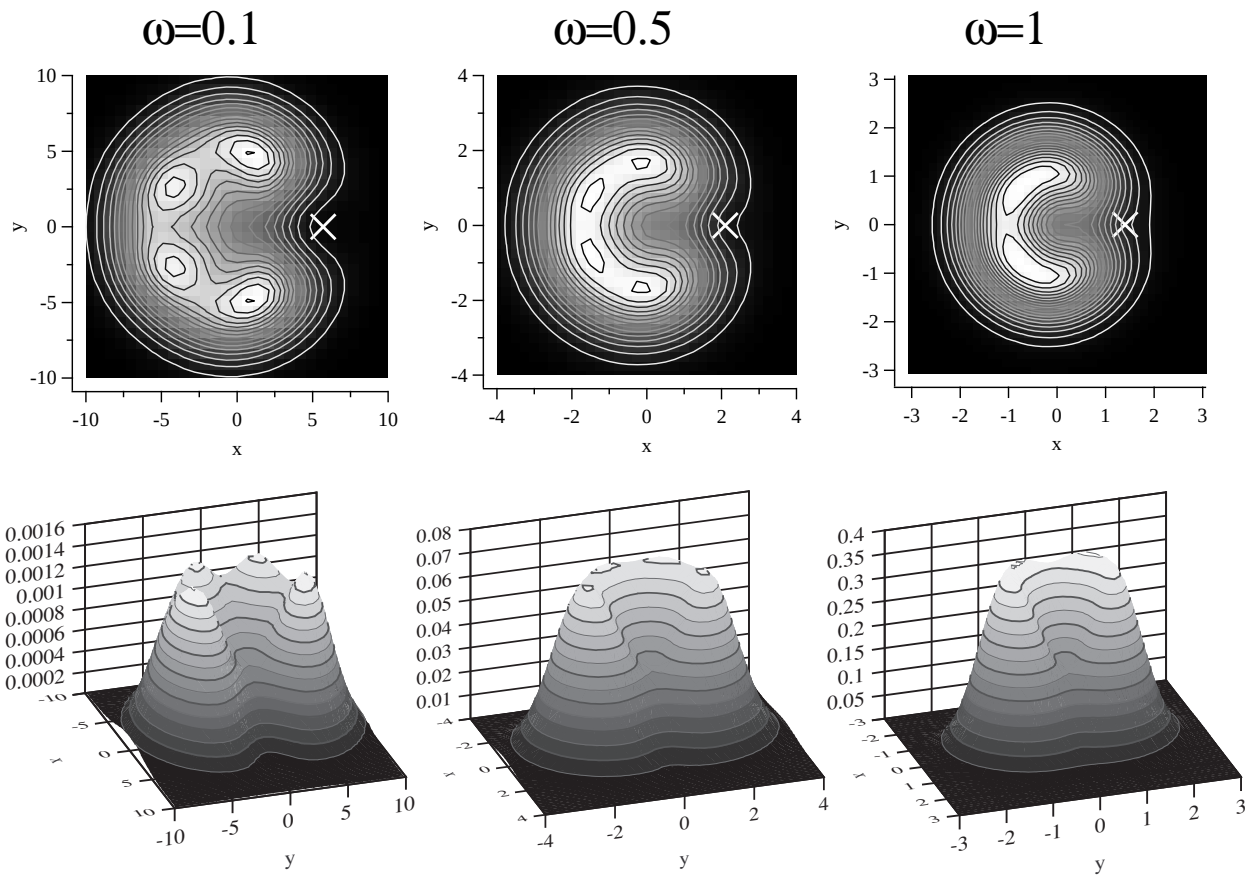

FIG. 12 Pair correlation function of the ground state $(M, S) = (1, 1/2)$ of 2D five-electron system as a function of the frequency ω of the harmonically confining potential. The white cross denotes $\mathbf{r}_0$. Atomic units are used.

description of the collision process involves many partial waves. Imagine, in contrast, that two atoms, which interact through a spherically symmetric interaction potential, collide at an ultracold temperature. In this case, λ_{dB} is large compared to the interaction or effective range of the underlying interaction potential and the collision outcome is governed by the lowest partial wave allowed by symmetry. For identical bosons or distinguishable particles, this is the s-wave. For identical fermions, in contrast, this is the p-wave since s-wave scattering is forbidden by symmetry (Chin *et al.*, 2010).

As will be illustrated in this section, s-wave interacting few-particle systems exhibit a variety of intriguing universal features that can be conveniently described by the ECG approach. Subsection VIII.A considers non-relativistic two-component Fermi gases with interspecies s-wave scattering length a_s and vanishing intraspecies interactions under external spherically symmetric confinement. The s-wave scattering length a_s is a parameter that

characterises the low energy scattering dynamics. It is defined in terms of the s-wave phase shift δ, $a_s = -\lim_{k\to 0}\tan(\delta)/k$ (here, k denotes the relative wave vector of the two colliding atoms), and determines the zero energy cross section σ, $\sigma = 4\pi a_s^2$. Subsection VIII.B outlines a recently developed methodology that combines the ECG and hyperspherical coordinate approaches. Applications of this methodology to bosonic systems are described in Subsec. VIII.C. Lastly, Subsec. VIII.D provides an outlook on the future.

A. Two-component Fermi gases

The model Hamiltonian for two-component s-wave interacting Fermi gases under external spherically symmetric harmonic confinement reads

$$H = \sum_{j=1}^{N_1}\sum_{k=N_1+1}^{N} V_{\rm tb}(r_{jk}) + \sum_{j=1}^{N_1}\left(\frac{-\hbar^2}{2m_1}\nabla^2_{\mathbf{r}_j} + \frac{1}{2}m_1\omega^2\mathbf{r}_j^2\right) + \sum_{j=N_1+1}^{N}\left(\frac{-\hbar^2}{2m_2}\nabla^2_{\mathbf{r}_j} + \frac{1}{2}m_2\omega^2\mathbf{r}_j^2\right), \tag{116}$$

where N_1 and N_2 denote respectively the number of fermions of species 1 with mass m_1 and the number of fermions of species 2 with mass m_2 ($N = N_1 + N_2$). In Eq. (116), the unlike atoms interact through a sum of central two-body potentials $V_{\rm tb}(r_{jk})$, where r_{jk} denotes the distance between particles j and k, $r_{jk} = |\mathbf{r}_j - \mathbf{r}_k|$; here, $\mathbf{r}_j$ ($j = 1, \cdots, N$) denotes the position vector of the jth fermion measured with respect to the trap center. Throughout this section, we assume that the atoms of components 1 and 2 occupy two different internal hyperfine states of the same species (implying $m = m_1 = m_2$). If the harmonic oscillator length a_{ho} that characterizes the external confinement [$a_{ho} = \sqrt{\hbar/(m\omega)}$, where ω denotes the angular trapping frequency] and the absolute value of the interspecies two-body s-wave scattering length $|a_s|$ are much larger than the range r_0 and the effective range r_e of $V_{\rm tb}$, then the two-component Fermi gas behaves universally, i.e., its properties are fully determined by the dimensionless quantities a_s/a_{ho}, N_1 and N_2.

The ECG approach is extremely well suited to describe universal aspects of small two-component Fermi gases for two primary reasons: *(i)* Since low-energy observables are, in general, independent of the details of the interaction potential $V_{\rm tb}$ (Giorgini *et al.*, 2008), the true atom-atom potential, which typically supports several tens or hundreds of bound states, can be replaced by a simple Gaussian model potential $V_{\rm g}$, $V_{\rm g}(r) = -V_0\exp[-r^2/(2r_0^2)]$,

whose depth V_0 and range r_0 are adjusted such as to reproduce the desired s-wave scattering length a_s and so that $V_{\rm g}$ supports no or one two-body s-wave bound state in free space. The advantage of the Gaussian model potential over, say, a square well model potential is that the matrix elements associated with the interaction potential are readily evaluated (Suzuki and Varga, 1998). Extrapolation of the energy and other observables to the $r_0 \to 0$ limit allows one to simulate zero-range interacting systems. *(ii)* The functional form of the basis functions employed in the ECG approach is sufficiently flexible to describe short-range correlations that occur at length scales of the order of the range of the interaction potential and long-range correlations that occur at length scales of the order of the external confining potential (Blume *et al.*, 2007; von Stecher and Greene, 2007; von Stecher *et al.*, 2008).

When a_s is negative and $|a_s|$ small, the N-fermion system behaves like a weakly-attractive atomic Fermi gas. When a_s is small and positive, the system can be described as consisting of N_2 repulsively interacting composite bosonic molecules and $|N_1 - N_2|$ unpaired fermions. These small $|a_s|$ regimes are, as has been shown through comparison with results obtained by the ECG approach and by MC approaches, quite well described perturbatively (von Stecher *et al.*, 2007, 2008). When $|a_s|/a_{ho}$ becomes of order one, non-perturbative approaches are needed. The ECG approach has been applied to determine the energies, structural properties, and dynamics of small trapped gases described by the Hamiltonian given in Eq. (116) as a function of the s-wave scattering length with up to $N = 6$ (Blume and Daily, 2009, 2011; Blume *et al.*, 2007; Daily and Blume, 2010; Rittenhouse *et al.*, 2011; von Stecher and Greene, 2007, 2009; von Stecher *et al.*, 2007, 2008). For the $(N_1, N_2) = (2, 2)$ system, for example, the ECG formalism was used to model the molecule formation rate in ramp experiments throughout the BCS-BEC crossover (von Stecher and Greene, 2007).

In the unitary regime, i.e., in the regime where the s-wave scattering length diverges, the system is strongly-correlated. In this regime, the s-wave scattering length does not define a meaningful length scale and the system is—when $r_0 \to 0$ (i.e., in the zero-range limit)—characterized by the same number of length scales as the non-interacting system (Giorgini *et al.*, 2008; Werner and Castin, 2006a). Like the non-interacting system, the unitary system is scale invariant and possesses ladders of states whose energies are separated by $2\hbar\omega$ (Werner and Castin, 2006a) and are associated with excitations along the hyperradial coordinate (see Sec. III.K for the definition of the hyperradius). The relative energy of the system at unitarity can be written as $E_{\rm rel} = (s_\nu + 2q + 1)\hbar\omega$ (Werner and Castin, 2006a), where s_ν is

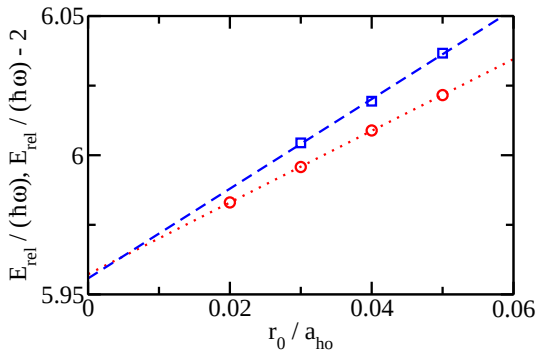

FIG. 13 (Color online) Relative energy $E_{\rm rel}$ of harmonically trapped equal-mass two-component Fermi gas with $(N_1, N_2) = (3, 2)$ and $L^\pi = 1^-$ at unitarity as a function of r_0. Circles and squares show $E_{\rm rel}$ (energetically lowest lying state) and $E_{\rm rel} - 2\hbar\omega$ (third lowest state), respectively. Dotted and dashed lines show linear fits to the ECG energies.

determined by the eigenvalues of the hyperangular Schrödinger equation (see also below) and q, $q = 0, 1, \cdots$, denotes the hyperradial quantum number. The first numerical verification of the $2\hbar\omega$ spacing for $N > 3$ was obtained by applying the ECG approach (Blume *et al.*, 2007).

Circles and squares in Fig. 13 show the energy of the $(N_1, N_2) = (3, 2)$ system with $1/a_s = 0$ as a function of r_0 for the lowest and third lowest states with $L^\pi = 1^-$ symmetry. In anticipation of the $2\hbar\omega$ spacing, the energy of the third lowest state is shifted down by $2\hbar\omega$. The basis sets contain between 2400 to 3000 properly anti-symmetrized basis functions. The ECG energies shown in Fig. 13 have not been extrapolated to the infinite basis set limit; the difference between the energies for the largest basis set considered and those for the infinite basis set limit is of the order of $0.002\hbar\omega$. Dotted and dashed lines show linear fits to the finite-range energies. In the $r_0 \to 0$ limit, the energies of the lowest and third lowest states are $5.957(3)\hbar\omega$ and $7.956(5)\hbar\omega$, respectively, where the number in parenthesis indicates the combined basis set extrapolation and $r_0 \to 0$ extrapolation errors; thus, the $2\hbar\omega$ spacing is verified to within the numerical accuracy of the extrapolated zero-range energies. For the $(N_1, N_2) = (3, 3)$ system (see Fig. 1 in (Blume *et al.*, 2007)), the hyperradial densities determined from the ECG wave functions were found to be in good agreement with analytic predictions (Werner and Castin, 2006a), thereby confirming the scale invariance of the trapped equal-mass two-component Fermi gas at unitarity.

TABLE XXII Relative energies for trapped two-component Fermi gas with equal masses in the zero-range limit at unitarity. Calculations performed by the ECG approach are marked by "*" (the numbers in parenthesis in the third column indicate the combined basis set and zero-range extrapolation errors).

(N_1, N_2)	L^π	$E_{\rm rel}/(\hbar\omega)$	Ref.
$(1,1)$	0^+	1/2	(Busch *et al.*, 1998)
$(2,1)$	1^-	2.772724	(Werner and Castin, 2006b)
$(3,1)$	1^+	5.08186(10)	(Rakshit *et al.*, 2011)*
$(4,1)$	0^-	7.45(9)	(Blume and Daily, 2010b)*
$(2,2)$	0^+	3.5092(4)	(von Stecher and Greene, 2009)*
$(3,2)$	1^-	5.957(3)	(Blume and Daily, 2011)*
$(3,3)$	0^+	6.84(9)	(Blume and Daily, 2011)*

Table XXII summarizes the zero-range energies of the energetically lowest lying gas-like state of various trapped (N_1, N_2) systems at unitarity. While analytical results exist for the two- and three-body systems, no analytical results are presently available for $N > 3$. The ECG energies for $L^\pi \neq 0^+$ reported in Table XXII have been obtained using basis functions that are written in terms of one or more global vectors (see Sec. II.D.2) and by extrapolating the energies to the $r_0 \to 0$ limit. These energies constitute the most precise energies for trapped two-component Fermi gases with $N = 4 - 6$ to date.

B. Hyperspherical ECG approach

The previous subsection considered bound states of trapped few-fermion systems. While some scattering properties such as the atom-dimer and dimer-dimer scattering lengths can be extracted from the energy spectrum of the harmonically trapped system (von Stecher *et al.*, 2007, 2008), an alternative approach, the hyperspherical ECG (HECG) approach (Rittenhouse *et al.*, 2011; von Stecher and Greene, 2009) (note, the authors refer to their method as the CGHS method), combined with, e.g., an R-matrix calculation allows for the description of multi-channel scattering processes. The HECG approach is distinctly different from the ECG based scattering applications described in Sec. IX. It solves the Schrödinger equation

in a two-step process by first considering the hyperangular degrees of freedom and by then considering the hyperradial degree of freedom. The key advantage of the HECG approach over, say, the HH expansion approach (see Sec. III.K) is that the ECG functions provide, at least in the low-energy regime considered here, a more flexible basis set than the HH.

We consider an N-particle system in three-dimensional space with position vectors $\mathbf{r}_j$ and masses m_j ($j = 1, \cdots, N$) with the interaction potentials of Eq. (3) only dependent on the relative distance coordinates. No external confining potential is considered), and the center of mass degrees of freedom has been separated off.

The starting point of the HECG approach is the hyperspherical representation (Rittenhouse *et al.*, 2011), which expands the relative wave function Ψ in terms of a complete set of channel functions $\Phi_\nu(\mathbf{\Omega}; R)$ which depend parametrically on the hyperradius R, and weight functions $F_{\nu q}(R)$ as given by Eq. (101). The idea of the HECG approach (von Stecher and Greene, 2009) is to expand the channel functions Φ_ν of Eq. (101) in terms of the basis functions given in Eq. (2). Such an expansion requires transforming the basis functions to hyperspherical coordinates and evaluating the overlap matrix element, the hyperangular kinetic energy matrix element and the interaction potential matrix element by integrating over all hyperangles while keeping the hyperradius R fixed. Once $U_\nu(R)$ and $\Phi_\nu(\mathbf{\Omega}; R)$ are known, the coupling matrix elements $P_{\nu'\nu}(R)$ and $Q_{\nu'\nu}(R)$ can also be obtained and the solutions to the coupled set of one-dimensional radial equations can be obtained using standard techniques. It is important to note that the coupled set of hyperradial equations can be solved using boundary conditions appropriate for bound or scattering states; in the latter case, single- and multi-channel scattering processes can be treated, i.e., the number of open and closed channels can be adjusted as needed.

To date, the HECG approach has been applied primarily to $N = 3$ and 4 systems with $L^\pi = 0^+$ symmetry. For states with this symmetry, compact expressions for the fixed-R matrix elements have been obtained for $N = 3$ while expressions that involve $N - 3$ numerical angular integrations have been obtained for $N > 3$ (Rittenhouse *et al.*, 2011; von Stecher and Greene, 2009). Application of the HECG approach to five-body systems seems possible but application of the HECG approach to six-body systems may be beyond current computational resources. Extensions of the HECG approach to higher angular momentum states appear feasible.

Fig. 14 shows the scaled hyperangular eigenvalues or effective potential curves

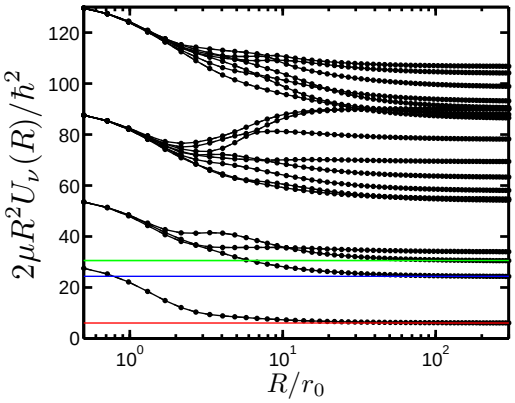

FIG. 14 (Color online) Scaled hyperradial potential curves $2\mu R^2 U_\nu/\hbar^2$ as a function of R/r_0 for the $(2,2)$ system with $L^\pi = 0^+$ symmetry and infinitely large interspecies scattering length a_s. The horizontal lines show the expected asymptotic large R behavior of the lowest three scaled hyperradial potential curves. The figure has been taken from Ref. (von Stecher and Greene, 2009) with permission.

$2\mu R^2 U_\nu(R)/\hbar^2$ for the $(2,2)$ system, described by the Hamiltonian given in Eq. (116) with $m_1 = m_2$ and $\omega = 0$, with $L^\pi = 0^+$ symmetry and infinitely large interspecies scattering length a_s as a function of R/r_0, where r_0 is the range of the Gaussian model potential (von Stecher and Greene, 2009). In the small R region (i.e., for $R/r_0 \lesssim 1$), the hyperradial potential curves are dominated by the hyperangular kinetic energy, resulting in potential curves whose degeneracies coincide with those of the non-interacting system. In the intermediate R region, in contrast, the behavior of the potential curves is governed by a competition between the hyperangular kinetic energy and the interaction energy. Lastly, in the large R region (i.e., for $R/r_0 \gtrsim 20$), the hyperradial potential curves are dominated by the interaction energy. The large-R potential curves at unitarity can be written as $2\mu R^2 U_\nu(R) = \hbar^2(s_\nu^2 - 1/4)$, where s_ν is R-independent. The horizontal lines in Fig. 14 show the asymptotic behavior of the three lowest scaled hyperradial potential curves, obtained by extracting s_ν from the relative ECG energies at unitary (see discussion in fourth paragraph of Sec. VIII.A). The fact that the scaled hyperradial potential curves in the small and large R regions agree with the expected behavior shows that the basis sets employed in the HECG approach are flexible enough to describe the hyperangular dynamics. The next section discusses applications of the HECG approach to the four-boson system.

C. Bose systems and Efimov physics

Section VIII.A discussed the behavior of two-component Fermi gases with equal masses, whose behavior is, for $|a_s| \gg r_0$, fully governed by the s-wave scattering length. For these systems, there are no weakly bound three-body states and the atom-dimer scattering length a_{ad} is directly proportional to a_s (Giorgini *et al.*, 2008). For the three-boson system with large scattering length and zero-range interactions, the situation is different (Efimov, 1970, 1973). The lowest effective hyperradial potential curve with $L^\pi = 0^+$ symmetry is supercritical, i.e., the problem is undetermined unless augmented by a so-called Efimov or three-body parameter that determines the behavior of the hyperradial wave function in the small R region where all three particles are close together (Braaten and Hammer, 2006). It follows that the equal-mass three-boson system with infinitely large s-wave scattering length supports an infinite number of geometrically spaced three-body bound states (or Efimov trimers) with energy $E_{3,n}$, $E_{3,n+1} \approx E_{3,n}/515$ ($n = 1, 2, \cdots$), where $E_{3,1}$ is determined by the small R boundary condition. Solid lines in Fig. 15 schematically show the three-body Efimov spectrum as a function of $1/a_s$.

Since the early 1970s, when Efimov put this intriguing three-boson scenario forward (Efimov, 1970, 1973), the question "What happens in the four-body sector?" has been asked (Amado and Greenwood, 1973; Kröger and Perne, 1980). Is the behavior of the four-boson system fully determined by the s-wave scattering length and the three-body parameter, or is a four-body parameter needed? Answers to these questions have come from a number of analytical and numerical techniques (Deltuva, 2011a,b; D'Incao *et al.*, 2009; Hadizadeh *et al.*, 2011; Hammer and Platter, 2007; Platter *et al.*, 2004; von Stecher *et al.*, 2009). Using the HECG approach, the effective hyperradial potential curves of the four-boson system were calculated and it was found (von Stecher *et al.*, 2009), in agreement with earlier predictions (Hammer and Platter, 2007), that there are two weakly-bound four-body states with energies $E^{(1)}_{4,n}$ and $E^{(2)}_{4,n}$ "attached" to each Efimov trimer state with energy $E_{3,n}$: $E^{(1)}_{4,n} \approx 4.58 E_{3,n}$ and $E^{(2)}_{4,n} \approx 1.01 E_{3,n}$ (see dashed lines in Fig. 15). The proportionality constants 4.58 and 1.01 are universal, i.e., they are the same for all Efimov trimers and independent of the details of the underlying two-body potential. The fact that the energies $E^{(1)}_{4,n}$ and $E^{(2)}_{4,n}$ are universally linked to the energy of the n^{th} Efimov trimer suggests that a four-body parameter is not needed, i.e., that the short-range behavior of the four-body

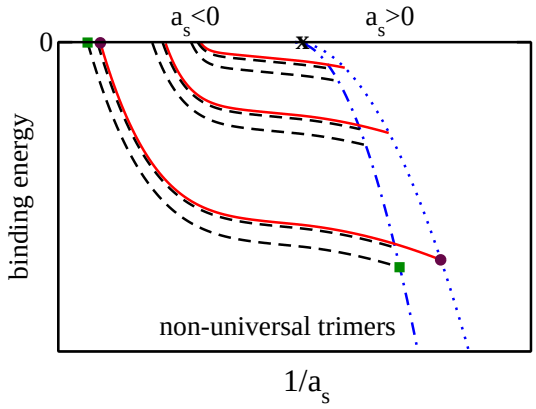

FIG. 15 (Color online) Schematic of the extended Efimov scenario for equal-mass boson system as a function of $1/a_s$ ($|a_s|$ large). The solid lines show the energy of three Efimov trimers (the accumulation of infinitely many bound states for slightly negative energy is not shown). Dashed lines show the energy of the two four-body states attached to each Efimov trimer. The dotted and dash-dotted lines show the energy of the weakly-bound two-body state and twice the energy of the weakly-bound two-body state. The scattering lengths at which the most strongly-bound Efimov trimer dissociates into three free atoms or a dimer and a free atom are marked by circles. The scattering lengths at which the more deeply bound tetramer attached to the most strongly-bound Efimov trimer dissociates into four free atoms or two dimers are marked by squares. The point $(1/a_s, E) = (0, 0)$ is marked by an "x".

hyperradial potential curves is not supercritical. We note that alternative interpretations exist (Hadizadeh *et al.*, 2011).

Furthermore, application of the HECG approach showed that the s-wave scattering lengths $a_{4,n}^{(1),-}$ and $a_{4,n}^{(2),-}$ at which the four-body states dissociate into four free atoms are universally related to the scattering lengths $a_{3,n}^{-}$ at which the Efimov trimers dissociate into three free atoms, $a_{4,n}^{(1),-} \approx 0.43 a_{3,n}^{-}$ and $a_{4,n}^{(2),-} \approx 0.90 a_{3,n}^{-}$ (von Stecher *et al.*, 2009). On the positive scattering length side, the HECG calculations predicted that the scattering lengths $a_{4,n}^{(1),+}$ and $a_{4,n}^{(2),+}$ at which the tetramers dissociate into two dimers are universally related to the scattering lengths $a_{3,n}^{+}$ at which the trimers dissociate into a dimer and a free atom (D'Incao *et al.*, 2009). Recent scattering calculations (Deltuva, 2011a,b) based on momentum space equations confirmed these findings and significantly improved upon the numerical accuracy of the proportionality constants.

The extended Efimov scenario for equal-mass boson systems with $N > 4$ is presently less

well understood. Recent ECG calculations suggest that there also exist two five-body states that are attached to each Efimov trimer (von Stecher, 2010, 2011). Indeed, preliminary experimental results show evidence for enhanced loss features at the expected s-wave scattering lengths (Ferlaino, 2011). The ECG and HECG results for the four- and five-body energy spectra are in agreement with an earlier approximate hyperspherical MC study (Blume and Greene, 2000), which found two bound states for $N = 4 - 10$ for an interaction model that supports one weakly-bound trimer state, and with a ground state DMC study (Hanna and Blume, 2006), which found evidence that four- or higher-body parameters are not needed to describe the low-energy states of bosonic systems with $N > 3$. Altogether, these results point toward a unified picture of the low-energy behavior of few-boson systems with large s-wave scattering length ($N > 3$), namely, that the low-energy observables of the N-body system are universally linked to two- and three-body observables.

In addition to the equal-mass s-wave interacting boson system, Efimov physics plays a role in the three-boson system with anisotropic dipolar interactions (Wang *et al.*, 2011b) and in unequal-mass two-component Fermi gases with sufficiently large mass ratio (Petrov, 2003). It is expected that applications of the ECG and HECG approaches will contribute to the construction of extended Efimov scenarios that include three- and four-body physics for these systems in the future. In the regime where Efimov physics is absent, the ECG approach has already been applied to investigate three- and four-body resonances of trapped unequal-mass two-component Fermi gases (Blume and Daily, 2010a,b).

D. Outlook

As mentioned in the introduction, the ECG approach is most powerful if applied to four- and higher-body systems where a variety of other numerical approaches have limitations because of their unfavorable scaling with increasing number of degrees of freedom. The study of few-body phenomena for systems with more than three constituents in the ultracold has just started. Tremendous experimental progress has paved the way for measurements of observables that have been attributed to four-body physics (Ferlaino *et al.*, 2009; Pollack *et al.*, 2009; Zaccanti *et al.*, 2009). As experiment and theory continue to mature, it is expected that the ECG approach, with its variants, will play an increasingly prominent role in the study of low-energy bound state and scattering observables of systems consisting of

more than three particles. For example, there are presently many open questions related to the extended Efimov scenario of the five-boson system, of unequal-mass two-component Fermi systems, and of dipolar systems. Furthermore, the study of N-body resonances in three dimensions or in effectively low-dimensional geometries promises rich physics, with direct consequences for possible pairing scenarios that involve N-body clusters.

Indeed, the ECG approach has already been applied to dipolar systems in effectively low-dimensional confining geometries (Volosniev *et al.*, 2011). A key motivation behind these studies is the tremendous experimental progress in cooling polar molecules down to the near-degenerate regime (Ni *et al.*, 2008). The dipole-dipole interaction is long-range and anisotropic, and couples different angular momentum states. Generally speaking, "head to tail collisions" of aligned dipoles are attractive and can lead to detrimental losses. The application of effectively low-dimensional confining geometries has been shown theoretically and experimentally to stabilize dipolar systems significantly (de Miranda *et al.*, 2011; Lahaye *et al.*, 2009). In one set of ECG applications (Volosniev *et al.*, 2011), the system wave functions have been expanded in terms of shifted Gaussians. The emergence of weakly-bound few-body states—involving, e.g., aligned dipoles located in two different layers—is of particular interest, as the few-body spectra provide crucial insights into the many-body behavior of these highly non-trivial and strongly-correlated systems.

IX. SCATTERING AND RESONANCES

While the possibility of employing bound state methods to treat scattering states has always been desirable, there have been fewer applications of ECG technologies to collision systems (Aoyama *et al.*, 2012; Hiyama *et al.*, 2006, 2003; Ivanov *et al.*, 2001, 2002a; Matsumoto *et al.*, 2003; Mitroy *et al.*, 2008b; Zhang and Mitroy, 2011; Zhang *et al.*, 2008). However, the few scattering calculations that have been done have often been on systems that would be difficult to treat by other means.

The diversity of scattering problems can be divided into two classes. First one has a class of low-energy systems in which only elastic scattering is possible. Such systems can be treated as quasi-bound state systems with an ad-hoc procedure used to graft on the scattering boundary conditions. The other class of systems would have multiple open channels and are best treated by embedding ECG basis functions into an established scattering theory.

A. Single channel elastic scattering systems

1. *Confining potentials*

While the overall goal is the determination of the scattering wave function, it is useful to divide the calculation into two stages. The first stage of the calculation is to generate a basis that gives a good representation of the dynamics when the projectile and target are close together. The next step involves using this basis to calculate the scattering information.

The first stage can be achieved by adding a confining potential to the Hamiltonian. Two forms have so far been adopted. In initial applications, the form was

$$V_{\rm CP}(r) = \lambda r^n. \tag{117}$$

One choice adopted was $\lambda \approx 10^{-19}$ hartree/a_0^{12} and $n = 12$ (Zhang and Mitroy, 2008). This gave a potential that was small in the interaction region for the system under consideration. A more refined version was

$$V_{\rm CP}(r) = G\Theta(r - R_0)(r - R_0)^2, \tag{118}$$

where Θ is the Heaviside function.

With these potentials, the generation of the interaction region basis reduces to a standard bound state calculation. So far, the confining potential concept has only been applied to systems with an infinitely heavy scattering center. It has not been applied to systems where the projectile and scattering particle are of comparable mass. It should be noted that the first set of ECG based calculations on atomic systems did not use confining potentials. In this case confinement was achieved by constraining the α_{ij} coefficients in Eq. (2) to be positive and to not fall below a critical minimum size (Ivanov *et al.*, 2001, 2002a,b).

2. *The asymptotic basis*

A linear combination of ECGs is not a particularly efficient way to represent the wave function in the asymptotic region since the wave function takes a simple product form at large separations. For example, the asymptotic wave function for e^-–He scattering would be written (with implied anti-symmetrization) as

$$\Psi = \psi_{\rm He}(\mathbf{r}_1, \mathbf{r}_2)\phi(\mathbf{r}_3)\ . \tag{119}$$

This part of the wave function can be best incorporated by adding basis functions of the form (Zhang *et al.*, 2008), e.g.

$$\begin{aligned} \Psi_{i,\text{out}} &= \psi_{\text{He}}(\mathbf{r}_1, \mathbf{r}_2)\psi_i(\mathbf{r}_3) \ , \\ \psi_{\text{He}}(\mathbf{r}_1, \mathbf{r}_2) &= \sum_k d_k \exp(-\beta_{k1} r_1^2 - \beta_{k2} r_2^2 - \beta_{k12} r_{12}^2) \ , \\ \psi_i(\mathbf{r}_3) &= \exp\left(-\alpha_i r_3^2\right) \ . \end{aligned} \tag{120}$$

to the three-electron ECGs resulting from the optimization of the energy within the confining potential. The target wave function can be represented as a linear combination of ECGs and the α_i are chosen as a geometric progression obeying $\alpha_i = \alpha_1/T^{i-1}$ (where T is typically set to be about 1.45). Each asymptotic basis function is actually composed of a linear combination of ECGs.

The utility of the asymptotic basis can be seen by reference to the e^-–He ($^2S^e$) phase shift. A basis of 800 three-electron ECGs supplemented by 40 additional asymptotic basis functions given by Eq. (120) gave a phase shift that was closer to convergence than a basis of 1600 three electron ECGs without any asymptotic basis function (Zhang *et al.*, 2008).

3. Getting scattering information

Once a good basis for the interaction region has been generated, there are a number of methods that can be used to extract the scattering information. For example, it is possible to determine the phase shifts directly from the energies of the system confined by Eq. (118) (Mitroy *et al.*, 2008b; Zhang *et al.*, 2008). In addition, in terms of increasing complexity, one can use stabilization ideas (Hazi and Taylor, 1970), the Harris variational method (Harris, 1967; Kievsky *et al.*, 2010), the Kohn variational method (Burke and Joachain, 1995), or a Green's function method (Suzuki *et al.*, 2009).

4. Stabilization calculations

Two types of states occur when a large square integrable basis is diagonalized in a potential. The first class of states are those with negative energies that approximate the exact bound states of the potential. Another class of states have positive energy but do not have the long range character of true continuum states. However, the shape of the wave function

for these positive energy states often resembles that of the true continuum state over a finite range at that energy. This is demonstrated in Fig. 16 where the pseudo-state with energy E obtained by diagonalizing the free particle Hamiltonian in a basis of Laguerre type orbitals is compared to $\sin(\sqrt{2mE/\hbar}r)$. Phase shifts accurate to about 1% can be determined by making a least squares fit of the L^2 wave function to the known asymptotic form outside the interaction region (Ivanov *et al.*, 2001, 2002a).

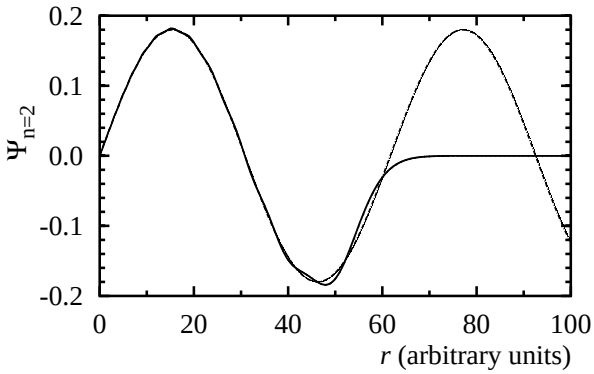

FIG. 16 Comparison between $\sin(kr)$ and a pseudo state obtained by diagonalization of the free particle Hamiltonian in a large basis of Laguerre type orbitals. The value of k is taken to be $\sqrt{2E}$ where E is the energy of the pseudo state.

Stabilization calculations utilizing ECGs have been applied to a number of difficult to solve few-body systems. One of the first series of stabilization calculations was an application to the Ps–H, Ps–He (and other rare gases) and Ps–Ps systems. These represent difficult to treat systems since both projectile and target are composite systems with internal structures. The optimizations for these systems were done without the advantage of a confining potential (Ivanov *et al.*, 2001, 2002a,b). Despite this limitation, the first estimates of the low energy scattering parameters utilizing SVM wave functions were as accurate as any published to that time (Ivanov *et al.*, 2001, 2002a,b)

One of the key results of this early work was an estimate of the scattering length for ^{3}Ps-^{3}Ps scattering. A stabilization SVM calculation gave a scattering length of 8.44 a_0 (Ivanov *et al.*, 2002b). The only other first principles estimates of the scattering length, namely 9.15(4) a_0, came from the QMC (Shumway and Ceperley, 2001). The interest in this system derives from proposals to form a BEC made up of triplet positronium (Platzman and Mills, Jr., 1994) (the lifetime of ^{3}Ps is 0.125×10^{-7} sec^{-1}). The light mass means the critical temperature will lie between 20–30 K and the positive scattering length means the BEC

would be stable.

The Ps-He system is an example of a calculation that is technically challenging. This is a five-body system with a target that cannot be represented with an analytic wave function while the projectile is a two-body system. The only observable that has been directly measured with any reliability is the *pick-off* annihilation rate. The pickoff annihilation rate is proportional to the annihilation cross section resulting from contact between the positron in positronium and the electrons in the target (Charlton, 1985; Charlton and Humberston, 2001). Despite being one of the standard observables extracted from positron annihilation experiments (Charlton, 1985; Charlton and Humberston, 2001), there has never been a first principles calculation of ${}_1Z_{\rm eff}$ for any physical system that is expected to be accurate to within a factor of 2.

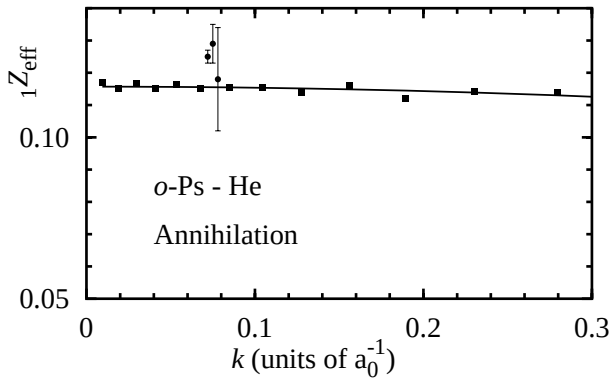

FIG. 17 The s-wave pickoff annihilation parameter for Ps-He scattering as a function of k (units of a_0^{-1}) (Zhang and Mitroy, 2008). The solid line is the fit to the data using effective range theory while the data points with the error bars are experimental (Canter *et al.*, 1975; Coleman *et al.*, 1975; Duff and Heyman, 1962).

The variation of the pick-off annihilation rate ${}_1Z_{\rm eff}$, as a function of k for $k < 0.30\ a_0^{-1}$ is shown in Fig. 17 as an effective range fit to the calculated values (Zhang and Mitroy, 2008). The value of ${}_1Z_{\rm eff}$ at thermal energies was found to be 0.1157. The agreement with experiment was acceptable when the uncertainties in extracting ${}_1Z_{\rm eff}$ from the experimental lifetime spectrum are taken into consideration.

5. Kohn variational calculations

The Kohn variation method is a well established approach to calculating low energy scattering information (Burke and Joachain, 1995). However, it presents additional complications due to the existence of matrix elements involving the continuum. The only ECG based Kohn variational calculations in atomic physics have involved a positron as the projectile (Zhang and Mitroy, 2011). The most complicated matrix elements have two continuum functions, e.g.

$$\langle \psi(\mathbf{r})\Phi(\mathbf{R})|(H-E)|\psi(\mathbf{r})\Psi(\mathbf{R})\rangle. \tag{121}$$

In this expression $\Psi(\mathbf{R})$ is a target many body wave function expressed in terms of ECGs and $\psi(\mathbf{r})$ is a continuum function. One can integrate over the collective set of target coordinates, i.e. $\mathbf{R}$, leaving a numerical integral over the last coordinate.

Potentially more complicated problems appear when there is an exchange interaction between the projectile and target (e.g. electron-atom scattering). One has to deal with integrals of the type

$$\langle \psi(\mathbf{r})\Psi(\mathbf{r}',\mathbf{R}')|(H-E)|\psi(\mathbf{r}')\Psi(\mathbf{r},\mathbf{R})\rangle, \tag{122}$$

which in general can only be reduced to an integral involving the coordinates of particles. However, the exchange interaction is a short range interaction and there are a number of ways for evaluating such integrals for example by separable expansion, or by replacing the continuum function at short distances by a linear combination of Gaussians (Kamimura, 1977; Rescigno and Orel, 1981; Rescigno and Schneider, 1988).

One recent landmark calculation was the application of the SVM to e^+-H_2 scattering (Zhang and Mitroy, 2011; Zhang *et al.*, 2009) which did not require any exchange interactions involving the projectile. This system had seen a number of attempts to calculate the low energy cross section using the Kohn variational method with Hylleraas basis sets (Armour and Baker, 1986; Cooper *et al.*, 2008). The accuracy of these Hylleraas basis calculations was effectively limited by the difficulties in calculating the matrix elements. Matrix element evaluation of the ECG basis did not pose any insuperable problems in a recent calculation of zero-energy e^+-H_2 scattering. The strategy of the calculation was to optimize the energies of the two lowest states of the e^+H_2 system inside a confining potential. The resulting ECG basis was then used in a Kohn variational calculation.

Fig. 18 shows the scattering length as a function of inter-nuclear distance. The interesting

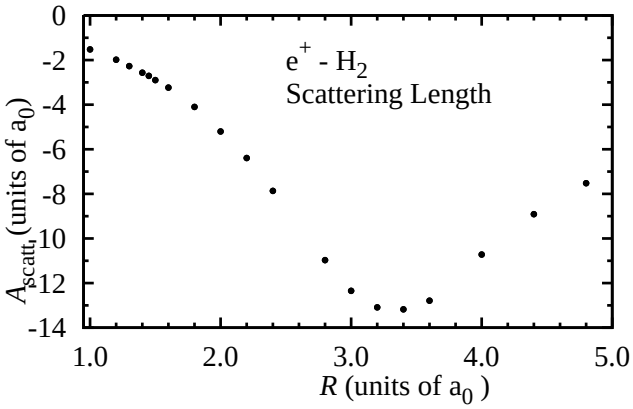

FIG. 18 The scattering length (in a_0) as a function of inter-nuclear distance, R, for positron scattering from H_2 (Zhang and Mitroy, 2011).

feature was the deep minimum in the scattering length near $R = 3.4\ a_0$ which was completely new and unexpected. The large negative scattering length indicates that the positron is close to being bound to the H_2 at this inter-nuclear distance. The zero-energy cross section for elastic e^+-H_2 scattering can be determined by integrating over the H_2 inter-nuclear distances of vibrational ground state.

The most important observable for low-energy e^+-H_2 scattering is the annihilation parameter, $Z_{\rm eff}$ for positrons at thermal energies. This quantity is related to the cross section for the annihilation of the positron due to contact with the target electrons (Charlton and Humberston, 2001). It is can be calculated for positrons colliing with an N-eelctron target using

$$Z_{\rm eff} = \sum_{i=1}^{N} \int d^3\tau\ d^3r_0\, |\Psi(\mathbf{r}_1, \ldots, \mathbf{r}_N; \mathbf{r}_0)|^2\, \delta(\mathbf{r}_i - \mathbf{r}_0)\ , \tag{123}$$

where $\Psi(\mathbf{r_1}, \ldots, \mathbf{r}_N; \mathbf{r}_0)$ is the scattering wave function, $d^3\tau$ represents the integration of electron co-ordinates $\mathbf{r}_1$ to $\mathbf{r}_N$, and $\mathbf{r}_0$ is the positron coordinate.

Experimental values are 14.7(2) (McNutt *et al.*, 1979), 14.61(14) (Laricchia *et al.*, 1987) and 16.02(08) (Wright *et al.*, 1983). The differences between the experimental values can be ascribed to variations in how the positrons achieve thermal energies in the different experiments (Zhang and Mitroy, 2011). A Kohn variational calculation using ECGs generated in a confining potential gave $Z_{\rm eff}$=15.7 (Zhang and Mitroy, 2011) and is supportive of the experiment giving the large $Z_{\rm eff}$. Kohn variational calculations based on Hylleraas basis functions (Armour and Baker, 1986; Armour *et al.*, 2010; Cooper *et al.*, 2008, 2009) gave

values ranging from 10 to 13 with some uncertainty about which value to adopt.

The Kohn variational method has also been used with GEM wave functions to investigate nucleon-K meson system treated as a five quark system (Hiyama *et al.*, 2006). Two resonances at 500 and 520 MeV were identified (Hamaguchi *et al.*, 2007) by this approach.

B. Multi-channel scattering

1. Continuum discretized coupled-channels method

The continuum discretized coupled-channel (CDCC) method can be used to study break-up reactions in nuclear physics (Austern *et al.*, 1987; Yahiro *et al.*, 1982). The GEM has been used to construct the CDCC wave function for three-body (Egami *et al.*, 2004; Matsumoto *et al.*, 2003; Yahiro *et al.*, 1982) and four-body (Matsumoto *et al.*, 2006) break-up.

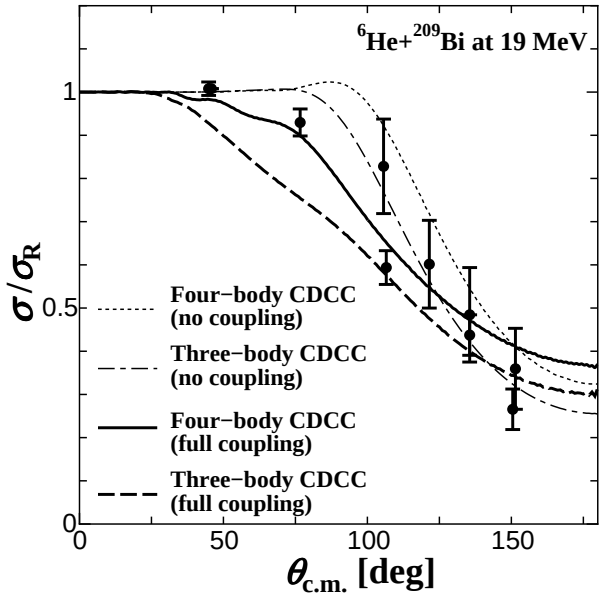

FIG. 19 Angular distribution of the ratio of the elastic differential cross section with respect to the Rutherford cross section for ^{6}He+^{209}Bi scattering at 19 MeV. The solid (dashed) and dotted (dot-dashed) lines show the results of the four-body CDCC (three-body) CDCC) calculation with and without breakup effects, respectively. The experimental data are at laboratory frame energies of 19.0 MeV (Aguilera *et al.*, 2000) and 19.1 MeV (Aguilera *et al.*, 2001).

The ^{6}He nucleus is a very weakly bound halo nucleus. As such, breakup reactions involving this nucleus have a contribution from the four body $^6\mathrm{He} + \mathrm{X} \rightarrow n+n+\alpha+X$ continuum

(Matsumoto *et al.*, 2006, 2004). The three-body model for describing this reaction with the two neutrons is treated as a single d-neutron, e.g. as $^2n+\alpha+X$. Fig. 19 shows the impact of the four-body continuum on the differential cross section for ^{6}He + ^{209}Bi *elastic* scattering (Matsumoto *et al.*, 2006). The four-body continuum leads to an increase in the differential cross section for center-of-mass scattering angles larger than 30°. The inclusion of the four-body continuum has larger impact on the *total reaction* cross section. The three-body CDCC calculation overestimated an optical potential analysis (Aguilera *et al.*, 2000) by 180% while the four-body calculation overestimated by 35%.

2. R-matrix calculations of few-nucleon reactions

Due to the complexity of the NN interaction, only a few approaches (Nollett *et al.*, 2007; Quaglioni and Navrátil, 2008; Suzuki *et al.*, 2009; Viviani *et al.*, 2011) have been applied to the *ab initio* study of nuclear scattering and reactions for $A > 3$ using realistic nuclear interactions. A common theme underpinning these approaches is to divide the configuration space into internal and external regions with the dynamical interactions confined to the internal region.

ECGs have recently been used to construct the interaction region basis in a microscopic R-matrix treatment of few-body nuclear scattering (Aoyama *et al.*, 2012; Arai *et al.*, 2011; Descouvemont and Baye, 2010). The total wave function in the internal region $\Psi^{\pi}_{\mathrm{int}JM}$, where J is the angular momentum and π is the parity, is expanded in terms of the channel functions

$$\Phi^{\pi}_{\alpha JM} = [[\Psi_{I_a} \times \Psi_{I_b}]_I \times F_{aI_abI_b}(r_\alpha) Y_\ell(\hat{\boldsymbol{r}}_\alpha)]_{JM}. \tag{124}$$

The channel wave functions are eigenstates of the total angular momentum of the system and couple the internal wave functions Ψ_{I_a} and Ψ_{I_b} of the fragments with a function describing the radial and angular dependence of the relative motion (vector $\mathbf{r}_\alpha$ connects center of mass of the fragments). The internal channel wave functions are represented by a linear combination of ECGs that are generated by diagonalizing the appropriate realistic NN potential. The wave function $F_{aI_abI_b}(r_\alpha)$ is represented in the interaction region as a set of Gaussians. Outside the interaction region (e.g. outside the R-matrix boundary) the wave function is represented by the appropriate asymptotic form that satisfies a prescribed asymptotic boundary condition.

The equation of motion for the internal region is

$$(H + \mathcal{L} - E)\Psi^{\pi}_{\mathrm{int}JM} = \mathcal{L}\Psi^{\pi}_{\mathrm{ext}JM}, \tag{125}$$

with the Bloch operator

$$\mathcal{L} = \sum_{\alpha} \frac{\hbar^2}{2\mu_\alpha R} |\Phi^{\pi}_{\alpha JM}\rangle \delta(r_\alpha - R) \Big(\frac{\partial}{\partial r_\alpha} - \frac{b_\alpha}{r_\alpha} \Big) r_\alpha \langle \Phi^{\pi}_{\alpha JM}|, \tag{126}$$

where b_α are arbitrary constants. The Bloch operator acts only at the surface R and ensures that the logarithmic derivative of the wave function is continuous at R. A solution of Eq. (125) determines the S-matrix from which cross sections can be computed.

The first few-body system investigated with the R-matrix/ECG approach consisted of reactions related to the four nucleon α-particle system (Aoyama *et al.*, 2012; Arai *et al.*, 2011; Descouvemont and Baye, 2010). The total wave function included the physical channels d+d, t+p, and ^{3}He+n, where d, t and ^{3}He ground states and excited pseudo-states were included in the expansion. Pseudo-states describing nn and pp channels were also added.

The particle transfer reactions for d-d collisions and the radiative capture of deuterons during these collisions are fundamental to an understanding of nuclear fusion. The three most important reactions are ^{2}H$(d,\gamma)^4$He, ^{2}H$(d,n)^3$He and ^{2}H$(d,p)^3$H. The latter two reactions can be directly calculated from the S-matrix coming from a solution of Eq. (125). The first reaction involves an electromagnetic transition matrix element from the scattering state to the ^{4}He ground state, which can be calculated by using first order perturbation theory.

Below the Coulomb barrier, the cross section is strongly dependent on energy dependent kinematic factors. To reduce this energy dependence, it is usual to convert the cross sections into the astrophysical S-factors, defined as

$$S_{J_f\pi_f}(E) = E \exp(2\pi\eta)\sigma_{J_f\pi_f}(E), \tag{127}$$

where $\eta = Z_1 Z_2 e^2/k$ is the Sommerfeld parameter.

Fig. 20 displays the calculated astrophysical S-factor for the ^{2}H$(d,\gamma)^4$He (Arai *et al.*, 2011) reaction. The angular momentum of the deuteron is 1. The radiative capture reaction to the ground state of ^{4}He proceeds from an incoming d+d channel $(^{2I+1}\ell_J)$ by particular electromagnetic multipole transitions: $E1$ for $^3P_1$, $M1$ for $^5D_1$, $E2$ for $^5S_2$, $^1D_2$, and $^5D_2$, etc. Because only the $^5S_2$ channel contains an s-wave scattering wave function, the radiative capture is expected to proceed predominantly via an $E2$ transition at least at low energies.

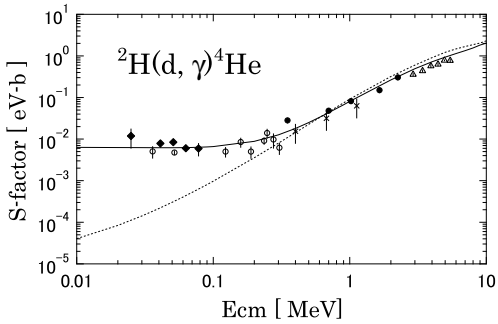

FIG. 20 Astrophysical S-factor of ^{2}H(d,γ)^{4}He reaction. Results with AV8′+3NF (solid line) and Minnesota interaction (Thompson *et al.*, 1977) (dotted line) are compared to experiment (Angulo *et al.*, 1999) (based on Fig 1 from (Arai *et al.*, 2011). The Minnesota interaction is a pure central interaction and due to the lack of tensor potential it does not reproduce the low energy behavior of the S-factor.

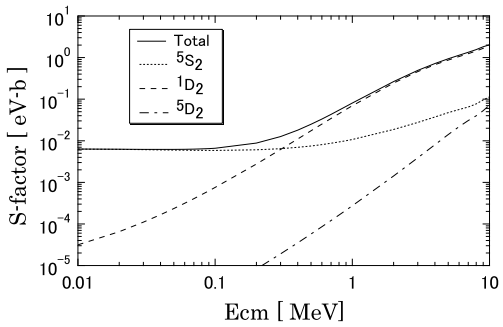

FIG. 21 Contributions of three incoming d+d channels, $^5S_2$, $^1D_2$, and $^5D_2$, to the astrophysical S-factor of the ^{2}H(d,γ)^{4}He reaction calculated with AV8′+3NF potential (taken from (Arai *et al.*, 2011)).

Results with the AV8′+3NF potential reproduce the experimental data very well. The simple Minnesota potential, which does not include the tensor interaction, grossly underestimates $S_{J_f\pi_f}(E)$ at the lowest $E_{\rm cm}$ since the scattering wave function does not have an s-wave at low energies. Fig. 21 shows the contributions of the $^5S_2$, $^1D_2$ and $^5D_2$ incoming dd channels to the S-factor. The first two channels give equal contributions at about 0.3 MeV. Below that energy, the $^5S_2$ channel overwhelms the $^1D_2$ channel as expected, yielding the flat behavior. Above 0.3 MeV, the $^1D_2$ channel contributes more than the $^5S_2$ channel. The contribution of the $^5D_2$ channel is negligible at low energies.

Fig. 22 shows the astrophysical S-factors for the particle transfer reactions, ^{2}H(d,p)^{3}H and ^{2}H(d,n)^{3}He (Arai *et al.*, 2011). All the states with J^π=0$^\pm$, 1$^\pm$, 2$^\pm$ are taken into account

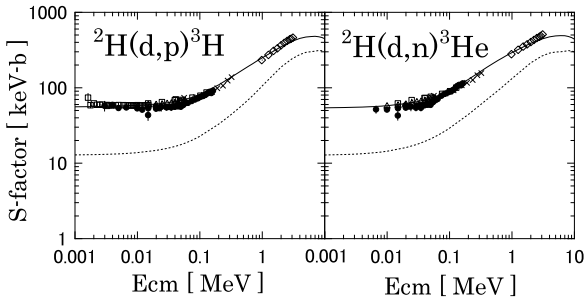

FIG. 22 Astrophysical S-factors of $^2\mathrm{H}(d,p)^3\mathrm{H}$ and $^2\mathrm{H}(d,n)^3\mathrm{He}$ reactions. Results with AV8′+3NF (solid line) and Minnesota interaction (dotted line) are compared to experiment (Angulo *et al.*, 1999; Leonard *et al.*, 2006) (taken from (Arai *et al.*, 2011)).

in the calculation. The results obtained with the realistic AV8'+3NF potential are in very good agreement with experiment. The simpler Minnesota potential grossly underestimated the capture cross section. The cross section at very low energy is found to be dominated by the 2^+ state that contains the transition from the initial $^5S_2$ to the final $^3D_2$ channel.

The R-matrix/ECG model is sufficiently flexible to permit the inclusion of the most important dynamical interactions in the description of the collision. It also permits the use of a modern realistic NN interaction. The excellent agreement with experiment suggests that further applications to other few-body systems might be worthwhile.

C. Complex rotation calculations of resonances

There have been relatively few calculations of resonances with ECG based wave functions. Most of the calculations have been performed with the complex rotation method (Ho, 1983; Moiseyev, 1998; Moiseyev *et al.*, 1978). In the method the Hamiltonian and wave function are transformed by a coordinate rotation

$$\mathbf{r} \;\rightarrow\; \alpha \exp(i\theta)\mathbf{r}. \tag{128}$$

Rotating the coordinates into the complex plane leads to the resonant wave function being made square integrable and accessible to a basis set expansion. When the interactions are purely Coulombic, the complex scaled Hamiltonian can be written as

$$H_\theta = \exp(-2i\theta)T + \exp(-i\theta)V_C, \tag{129}$$

TABLE XXIII Selected frequencies for transitions between states in $\bar{p}^4He^+$. The experimental frequencies (Hori *et al.*, 2006), and frequencies from a Hylleraas type (HYL) calculation (Korobov, 2008) and a GEM calculation (Kino *et al.*, 2003) are listed. Numbers in parentheses are the estimated experimental uncertainties at the 1σ level.

Transition $(n,\ell) \rightarrow (n',\ell')$	Method	Transition frequency (MHz)
(36,34) → (35,33)	Exp.	717 474 004(10)
	HYL	717 474 001.1
	GEM	717 473 893
(35,33) → (34,32)	Exp.	804 633 059(8)
	HYL	804 633 058.1
	GEM	804 633 026
(32,31) → (31,30)	Exp.	1 132 609 209(15)
	HYL	1 132 609 223.5
	GEM	1 132 609 194

where the complex scaling parameter θ is an arbitrary real parameter satisfying the inequality $0 < \theta < \pi/2$. A generalized variational principle (Ho, 1983; Moiseyev, 1998) can be applied to the complex scaled Hamiltonian. Resonant states can be identified by adjusting the θ parameter. The complex energies of scattering states rotate in an approximately circular trajectory on the complex plane at θ is adjusted while resonant state energies show relatively little change as θ changes. The variational principle for the complex scaled Hamiltonian, Eq. (129) is only a stationary principle. There is no guarantee that the calculated position of the resonance is a lower or upper bound for the true value. The energies of scattering states can also slide through the resonance energy during optimization. For these reasons, some of the first complex scaling calculations of resonances using ECGs were performed with the GEM approach without extensive optimization process.

1. Antiprotonic helium

One application of the ECG based GEM has been to the metastable states of the exotic $\bar{p}\mathrm{He}^+$ system (Hayano *et al.*, 2007). These consist of states with the antiproton trapped in highly excited states with large angular momentum ($L \sim 30$). These states are metastable since the antiproton can have an Auger decay resulting in the $\bar{p}\mathrm{He}^{2+}$ state. The transition frequencies between optical transitions provide limits on the accuracy of the antiproton mass.

Table XXIII lists the calculated frequencies of the GEM calculation (Kino *et al.*, 2003) for some selected transitions of the $\bar{p}\mathrm{He}^+$ system and compares them with Hylleraas type (Korobov, 2006) and experiment (Hori *et al.*, 2006). The theoretical transition frequencies do include relativistic corrections. The comparison between theory and experiment yielded an estimate of the antiproton to electron mass ratio of 1836.152674(5) (Hori *et al.*, 2006).

The energies of the Hylleraas type basis are a couple of orders of magnitude more precise than the GEM calculation. This is expected since $\bar{p}\mathrm{He}^+$ is a three-body system. The GEM calculations were performed in double precision arithmetic and it would be possible to improve the accuracy by adopting quadruple precision arithmetic as is done in the Hylleraas type calculations. The GEM calculation acts as an independent validation of the more precise Hylleraas type calculation.

2. Complex Scaling calculation with SVM

Recently a modified and more sophisticated SVM optimization process was developed to improve resonance parameters as the basis set increases (Mezei *et al.*, 2007). Test calculations of the lowest resonances for the Ps^-, H^- systems (p, p, μ^-) and the two-dimensional He atoms using a modified SVM gave resonance energies and widths that were in very good agreement with the best calculations in the literature.

In semiconductors the relevant charged particles are electrons in the conduction band and holes in the valence band. A vacancy in the valence band is called a hole and has equal but opposite charge to the electron. For small energies the holes and electrons can be described as free particles having an effective mass which varies from material to material. In general the hole mass (m_h) is larger than the electron mass m_e, e.g., in GaAs m_h/m_0=0.34 and $m_e/m_0 = 0.067$, where m_0 is the electron mass in vacuum. The bound electron-hole system

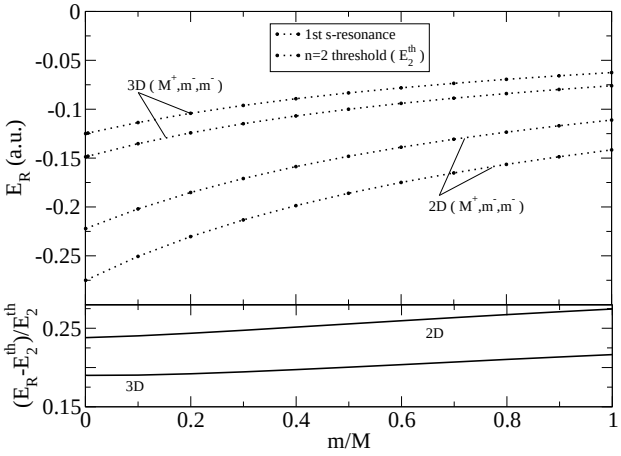

FIG. 23 The position (real part of the energy) of the resonance state as the function of the mass ratio for negatively charged trions in 2D and 3D. The resonance energy is given by $E_R - \frac{i}{2}\Gamma$. The second thresholds are also shown both for 2D and 3D systems.

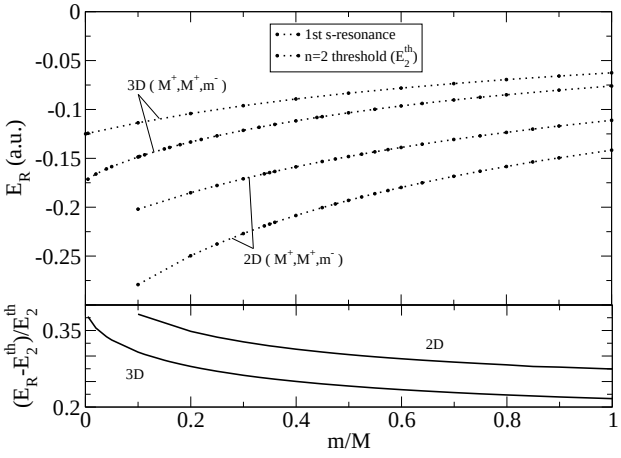

FIG. 24 The position (real part of the energy) of the resonance state as the function of the mass ratio for positively charged trions in 2D and 3D. The resonance energy is given by $E_R - \frac{i}{2}\Gamma$. The second thresholds are also shown both for 2D and 3D systems.

is called an exciton. When an additional charge binds to such an exciton, it forms a charged exciton (trion). We distinguish between negative (X^-) and positive (X^+) trions depending on whether an electron or a hole is added.

Knowing that these Coulombic systems have infinite number of resonances accumulating

at thresholds, in order to perform the study of mass dependence we have chosen the resonance closest to the $N = 1$ threshold. The position of this resonance for the $X^- = (m_h^+, m_e^-, m_e^-)$ and $X^+ = (m_h^+, m_h^+, m_e^-)$ systems as the function of the mass ratio are shown in Figs. 23 and 24. The $n = 2$ thresholds (both 2D and 3D) are also shown. The position of the resonance E_R in both cases shows a very smooth behavior. In the case of X^- it runs almost parallel with the threshold. This is shown in the lower part of Fig. 23 and 24, where the quantity $(E_R - E_2^{\rm th})/E_2^{\rm th}$ is plotted, where $E_2^{\rm th}$ is the second threshold.

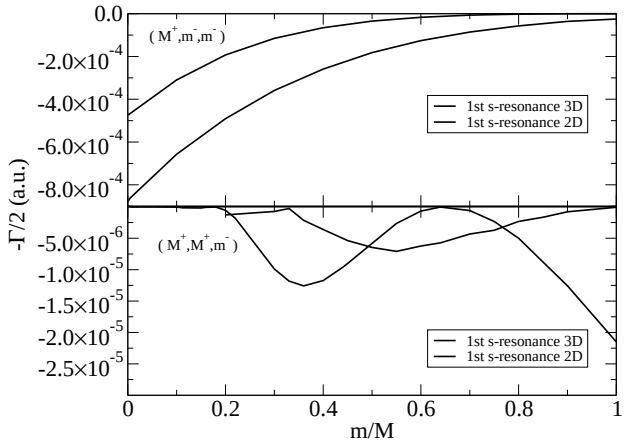

FIG. 25 The imaginary part of the energy of the resonance state as the function of the mass ratio for positively and negatively charged trions in 2D and 3D. The resonance energy is given by $E_R - \frac{i}{2}\Gamma$.

The width of the resonance Γ is also smooth as the function of the mass ratio in the case of X^-. In contrast, there are interesting variations in the X^+ case. In the 3D case, around $\sigma = 0.64$, the width of the state becomes very narrow (large lifetime). These changes may be due to a structural change: a molecule like system is transformed into an atom like system by changing the mass ratio. From Fig. 25 we may conclude that the X^+ system is generally more stable than the X^-.

One can observe that for an atom-like anion system (X^-) the resonance width is insensitive to the dimensionality. The 2D and 3D results have the same tendency. This outcome is in agreement with the conclusion of work (Madroero *et al.*, 2005) where the He atom was investigated both in 2D and in 3D. However, for molecule-like cation system the dimensionality strikingly influences the resonance width. The 2D and the 3D results behave differently

as a function of the mass ratio.

3. Electric dipole response of ^{4}He

Another application of the ECG+GVR approach to continuum problems was the electric dipole response of ^{4}He computed using the complex scaling method (Horiuchi *et al.*, 2012; Moiseyev, 1998). Application of the CSM in nuclear physics is not trivial (Witała and Glöckle, 1999), because the NN potential contains an exponential form $\mathrm{e}^{-\rho r}$. This transform to $\mathrm{e}^{-\rho r(\cos\theta + i\sin\theta)}$ upon coordinate rotation extending to large distances as θ increases.

The response function due to the electric dipole operator $\mathcal{E}_{1\mu}$ acting on the initial state Ψ^+_{00} reads

$$\begin{aligned} S(E) &= \sum_{\mu f} |\langle \Psi^-_{J_f M_f} | \mathcal{E}_{1\mu} | \Psi^+_{00} \rangle|^2 \delta(E_f - E_0 - E) \\ &= -\frac{1}{\pi} \sum_{\mu} \mathrm{Im} \langle \Psi^+_{00} | \mathcal{E}^\dagger_{1\mu} \frac{1}{E - H + E_0 + i\epsilon} \mathcal{E}_{1\mu} | \Psi^+_{00} \rangle, \end{aligned} \tag{130}$$

where the $\sum_{\mu f}$ represents a sum over all bound states and an integration over the continuum over all possible final states with energy E_f and magnetic projection, M_f. The summation over the final states is performed using the closure relation, resulting in the resolvent $1/(E - H + E_0 + i\epsilon)$.

After the rotation $U(\theta)$ of the coordinate and momentum on a complex plane by the angle θ, the resolvent of CSM can be expanded in terms of the eigenfunctions of the rotated Hamiltonian $H(\theta) = U(\theta) H U^{-1}(\theta)$ (Aoyama *et al.*, 2006; Suzuki *et al.*, 2010):

$$H(\theta) \Psi^-_{J_f M_f \kappa}(\theta) = E^\kappa_{J_f}(\theta) \Psi^-_{J_f M_f \kappa}(\theta). \tag{131}$$

A key point is that $\Psi^-_{J_f M_f \kappa}(\theta)$ is bound in a suitable range of β and can be obtained in a combination of square-integrable functions like the ECG.

The observed photo-absorption cross section is related to $S(E)$ by

$$\sigma_\gamma(E) = \frac{4\pi^2}{3\hbar c} E S(E). \tag{132}$$

Fig. 26 compares results of CSM calculation with experiment for $\sigma_\gamma(E)$. The agreement between theory and experiment is satisfactory. The calculation reproduces the energy and height of the peak of most of the data, with one exception (Shima *et al.*, 2005). The

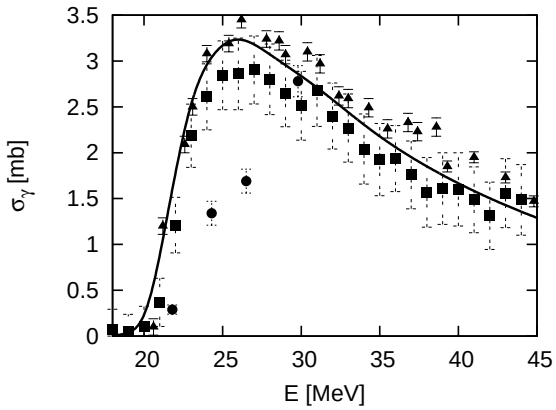

FIG. 26 Photo-absorption cross section computed using CSM with θ=17°. AV8′+3NF potential is used. Experimental data are taken from Refs. (Arkatov, 1974) (closed triangle), (Shima *et al.*, 2005) (closed circle), (Nilsson, 2007) (open circle), (Tornow, 2011) (open triangle). (based on Figure 9 of (Horiuchi *et al.*, 2012)). The last two data are obtained by doubling the (γ, n) and (γ, p) cross sections, respectively. Photo-absorption cross section using the CSM with θ=17°. AV8′+3NF potential is used. Experimental data are taken from Refs. (Arkatov, 1974) (triangle), (Shima et al., 2005) (circle), and (Nakayama, 2007) (square)." ,where the Ref. (Nakayama, 2007) is S. Nakayama et al. Phys. Rev. C 76 021305 (2007).

ECG based calculation gives results are consistent with other calculations using different methods (Gazit *et al.*, 2006; Quaglioni and Navrátil, 2007).

D. Outlook

So far there have been fewer applications of ECG basis sets to scattering problems than to bound state calculations. One common feature of these applications has been that they generally been to scattering systems that would be difficult to describe by other methods, for example having a target and projectile with internal structure. The embedding of ECGs into a conventional scattering theory such as the R-matrix for the $4N$ class of systems constitutes a significant achievement.

The possibility exists for accurate calculations of low energy nuclear reactions and scattering for systems with $N < 8$ using microscopic NN interactions. The target and projectile internal wave functions can be described with ECGs while the relative motion between the fragments can be described by gaussians. This will assist in one of the over-arching goals

TABLE XXIV Relative performance of selected approaches to solving various few-body systems.

System/Property	Hylleraas	CI and related Methods	Hyperspherical	QMC	ECG methods
Atomic systems $N \leq 3$	Extreme precision	Good	Rarely used	Good	High precision
Atomic systems $4 \leq N \leq 6$	Not used	Very Good	Hardly used	Good	Excellent
Single cluster systems	Good	Fair	Excellent	Very Good	Excellent
Double cluster systems	Fair	Poor	Poor	Very Good	Excellent
Small Molecular Systems	Only for H_2	Good	Hardly Used	Good	Excellent
Scattering	Excellent for Resonances	Very Good	Excellent	Good for difficult systems	Good for difficult systems
Cold Atoms	Hardly used	Hardly used	Excellent	Excellent	Excellent
Electronic Quantum dots	Hardly used	Very Good	Hardly used	Very Good	Very good
Excitons and related systems	Hardly used	Hardly used	Hardly used	Very good	Excellent
Nuclear and sub-nuclear systems ($N \leq 5$)	Hardly used	Very Good	Hardly used	Very Good	Very good
All systems ($N > 6$)	Not used	Very good	Not used	Excellent	Rarely used

of theoretical nuclear physics, namely the description description of nuclear structure and dynamics starting from first principles calculations.

X. CONCLUSIONS

Quantum mechanical few-body studies have played a key role in nearly all areas of physics and chemistry since the very early days of quantum mechanics. Over the years, a large number of analytical and numerical approaches have been developed to solve few-body bound state and scattering problems of various complexity. A subset of approaches builds, like ECG based approaches, on the variational principle and expands, in one way or another, the non-relativistic or relativistic few-body wave function in terms of a conveniently chosen basis set. Other approaches are based on the propagation in imaginary time, semi-classical ideas, or on effective low-energy Hamiltonian derived within the frameworks of "standard" quantum mechanics or effective field theory.

The preceding sections have seen significant applications of ECG based approaches to atomic structure, exotic atoms, quantum chemistry, nuclear structure, soft condensed matter physics, cold atom physics and few-body collision physics. The reason for this success over such a variety of different quantum systems relies on three features inherent to ECGs. First,

the center of mass motion of the system is easily removed. Next, the matrix elements of any one- or two-body operator reduce at most to a one dimensional numerical integral multiplied by a factor that can be obtained by standard matrix operations. Finally, the ECG is democratic in nature in that the interactions between all pairs of particles are given equal prominence. The inherent flexibility of the ECG basis means that they are capable of adapting to accommodate different inter-particle masses and almost all interactions.

ECG basis sets have been applied to generate very accurate wave functions for systems with N = 3–7. They have not achieved the hyper-accuracy achievable with Hylleraas techniques for N=3 Coulombic systems, but achieving twelve significant figures for the helium ground state energy is certainly very respectable. The real advantage of ECGs becomes apparent when N=4. For example, the fully *ab-initio* calculations for the H_2 molecule without making the BO approximation stands as a significant achievement in the technology of computational few-body physics. Looking at N=5, the SVM was used to demonstrate that e^+Li was electronically stable and solved a long-standing problem in positron physics. At the present time, the only other *ab initio* calculation for this system is a DMC calculation which underestimates the binding energy by 5%.

In general, scattering calculations are more challenging than bound state calculations, and there have been relatively few applications of ECG based approaches to scattering calculations until recently. However, ECGs have now been embedded into scattering calculations based on the regular and hyperspherical-harmonic R-matrix approaches. These are very significant developments since ECG basis sets can now be utilized in general treatments of reactive and rearrangement collisions for systems with N=3 and 4. For three-body systems, ECG based approaches are not, at least not in general, competitive with DVR, finite-element, or B-spline based approaches, which can treat a large number of closed and open channels out to large interparticle separations with good to excellent accuracy. ECG based approaches have, however, proven to be competitive for certain four-body systems. A recent ECG based development, for example, formulated the four-body scattering problem within the hyperspherical framework, which goes back to Fano and has helped in many instances to elucidate the underlying physical mechanisms. In the future, it will be interesting to further refine ECG based scattering calculations for four-body systems, within the regular R-matrix and hyperspherical frameworks, and to extent the formalisms to treating five- and six-body scattering problems.

One of the unusual features about ECG research is that there has been a large number of application results arising from the efforts of a relatively small number of research groups. This might change in the future as one could expect that ECGs will become widely used in the field of few-body physics as there is more appreciation of their remarkable adaptability.

Acknowledgments

W.H. and Y.S. thank S. Aoyama and K. Arai for discussions and help that were vital to complete the manuscript. One of us, J.M. thanks Dr G. G. Ryzhikh for correcting his prejudices regarding the use of exponential basis functions with arguments consisting of quadratic factors in the interparticle distances. The work of J.M. was supported in part by the Australian Research Council Discovery Project DP-1092620. The work of Y.S. is in part supported by a Grant-in-Aid for Scientific Research (No. 21540261) of Japan Society for the Promotion of Science. The work of W.C. and K.S. was supported by the National Science Foundation grant CHE-0848589. J.K. acknowledges support by the Polish Ministry of Science and Higher Education Grant No. N N204 015338 and by a computing grant from Poznań Supercomputing and Networking Center. D.B. gratefully acknowledges support by the NSF through grant PHY-0855332.

References

Adamowicz, L., 1978, Int. J. Quantum Chem. **13**, 265.

Adamowicz, L., and A. J. Sadlej, 1978, J. Chem. Phys. **69**, 3992.

Adler, T. B., G. Knizia, and H.-J. Werner, 2007, J. Chem. Phys. **127**, 221106.

Aguilera, E. F., J. J. Kolata, F. D. Becchetti, P. A. DeYoung, J. D. Hinnefeld, A. Horváth, L. O. Lamm, H.-Y. Lee, D. Lizcano, E. Martinez-Quiroz, P. Mohr, T. W. O'Donnell, *et al.*, 2001, Phys. Rev. C **63**, 061603.

Aguilera, E. F., J. J. Kolata, F. M. Nunes, F. D. Becchetti, P. A. DeYoung, M. Goupell, V. Guimarães, B. Hughey, M. Y. Lee, D. Lizcano, E. Martinez-Quiroz, A. Nowlin, *et al.*, 2000, Phys. Rev. Lett. **84**, 5058.

Ahn, K. *et al.*., 2001, in *American Institute of Physics Conference Series*, edited by I. T. *et al.* Cheonet (American Institute of Physics, New York, USA), volume 594 of *American Institute of*

Physics Conference Series, p. 180.

Al-Hujaj, O.-A., and P. Schmelcher, 2003, Phys. Rev. A **67**, 023403.

Alexander, S. A., H. J. Monkhorst, R. Roeland, and K. Szalewicz, 1990, J. Chem. Phys. **93**, 4230.

Alexander, S. A., H. J. Monkhorst, R. D. Roeland, and K. Szalewicz, 1990, J. Chem. Phys. **93**, 4230.

Alexander, S. A., H. J. Monkhorst, and K. Szalewicz, 1986, J. Chem. Phys. **85**, 5821.

Alexander, S. A., H. J. Monkhorst, and K. Szalewicz, 1988, J. Chem. Phys. **89**, 355.

Ali, S., 1966, Nucl. Phys. A **80**, 99.

Almora-Diaz, C. X., and C. F. Bunge, 2010, Int. J. Quant. Chem. **110**, 2982.

Amado, R. D., and F. C. Greenwood, 1973, Phys. Rev. D **7**, 2517.

Anderson, J. B., 2004, J. Chem. Phys. **120**, 9886.

Angel, J. R. P., E. F. Borra, and J. D. Landstreet, 1981, Astrophys. J. **45**, 457.

Angulo, C., M. Arnould, M. Rayet, P. Descouvemont, D. Baye, C. Leclercq-Willain, A. Coc, S. Barhoumi, P. Aguer, C. Rolfs, R. Kunz, J. W. Hammer, *et al.*, 1999, Nucl. Phys. A **656**, 3.

Aoyama, S., K. Arai, Y. Suzuki, P. Descouvemont, and D. Baye, 2012, Few. Body Sys. **52**, 97.

Aoyama, S., T. Myo, K. Katō, and K. Ikeda, 2006, Prog. Theor. Phys. **116**, 1.

Arai, K., S. Aoyama, Y. Suzuki, P. Descouvemont, and D. Baye, 2011, Phys. Rev. Lett. **107**, 132502.

Arai, K., Y. Ogawa, Y. Suzuki, and K. Varga, 2001, Prog. Theor. Phys. Supplement **142**, 97.

Araki, H., 1958, Prog. Theor. Phys. **17**, 619.

Arkatov, Y. M. *et al.*., 1974, Yad. Fiz. **19**, 1172.

Armour, E. A. G., and D. J. Baker, 1986, J. Phys. B **19**, L871.

Armour, E. A. G., J. N. Cooper, M. R. Gregory, S. Jonsell, M. Plummer, and A. C. Todd, 2010, J. Phys. Conference Series **199**, 012007.

Austern, N., Y. Iseri, M. Kamimura, M. Kawai, G. Rawitscher, and M. Yahiro, 1987, Phys. Rep. **154**, 125.

Bachorz, R., W. Cencek, R. Jaquet, and J. Komasa, 2009, J. Chem. Phys. **131**, 024105.

Barnea, N., W. Leidemann, and G. Orlandini, 2000, Phys. Rev. C **61**, 054001.

Bartlett, R. J., and M. Musiał, 2007, Rev. Mod. Phys. **79**, 291.

Baye, D., P. Capel, P. Descouvemont, and Y. Suzuki, 2009, Phys. Rev. C **79**, 024607.

Ben-Itzhak, I., E. Wells, K. D. Carnes, V. Krishnamurthi, O. L. Weaver, and B. D. Esry, 2000,

Phys. Rev. Lett. **85**, 58.

Bendazzoli, G. L., and A. Monari, 2004, Chem. Phys. **306**, 153.

Bethe, H. A., and E. E. Salpeter, 1977, *Quantum mechanics of one- and two-electron atoms* (Plenum, New York).

Birkedal, D., J. Singh, V. G. Lyssenko, J. Erland, and J. M. Hvam, 1996, Phys. Rev. Lett. **76**, 672.

Blanco, M., and E. J. Heller, 1983, J. Chem. Phys. **78**(5), 2504.

Blankenbecler, R., D. J. Scalapino, and R. L. Sugar, 1981, Phys. Rev. D **24**, 2278.

Bloch, I., J. Dalibard, and W. Zwerger, 2008, Rev. Mod. Phys. **80**, 885.

Blume, D., and K. M. Daily, 2009, Phys. Rev. A **80**, 053626.

Blume, D., and K. M. Daily, 2010a, Phys. Rev. Lett. **105**, 170403.

Blume, D., and K. M. Daily, 2010b, Phys. Rev. A **82**, 063612.

Blume, D., and K. M. Daily, 2011, C. R. Physique **12**, 86.

Blume, D., and C. H. Greene, 2000, J. Chem. Phys. **112**, 8053.

Blume, D., J. von Stecher, and C. H. Greene, 2007, Phys. Rev. Lett. **99**, 233201.

Bolton, F., 1996, Phys. Rev. B **54**, 4780.

Bonifacic, V., and J. Huzinga, 1974, J. Chem. Phys. **60**, 7.

Boninsegni, M., N. V. Prokof'ev, and B. V. Svistunov, 2006, Phys. Rev. E **74**, 036701.

Boys, S. F., 1950, Proc. Roy. Soc. London, Ser. A **200**, 542.

Boys, S. F., 1960, Proc. R. Soc. London, Ser. A **258**, 402.

Braaten, E., and H.-W. Hammer, 2006, Phys. Rep. **428**, 259.

Bressanini, D., M. Mella, and G. Morosi, 1997, Phys. Rev. A **55**, 200.

Bressanini, D., M. Mella, and G. Morosi, 1998, Phys. Rev. A **57**, 4956.

Brinkmann, K., and H. Kleindienst, 1991, J. Math. Chem. **6**, 267.

Bromley, M. W. J., and J. Mitroy, 2002a, Phys. Rev. A **65**, 062506.

Bromley, M. W. J., and J. Mitroy, 2002b, Phys. Rev. A **66**, 062504.

Bromley, M. W. J., and J. Mitroy, 2006a, Phys. Rev. Lett. **97**, 183402.

Bromley, M. W. J., and J. Mitroy, 2006b, Phys. Rev. A **73**, 032507.

Bromley, M. W. J., and J. Mitroy, 2007a, Int. J. Quantum Chem. **107**, 1150.

Bromley, M. W. J., and J. Mitroy, 2007b, Phys. Rev. A **75**, 042506.

Bromley, M. W. J., and J. Mitroy, 2010, Phys. Rev. A **81**, 052708.

Bubin, S., and L. Adamowicz, 2004, J. Chem. Phys. **121**, 6249.

Bubin, S., and L. Adamowicz, 2006, J. Chem. Phys. **124**, 224317.

Bubin, S., and L. Adamowicz, 2007, J. Chem. Phys. **126**, 214305.

Bubin, S., and L. Adamowicz, 2008, J. Chem. Phys. **128**, 114107.

Bubin, S., and L. Adamowicz, 2009, Phys. Rev. A **79**, 022501.

Bubin, S., and L. Adamowicz, 2011, Phys.Rev. A **83**, 022505.

Bubin, S., L. Adamowicz, and M. Molski, 2005a, J. Chem. Phys. **123**, 134310.

Bubin, S., E. Bednarz, and L. Adamowicz, 2005b, J. Chem. Phys. **122**, 041102.

Bubin, S., M. Cafiero, and L. Adamowicz, 2005c, Adv. Chem. Phys. **131**, 377.

Bubin, S., J. Komasa, M. Stanke, and L. Adamowicz, 2009a, J. Chem. Phys. **131**, 234112.

Bubin, S., J. Komasa, M. Stanke, and L. Adamowicz, 2010a, Phys. Rev. A **81**, 052504.

Bubin, S., J. Komasa, M. Stanke, and L. Adamowicz, 2010b, J. Chem. Phys. **132**, 114109.

Bubin, S., F. Leonarski, M. Stanke, and L. Adamowicz, 2009b, Chem. Phys. Lett. **477**, 12 .

Bubin, S., M. Stanke, and L. Adamowicz, 2009c, J. Chem. Phys. **131**, 044128.

Bubin, S., M. Stanke, and L. Adamowicz, 2010c, Chem. Phys. Lett. **500**, 229 .

Bubin, S., M. Stanke, and L. Adamowicz, 2011a, J. Chem. Phys. **135**, 074110.

Bubin, S., M. Stanke, and L. Adamowicz, 2011b, Phys. Rev. A **83**, 042520.

Bubin, S., M. Stanke, and L. Adamowicz, 2011c, J. Chem. Phys. **134**, 024103.

Bubin, S., M. Stanke, D. Kędziera, and L. Adamowicz, 2007, Phys. Rev. A **75**, 062504.

Bubin, S., and K. Varga, 2011, Phys. Rev. A **84**, 012509.

Buck, B., H. Friedrich, and C. Wheatley, 1977, Nucl. Phys. A **275**, 246.

Bukowski, R., W. Cencek, P. Jankowski, M. Jeziorska, B. Jeziorski, S. A. Kucharski, V. F. Lotrich, A. J. Misquitta, R. Moszyński, K. Patkowski, R. Podeszwa, S. Rybak, *et al.*, 2011, SAPT2011: An *ab initio* program for many-body symmetry-adapted perturbation theory calculations of intermolecular interaction energies, University of Delaware and University of Warsaw, URL http://www.physics.udel.edu/~szalewic/SAPT/SAPT.html.

Bukowski, R., B. Jeziorski, R. Moszyński, and W. Kołos, 1992, Int. J. Quantum Chem. **42**, 287.

Bukowski, R., B. Jeziorski, S. Rybak, and K. Szalewicz, 1995, J. Chem. Phys. **102**, 888.

Bukowski, R., B. Jeziorski, and K. Szalewicz, 1994, J. Chem. Phys. **100**, 1366.

Bukowski, R., B. Jeziorski, and K. Szalewicz, 1996, J. Chem. Phys. **104**, 3306.

Bukowski, R., B. Jeziorski, and K. Szalewicz, 1999, J. Chem. Phys. **110**, 4165.

Bukowski, R., B. Jeziorski, and K. Szalewicz, 2003, in *Explicitly Correlated Functions in Chemistry*

and Physics, edited by J. Rychlewski (Kluwer, Dordrecht), pp. 185–248.

Bunge, C. F., 2010, Theor. Chem. Acc. **126**, 139.

Burke, P. G., and C. J. Joachain, 1995, *Theory of electron-atom collisions. Part 1 potential scattering* (Plenum, New York).

Busch, T., B.-G. Englert, K. Rzążewski, and M. Wilkens, 1998, Foundations of Phys. **28**, 549.

Cafiero, M., and L. Adamowicz, 2001, Int. J. Quantum Chem. **82**, 151.

Campargue, A., S. Kassi, K. Pachucki, and J. Komasa, 2011, Phys. Chem. Chem. Phys. In press.

Canter, K. F., J. D. McNutt, and L. O. Roellig, 1975, Phys. Rev. A **12**, 375.

Carrington, A., I. R. McNab, C. A. Montgomerie-Leach, and R. A. Kennedy, 1991, Mol. Phys. **72**, 735.

Carroll, D. P., H. J. Silverstone, and R. P. Metzger, 1979, J. Chem. Phys. **71**, 4142.

Caswell, W. E., and G. P. Lepage, 1986, Phys. Lett. B **167**, 437.

Cencek, W., M. Jeziorska, R. Bukowski, M. Jaszuński, B. Jeziorski, and K. Szalewicz, 2004, J. Phys. Chem. A **108**, 3211.

Cencek, W., J. Komasa, K. Pachucki, and K. Szalewicz, 2005, Phys. Rev. Lett. **95**, 233004.

Cencek, W., J. Komasa, and J. Rychlewski, 1995, Chem. Phys. Lett. **246**, 417.

Cencek, W., J. Komasa, and K. Szalewicz, 2011, J. Chem. Phys. **135**, 014301.

Cencek, W., and W. Kutzelnigg, 1996, J. Chem. Phys **105**, 5878.

Cencek, W., and J. Rychlewski, 1993, J. Chem. Phys. **98**, 1252.

Cencek, W., and J. Rychlewski, 1995, J. Chem. Phys. **102**, 2533.

Cencek, W., and J. Rychlewski, 2000, Chem. Phys. Lett. **320**, 549.

Cencek, W., J. Rychlewski, R. Jaquet, and W. Kutzelnigg, 1998, J. Chem. Phys. **108**, 2831.

Cencek, W., and K. Szalewicz, 2008, Int. J. Quantum Chem. **108**, 2191.

Cencek, W., K. Szalewicz, and B. Jeziorski, 2001, Phys. Rev. Lett. **86**, 5675.

Ceperley, D., and B. Alder, 1986, Science **231**, 555.

Ceperley, D. M., 1995, Rev. Mod. Phys. **67**, 279.

Ceperley, D. M., and B. J. Alder, 1984, J. Chem. Phys. **81**, 5833.

Chakravorty, S. J., S. R. Gwaltney, E. R. Davidson, F. A. Parpia, and C. F. P. Fischer, 1993, Phys. Rev. A **47**, 3649.

Chalasinski, G., B. Jeziorski, J. Andzelm, and K. Szalewicz, 1977, Mol. Phys. **33**, 971.

Challacombe, M., and J. Cioslowski, 1994, J. Chem. Phys. **100**, 464.

Charlton, M., 1985, Rep. Prog. Phys. **48**, 737.

Charlton, M., and J. W. Humberston, 2001, *Positron Physics* (Cambridge University Press, Cambridge, UK).

Chen, B., and J. B. Anderson, 1995, J. Chem. Phys. **102**, 4491.

Chernykh, M., H. Feldmeier, T. Neff, P. von Neumann-Cosel, and A. Richter, 2007, Phys. Rev. Lett. **98**, 032501.

Chin, C., R. Grimm, P. Julienne, and E. Tiesinga, 2010, Rev. Mod. Phys. **82**, 1225.

Cioslowski, J., and R. Lopez-Boada, 1998, J. Chem. Phys. **109**, 1230.

Cizek, J., 1966, J. Chem. Phys. **45**, 4256.

Clary, D. C., and N. C. Handy, 1977, Chem. Phys. Lett. **51**, 483.

Coleman, P. G., T. C. Griffith, G. R. Heyland, and T. L. Killeen, 1975, J. Phys. B **8**, L185.

Cooper, J. N., E. A. G. Armour, and M. Plummer, 2008, J. Phys. B **41**, 245201.

Cooper, J. N., E. A. G. Armour, and M. Plummer, 2009, J. Phys. A **42**, 095207.

Dahle, P., T. Helgaker, D. Jonsson, and P. R. Taylor, 2007, Phys. Chem. Chem. Phys. **9**, 3112.

Daily, K. M., and D. Blume, 2010, Phys. Rev. A **81**, 053615.

Dalfovo, F., S. Giorgini, L. P. Pitaevskii, and S. Stringari, 1999, Rev. Mod. Phys. **71**, 463.

Danby, G., and J. Tennyson, 1988, Phys. Rev. Lett. **61**, 2737.

de Miranda, M. H. G., A. Chotia, B. Neyenhuis, D. Wang, G. Quemener, S. Ospelkaus, J. L. Bohn, J. Ye, and D. S. Jin, 2011, Nat. Phys. **7**, 502.

Deltuva, A., 2011a, Europhys. Lett. **95**, 43002.

Deltuva, A., 2011b, Phys. Rev. A **84**, 022703.

Descouvemont, P., and D. Baye, 2010, Rep. Prog. Phys. **73**, 036301.

D'Incao, J. P., J. von Stecher, and C. H. Greene, 2009, Phys. Rev. Lett. **103**, 033004.

Drachman, R. J., 1981, J. Phys. B **14**, 2733.

Drake, G. W. F., 1987, Phys. Rev. Lett. **59**, 1549.

Drake, G. W. F., 1996, *Handbook of Atomic, Molecular and Optical Physics* (American Institute of Physics, New York).

Drake, G. W. F., M. M. Cassar, and R. A. Nistor, 2002, Phys. Rev. A **65**, 054501.

Druin, A., 2010, in *International Conference on High Resolution Molecular Spectroscopy, Poznań, Sept. 7-11*, Jet Propulsion Laboratory (THz spectroscopy for space applications).

Duff, B. G., and F. F. Heyman, 1962, Proc. Phys. Soc. London, Ser. A **517**, 281.

Dzuba, V. A., V. V. Flambaum, G. F. Gribakin, and W. A. King, 1995, Phys. Rev. A **52**, 4541.

Efimov, V., 1970, Phys. Lett. **33B**, 563.

Efimov, V. N., 1973, Nucl. Phys. A **210**, 157.

Egami, T., K. Ogata, T. Matsumoto, Y. Iseri, M. Kamimura, and M. Yahiro, 2004, Phys. Rev. C **70**, 047604.

Egger, R., W. Häusler, C. H. Mak, and H. Grabert, 1999, Phys. Rev. Lett. **82**, 3320.

Epelbaum, E., H.-W. Hammer, and U.-G. Meißner, 2009, Rev. Mod. Phys. **81**, 1773.

Fabre de La Ripelle, M., 1983, Annals of Physics **147**, 281.

Fasth, C., A. Fuhrer, L. Samuelson, V. N. Golovach, and D. Loss, 2007, Phys. Rev. Lett. **98**, 266801.

Feldmeier, H., W. Horiuchi, T. Neff, and Y. Suzuki, 2011, ArXiv e-prints eprint 1107.4956.

Fellmuth, B., C. Gaiser, and J. Fischer, 2006, Meas. Sci. Technol. **17**, 145.

Ferlaino, F., 2011, talk at 42nd Annual Meeting of the APS Division of Atomic, Molecular and Optical Physics (June 13-17, 2011; Atlanta, Georgia).

Ferlaino, F., S. Knoop, M. Berninger, W. Harm, J. P. D'Incao, H.-C. Nägerl, and R. Grimm, 2009, Phys. Rev. Lett. **102**, 140401.

Fischer, J., and B. Fellmuth, 2005, Rep. Prog. Phys. **68**, 1043.

Fletcher, R., 1987, *Practical Methods of optimization (2nd Ed.)*, volume I (Wiley, New York).

Forest, J., V. pandharipande, S. Pieper, R. Wiringa, R. Schiavilla, and A. Arriaga, 1996, Phys. Rev. C **54**, 646.

Frolov, A. M., and V. H. Smith, Jr., 1995, J. Phys. B **28**, L449.

Fujito, M., A. Natori, and H. Yasunaga, 1996, Phys. Rev. B **53**(15), 9952.

Gadéa, F. X., and T. Leininger, 2006, Theor. Chem. Acct. **116**, 566.

Gazit, D., S. Bacca, N. Barnea, W. Leidemann, and G. Orlandini, 2006, Phys. Rev. Lett. **96**, 112301.

Giorgini, S., L. P. Pitaevskii, and S. Stringari, 2008, Rev. Mod. Phys. **80**, 1215.

Glöckle, W., and H. Kamada, 1993, Phys. Rev. Lett. **71**, 971.

Glozman, L. Y., W. Plessas, K. Varga, and R. F. Wagenbrunn, 1998, Phys. Rev. D **58**, 094030.

Gribakin, G. F., J. A. Young, and C. M. Surko, 2010, Rev. Mod. Phys. **82**, 2557.

Grisenti, R. E., W. Schollkopf, J. P. Toennies, G. C. Hegerfeldt, T. Kohler, and M. Stoll, 2000, Phys. Rev. Lett. **85**, 2284.

Guan, X., and B. Li, 2001, Phys. Rev. A **63**, 043413.

Hadizadeh, M. R., M. T. Yamashita, L. Tomio, A. Delfino, and T. Frederico, 2011, Phys. Rev. Lett. (to appear) .

Hamaguchi, K., T. Hatsuda, M. Kamimura, Y. Kino, and T. T. Yanagida, 2007, Phys. Lett. B **650**, 268.

Hammer, H. W., and L. Platter, 2007, Eur. Phys. J. A **32**, 113.

Hammond, B. L., W. A. Lester, Jr., and P. J. Reynolds, 1994, *Monte Carlo Methods in ab-initio Quantum Chemisty* (World Scientific, Singapore).

Handy, N. C., 1973, Mol. Phys. **26**, 169.

Hanna, G. J., and D. Blume, 2006, Phys. Rev. A **74**, 063604.

Hanson, R., L. P. Kouwenhoven, J. R. Petta, S. Tarucha, and L. M. K. Vandersypen, 2007, Rev. Mod. Phys. **79**, 1217.

Harju, A., V. A. Sverdlov, R. M. Nieminen, and V. Halonen, 1999, Phys. Rev. B **59**, 5622.

Harris, F. E., 1967, Phys. Rev. Lett. **19**, 173.

Harris, F. E., and H. J. Monkhorst, 2006, Int. J. Quantum Chem. **106**(15), 3186.

Hawrylak, P., and D. Pfannkuche, 1993, Phys. Rev. Lett. **70**(4), 485.

Hayano, R. S., M. Hori, D. Horváth, and E. Widmann, 2007, Rep. Prog. Phys. **70**, 1995.

Hazi, A. U., and H. S. Taylor, 1970, Phys. Rev. A **1**, 1109.

Head-Gordon, M., and J. A. Pople, 1988, J. Chem. Phys. **89**, 5777.

Helgaker, T., W. Klopper, and D. P. Tew, 2008, Mol. Phys. **106**, 2107.

Herzberg, G., 1970, J. Mol. Spectrosc. **33**, 147.

Hibbert, A., 1975, Rep. Prog. Phys. **38**, 1217.

Hill, R. N., 1985, J. Chem. Phys. **83**, 1173.

Hill, R. N., 1998, Int. J. Quantum Chem. **68**, 357.

Hiller, J., J. Sucher, and G. Feinberg, 1978, Phys. Rev. A **18**, 2399.

Hirose, K., and N. S. Wingreen, 1999, Phys. Rev. B **59**, 4604.

Hiyama, E., B. F. Gibson, and M. Kamimura, 2004, Phys. Rev. C **70**, 031001.

Hiyama, E., M. Kamimura, A. Hosaka, H. Toki, and M. Yahiro, 2005, Nucl. Phys. A **755**, 411.

Hiyama, E., M. Kamimura, A. Hosaka, H. Toki, and M. Yahiro, 2006, Phys. Lett. B **633**, 237.

Hiyama, E., M. Kamimura, T. Motoba, T. Yamada, and Y. Yamamoto, 2002, Phys. Rev. C **66**, 024007.

Hiyama, E., M. Kamimura, Y. Yamamoto, and T. Motoba, 2010, Phys. Rev. Lett. **104**, 212502.

Hiyama, E., Y. Kino, and M. Kamimura, 2003, Prog. Part. Nucl. Phys. **51**, 223.

Ho, Y. K., 1983, Phys. Rep. **99**, 1.

Ho, Y. K., 1986, Phys. Rev. A **33**, 3584.

Holka, F., P. G. Szalay, J. Fremont, M. Rey, K. A. Peterson, and V. G. Tyuterev, 2011, J. Chem. Phys. **134**, 094306 (pages 14).

Hori, M., A. Dax, J. Eades, K. Gomikawa, R. S. Hayano, N. Ono, W. Pirkl, E. Widmann, H. A. Torii, B. Juhász, D. Barna, and D. Horváth, 2006, Phys. Rev. Lett. **96**, 243401.

Horiuchi, W., and Y. Suzuki, 2006, Phys. Rev. C **74**, 034311.

Horiuchi, W., and Y. Suzuki, 2007, Phys. Rev. C **76**, 024311.

Horiuchi, W., and Y. Suzuki, 2008, Phys. Rev. C **78**, 034305.

Horiuchi, W., Y. Suzuki, and K. Arai, 2012, Phys. Rev. C **85**, 054002, URL http://link.aps.org/doi/10.1103/PhysRevC.85.054002.

Hylleraas, E. A., 1928, Z. Phys. **48**, 469.

Hylleraas, E. A., 1929, Naturwissenschaften **17**, 982.

Hylleraas, E. A., 1929, Z. Phys. **54**, 347.

Hylleraas, E. A., 1930a, Z. Phys. **63**, 297.

Hylleraas, E. A., 1930b, Z. Phys. **65**, 759.

Hylleraas, E. A., 1963, Rev. Mod. Phys. **35**, 421.

Hylleraas, E. A., and A. Ore, 1947, Phys. Rev. **71**, 493.

Ichikawa, A., 2001, Ph.D. thesis, Kyoto University.

Ivanov, I. A., J. Mitroy, and K. Varga, 2001, Phys. Rev. Lett. **87**(6), 063201.

Ivanov, I. A., J. Mitroy, and K. Varga, 2002a, Phys. Rev. A **65**, 032703.

Ivanov, I. A., J. Mitroy, and K. Varga, 2002b, Phys. Rev. A **65**, 022704.

James, H. M., and A. S. Coolidge, 1934, J. Chem. Phys. **1**, 825.

Janzen, A. R., and R. A. Aziz, 1997, J. Chem. Phys. **107**, 914.

Jaquet, R., W. Cencek, W. Kutzelnigg, and J. Rychlewski, 1998, J. Chem. Phys. **108**, 2837.

Jeziorska, M., W. Cencek, K. Patkowski, B. Jeziorski, and K. Szalewicz, 2007, J. Chem. Phys. **127**, 124303.

Jeziorski, B., R. Bukowski, and K. Szalewicz, 1997, Int. J. Quantum Chem. **61**, 769.

Jeziorski, B., H. J. Monkhorst, K. Szalewicz, and J. G. Zabolitzky, 1984, J. Chem. Phys. **81**, 368.

Jeziorski, B., R. Moszyński, and K. Szalewicz, 1994, Chem. Rev. **94**, 1887.

Jeziorski, B., and K. Szalewicz, 1979, Phys. Rev. A **19**, 2360.

Jitrik, O., and C. Bunge, 1997, Phys. Rev. A **56**, 2614.

Jones, M. D., G. Ortiz, and D. M. Ceperley, 1996, Phys. Rev. A **54**, 219.

Jones, M. D., G. Ortiz, and D. M. Ceperley, 1997, Phys. Rev. E **55**, 6202.

Kamada, H., A. Nogga, W. Glöckle, E. Hiyama, M. Kamimura, K. Varga, Y. Suzuki, M. Viviani, A. Kievsky, S. Rosati, J. Carlson, S. C. Pieper, *et al.*, 2001, Phys. Rev. C **64**, 044001.

Kameyama, H., M. Kamimura, and Y. Fukushima, 1989, Phys. Rev. C **40**, 974.

Kamimura, M., 1977, Prog. Theor. Phys. Supplement **62**, 236.

Kamimura, M., 1981, Nucl. Phys. A **351**, 456.

Kamimura, M., 1988, Phys. Rev. A **38**, 621.

Kanada, H., T. Kaneko, S. Nagata, and M. Nomoto, 1979, Prog. Theor. Phys. **61**, 1327.

Karunakaran, K. M., and R. E. Christoffersen, 1977, J. Chem. Phys. **62**, 1992.

Karunakaran, K. M., and R. E. Christoffersen, 1982, Int. J. Quantum Chem. **22**, 11.

Kassi, S., and A. Campargue, 2011, J. Mol. Spectrosc. **267**, 36.

Kato, T., 1957, Commun. Pure. Appl. Math. **10**, 151.

Kellner, D. W., 1927, Z. Phys. **44**, 91.

Kemp, J. C., J. B. Swedlund, J. D. Landstreet, and J. R. P. Angel, 1970, Astrophys. J. Lett. **161**, L77.

Kievsky, A., M. Viviani, P. Barletta, C. Romero-Redondo, and E. Garrido, 2010, Phys. Rev. C **81**, 034002.

King, F. W., D. Quicker, and J. Langer, 2011, J. Chem. Phys. **134**, 124114.

King, H. F., 1967, J. Chem. Phys. **46**, 705.

Kinghorn, D. B., 1996, Int. J. Quantum Chem. **57**, 141.

Kinghorn, D. B., and L. Adamowicz, 1997, J. Chem. Phys. **106**, 4589.

Kinghorn, D. B., and L. Adamowicz, 1999, J. Chem. Phys. **110**, 7166.

Kinghorn, D. B., and L. Adamowicz, 1999, Phys. Rev. Lett. **83**, 2541.

Kinghorn, D. B., and R. D. Poshusta, 1993, Phys. Rev. A **47**, 3671.

Kino, Y., H. Kudo, and M. Kamimura, 2003, Mod. Phys. Letters A **18**, 388.

Kleinman, D. A., 1983, Phys. Rev. B **28**, 871.

Klopper, W., and J. Noga, 2003, in *Explicitly Correlated Wave Functions in Chemistry and Physics*,

edited by J. Rychlewski (Kluwer, Dordrecht), p. 149.

Kohn, A., 2009, J. Chem. Phys. **130**, 131101.

Kolos, W., and J. Rychlewski, 1993, J. Chem. Phys. **98**, 3960.

Kołos, W., and L. Wolniewicz, 1964a, J. Chem. Phys. **41**, 3663.

Kołos, W., and L. Wolniewicz, 1964b, J. Chem. Phys. **41**, 3674.

Kołos, W., and L. Wolniewicz, 1965, J. Chem. Phys. **43**, 2429.

Kolos, W., and L. Wolniewicz, 1968, J. Chem. Phys. **49**, 404.

Komasa, J., 2002, Phys. Rev. A **65**, 012506.

Komasa, J., W. Cencek, and J. Rychlewski, 1995, Phys. Rev. A **52**, 4500.

Komasa, J., K. Piszczatowski, G. Lach, M. Przybytek, B. Jeziorski, and K. Pachucki, 2011, J. Chem. Theory Comput. **7**, 3105.

Komasa, J., and J. Rychlewski, 2001, Chem. Phys. Lett. **342**, 185 .

Komasa, J., J. Rychlewski, and K. Jankowski, 2002, Phys. Rev. A **65**, 042507.

Komasa, J., and A. J. Thakkar, 1995, J. Mol. Struct. THEOCHEM **343**, 43 .

Korobov, V. I., 2000, Phys. Rev. A **61**, 064503.

Korobov, V. I., 2002, Phys. Rev. A **66**, 024501.

Korobov, V. I., 2006, Phys. Rev. A **73**, 022509.

Korobov, V. I., 2008, Phys. Rev. A **77**, 042506.

Korona, T., H. L. Williams, R. Bukowski, B. Jeziorski, and K. Szalewicz, 1997, J. Chem. Phys. **106**, 5109.

Koskinen, M., M. Manninen, and S. M. Reimann, 1997, Phys. Rev. Lett. **79**(7), 1389.

Kosztin, I., B. Faber, and K. Schulten, 1996, Am. J. Phys. **64**, 633.

Kouwenhoven, L. P., D. G. Austing, and S. Tarucha, 2001, Rep. Prog. Phys. **64**(6), 701.

Kozlowski, P. M., and L. Adamowicz, 1992, J. Chem. Phys. **96**(12), 9013.

Kozlowski, P. M., and L. Adamowicz, 1995, Int. J. Quantum Chem. **55**(5), 367.

Kramida, A., and W. C. Martin, 1997, J. Phys. Chem. Reference Data **26**, 1185.

Krivec, R., 1998, Few-Body Syst. **25**, 199.

Krivec, R., V. B. Mandelzweig, and K. Varga, 2000, Phys. Rev. A **61**, 062503.

Kröger, H., and R. Perne, 1980, Phys. Rev. C **22**, 21.

Kuang, J., and C. D. Lin, 1997, J. Phys. B **30**, 2529.

Kukulin, V. I., and V. M. Krasnopol'sky, 1977, J. Phys. G **3**, 795.

Kukulin, V. I., and V. N. Pomerantsev, 1978, Ann. Phys. **111**, 330.

Kutzelnigg, W., 1985, Theor. Chem. Acc. **68**, 445, ISSN 1432-881X.

Kutzelnigg, W., and R. Jaquet, 2006, Phil. Trans. R. Soc. A **364**, 2855.

Kutzelnigg, W., and W. Klopper, 1991, J. Chem. Phys. **94**, 1985.

Łach, G., B. Jeziorski, and K. Szalewicz, 2004, Phys. Rev. Lett. **92**, 233001.

Lahaye, T., C. Menotti, L. Santos, M. Lewenstein, and T. Pfau, 2009, Rep. Prog. Phys. **72**, 126401.

Laricchia, G., M. Charlton, C. D. Beling, and T. C. Griffith, 1987, J. Phys. B **20**, 1865.

Lee, R. M., N. D. Drummond, and R. J. Needs, 2009, Phys. Rev. B **79**, 125308.

Leonard, D. S., H. J. Karwowski, C. R. Brune, B. M. Fisher, and E. J. Ludwig, 2006, Phys. Rev. C **73**, 045801.

Lepage, G. P., 1997, eprint arXiv:nucl-th/9706029.

Lester, Jr., W. A., and M. Krauss, 1964, J. Chem. Phys. **41**, 1407.

Lester Jr., W. A., S. M. Rothstein, and S. Tanaka, 2002, *Recent Advances in Quantum Monte Carlo Methods, Part II* (World Scientific, Singapore).

Lin, C. D., 1995, Phys. Rep. **257**, 1.

Liu, J., E. J. Salumbides, U. Hollenstein, J. C. J. . Koelemeij, K. S. E. Eikema, W. Ubachs, and F. Merkt, 2009, J. Chem. Phys. **130**(17), 174306.

Liu, J., D. Sprecher, C. Jungen, W. Ubachs, and F. Merkt, 2010, J. Chem. Phys. **132**, 154301.

Longstaff, J. V. L., and K. Singer, 1960, Proc. R. Soc. London, Ser. A **258**, 421.

Longstaff, J. V. L., and K. Singer, 1964, Theor. Chim. Acta **2**, 265.

Longstaff, J. V. L., and K. Singer, 1965, J. Chem. Phys. **42**, 801.

MacDonald, J. K., 1933, Phys. Rev. **43**, 830.

Madroero, J., P. Schlagheck, L. Hilico, B. Grmaud, D. Delande, and A. Buchleitner, 2005, EPL (Europhysics Letters) **70**, 183.

Maksym, P. A., and T. Chakraborty, 1990, Phys. Rev. Lett. **65**(1), 108.

Margolis, H. S., 2009, J. Phys. B **41**, 154017.

Mathieu, V., 2009, Phys. Rev. D **80**, 014016.

Mathieu, V., C. Semay, and B. Silvestre-Brac, 2008, Phys. Rev. D **77**, 094009.

Matsumoto, T., T. Egami, K. Ogata, Y. Iseri, M. Kamimura, and M. Yahiro, 2006, Phys. Rev. C **73**, 051602.

Matsumoto, T., E. Hiyama, K. Ogata, Y. Iseri, M. Kamimura, S. Chiba, and M. Yahiro, 2004,

Phys. Rev. C **70**, 061601.

Matsumoto, T., T. Kamizato, K. Ogata, Y. Iseri, E. Hiyama, M. Kamimura, and M. Yahiro, 2003, Phys. Rev. C **68**, 064607.

Matsumura, H., M. Orabi, Y. Suzuki, and Y. Fujiwara, 2006, Nucl. Phys. A **776**, 1.

Matsumura, H., and Y. Suzuki, 2004, Nucl. Phys. A **739**, 238.

Matsumura, H., and Y. Suzuki, 2006, Nucl. Phys. A **772**, 55.

May, A., E. Valeev, R. Polly, and F. R. Manby, 2005, Phys. Chem. Chem. Phys. **7**, 2710.

May, A. J., and F. R. Manby, 2004, J. Chem. Phys. **121**, 4479.

McNutt, J. D., S. C. Sharma, and R. D. Brisbon, 1979, Phys. Rev. A **20**, 347.

McWeeny, R., 1950, Nature **166**, 21.

Mehl, J. B., 2009, C. R. Physique **10**, 859.

Mella, M., M. Casalegno, and G. Morosi, 2002, J. Chem. Phys **117**, 1450.

Mella, M., G. Morosi, and D. Bressanini, 1999, J. Chem. Phys **111**, 108.

Mezei, J. Z., A. T. Kruppa, and K. Varga, 2007, Few-Body Syst. **41**, 233.

Mezei, J. Z., J. Mitroy, R. G. Lovas, and K. Varga, 2001, Phys. Rev. A **64**, 032501.

Mitroy, J., 2000, J. Phys. B **33**, 5307.

Mitroy, J., 2004, Phys. Rev. A **70**, 024502.

Mitroy, J., 2005a, Phys. Rev. A **72**, 032503.

Mitroy, J., 2005b, Phys. Rev. Lett. **94**, 033402.

Mitroy, J., 2010, Phys. Rev. A **82**, 052516.

Mitroy, J., 2010, J. At. Mol. Sci. **1**, 275.

Mitroy, J., 2011, (private communication, unpublished).

Mitroy, J., M. W. J. Bromley, and G. G. Ryzhikh, 1999, J. Phys. B **32**, 2203.

Mitroy, J., M. W. J. Bromley, and G. G. Ryzhikh, 2001, *Positronic Atoms* (Kluwer Academic Publishers, The Netherlands), p. 199.

Mitroy, J., M. W. J. Bromley, and G. G. Ryzhikh, 2002, J. Phys. B **35**, R81.

Mitroy, J., and G. G. Ryzhikh, 1999a, J. Phys. B **32**, 1375.

Mitroy, J., and G. G. Ryzhikh, 1999b, J. Phys. B **32**, L621.

Mitroy, J., and G. G. Ryzhikh, 1999c, Comput. Phys. Commun. **123**, 103.

Mitroy, J., M. S. Safronova, and C. W. Clark, 2010, J. Phys. B **43**, 202001.

Mitroy, J., J. Y. Zhang, M. W. J. Bromley, and S. I. Young, 2008a, Phys. Rev. A **78**, 012715.

Mitroy, J., J. Y. Zhang, and K. Varga, 2008b, Phys. Rev. Lett. **101**, 123201.

Mohr, P. J., and B. N. Taylor, 2005, Rev. Mod. Phys. **77**, 1.

Moiseyev, N., 1998, Phys. Rep. **302**, 212.

Moiseyev, N., P. Certain, and F. Weinhold, 1978, Mol. Phys. **36**, 1613.

Müller, H., and W. Kutzelnigg, 2000, Phys. Chem. Chem. Phys. **2**, 2061.

Müller, H.-M., and S. E. Koonin, 1996, Phys. Rev. B **54**, 14532.

Nakashima, H., and H. Nakatsuji, 2007, J. Chem. Phys. **127**, 224104.

Nakashima, H., and H. Nakatsuji, 2010, Astrophys. J. **725**, 528.

Nakatsuji, H., H. Nakashima, Y. Kurokawa, and A. Ishikawa, 2007, Phys. Rev. Lett. **99**, 240402.

Navrátil, P., and B. R. Barrett, 1999, Phys. Rev. C **59**, 1906.

Navrátil, P., S. Quaglioni, I. Stetcu, and B. R. Barrett, 2009, J. Phys. G **36**, 083101.

Nemura, H., and C. Nakamoto, 2007, Prog. Theor. Phys. Supplement **168**, 115.

Ni, K.-K., S. Ospelkaus, M. H. G. de Miranda, A. Pe'er, B. Neyenhuis, J. J. Zirbel, S. Kotochigova, P. S. Julienne, D. S. Jin, and J. Ye, 2008, Science **322**, 231.

Nilsson, B. *et al.*., 2007, Phys. Rev. C **75**, 014007.

Noga, J., D. Tunega, W. Klopper, and W. Kutzelnigg, 1995, J. Chem. Phys. **103**, 309.

Nollett, K. M., S. C. Pieper, R. B. Wiringa, J. Carlson, and G. M. Hale, 2007, Phys. Rev. Lett. **99**, 022502.

Obara, S., and A. Saika, 1986, J. Chem. Phys. **84**, 3963.

Okumura, S., and T. Ogawa, 2001, Phys. Rev. B **65**, 035105.

Ore, A., 1951, Phys. Rev. **83**, 665.

Ospadov, E., D. G. Oblinsky, and S. M. Rothstein, 2011, Phys. Chem. Chem. Phys. (Incorporating Faraday Transactions) **13**, 8031.

Ottschofski, E., and W. Kutzelnigg, 1997, J. Chem. Phys. **106**, 6634.

Pachucki, K., 1997, Phys. Rev. A **56**, 297.

Pachucki, K., 2005, Phys. Rev. A **71**, 012503.

Pachucki, K., 2006a, Phys. Rev. A **74**, 022512.

Pachucki, K., 2006b, Phys. Rev. A **74**, 062510.

Pachucki, K., 2007, Phys. Rev. A **76**(5), 059906.

Pachucki, K., 2010, Phys. Rev. A **82**, 032509.

Pachucki, K., W. Cencek, and J. Komasa, 2005, J. Chem. Phys. **122**, 184101.

Pachucki, K., and J. Komasa, 2003, Phys. Rev. A **68**, 042507.

Pachucki, K., and J. Komasa, 2004, Chem. Phys. Lett. **389**, 209.

Pachucki, K., and J. Komasa, 2004, Phys. Rev. Lett. **92**, 213001.

Pachucki, K., and J. Komasa, 2004, Phys. Rev. A **70**, 022513.

Pachucki, K., and J. Komasa, 2006a, J. Chem. Phys. **125**, 204304.

Pachucki, K., and J. Komasa, 2006b, Phys. Rev. A **73**, 052502.

Pachucki, K., and J. Komasa, 2008, J. Chem. Phys. **129**, 034102.

Pachucki, K., and J. Komasa, 2009, J. Chem. Phys. **130**, 164113.

Pachucki, K., and J. Komasa, 2010, Phys. Chem. Chem. Phys. **12**, 9188.

Pachucki, K., and J. Sapirstein, 2001, Phys. Rev. A **63**, 012504.

Pan, K. C., and H. F. King, 1970, J. Chem. Phys. **53**, 4397.

Pan, K. C., and H. F. King, 1972, J. Chem. Phys. **56**, 4667.

Patkowski, K., W. Cencek, P. Jankowski, K. Szalewicz, J. B. Mehl, G. Garberoglio, and A. H. Harvey, 2008, J. Chem. Phys. **129**, 094304.

Patkowski, K., W. Cencek, M. Jeziorska, B. Jeziorski, and K. Szalewicz, 2007, J. Phys. Chem. A **111**, 7611.

Patkowski, K., and K. Szalewicz, 2010, J. Chem. Phys. **133**, 094304.

Pavanello, M., W. C. Tung, and L. Adamowicz, 2009, J. Chem. Phys. **131**, 184106.

Pederiva, F., C. J. Umrigar, and E. Lipparini, 2000, Phys. Rev. B **62**, 8120.

Peierls, R. E., and J. Yoccoz, 1957, Proc. Phys. Soc. London, Sec. A **70**(5), 381.

Persson, B. J., and P. R. Taylor, 1996, J. Chem. Phys. **105**, 5915.

Petersson, T., and B. Hellsing, 2010, Eur. J. Phys. **31**, 37.

Petrov, D. S., 2003, Phys. Rev. A **67**, 010703(R).

Piela, L., 2007, *Ideas of Quantum Chemistry* (Elsevier, Amsterdam).

Piszczatowski, K., G. Lach, M. Przybytek, J. Komasa, K. Pachucki, and B. Jeziorski, 2009, J. Chem. Theor. Comput. **5**, 3039.

Pitre, L., M. R. Moldover, and W. L. Tew, 2006, Metrologia **43**, 142.

Platter, L., H. W. Hammer, and U. G. Meissner, 2004, Phys. Rev. A **70**, 052101.

Platzman, P. M., and A. P. Mills, Jr., 1994, Phys. Rev. B **49**, 454.

Pollack, S. E., D. Dries, and R. G. Hulet, 2009, Science **326**, 1683.

Poshusta, R. D., 1979, Int. J. Quantum Chem. Symp. **13**, 59.

Powell, M. J. D., 1964, Comput. J. **7**, 155.

Press, W. H., B. P. Flannery, S. A. Teukolsky, and W. T. Vetterling, 1992, *Numerical Recipes in Fortran, 2nd edition* (Cambridge University Press, Cambridge).

Proschel, P., W. Rosner, G. Wunner, H. Ruder, and H. Herold, 1982, J. Phys. B **15**, 1959.

Przybytek, M., W. Cencek, J. Komasa, G. Łach, B. Jeziorski, and K. Szalewicz, 2010, Phys. Rev. Lett. **104**, 183003.

Przybytek, M., B. Jeziorski, and K. Szalewicz, 2009, Int. J. Quantum Chem. **109**, 2872.

Puchalski, K., D. Kedziera, and K. Pachucki, 2011, Phys. Rev. A **84**, 052518.

Puchalski, M., D. Kędziera, and K. Pachucki, 2009, Phys. Rev. A **80**, 032521.

Puchalski, M., and A. Czarnecki, 2008, Phys. Rev. Lett. **101**, 183001.

Puchalski, M., and K. Pachucki, 2006, Phys. Rev. A **73**, 022503.

Puchalski, M., and K. Pachucki, 2008, Phys. Rev. A **78**, 052511.

Puchalski, M., and K. Pachucki, 2010, Phys. Rev. A **81**, 052505.

Pudliner, B. S., V. R. Pandharipande, J. Carlson, S. C. Pieper, and R. B. Wiringa, 1997, Phys. Rev. C **56**, 1720.

Quaglioni, S., and P. Navrátil, 2007, Phys. Lett. B **652**, 370.

Quaglioni, S., and P. Navrátil, 2008, Phys. Rev. Lett. **101**, 092501.

Rakshit, D., K. M. Daily, and D. Blume, 2011.

Ralchenko, Y., A. Kramida, J. Reader, and NIST ASD Team, 2008, NIST Atomic Spectra Database Version 3.1.5, URL http://physics.nist.gov/asd3.

Rassolov, V. A., and D. M. Chipman, 1996, J. Chem. Phys. **105**, 1470.

Regier, P. E., and A. J. Thakkar, 1985, J. Phys. B **18**, 3061.

Reich, E. S., 2004, New Scientist **April 24**, 34.

Rescigno, T. N., and A. E. Orel, 1981, Phys. Rev. A **24**, 1267.

Rescigno, T. N., and B. I. Schneider, 1988, Phys.!Rev. A **37**, 1044.

Reynolds, P. J., D. M. Ceperley, B. J. Alder, and W. A. Lester, 1982a, J. Chem. Phys. **77**, 5593.

Reynolds, P. J., D. M. Ceperley, B. J. Alder, and W. A. Lester, Jr., 1982b, J. Chem. Phys. **77**, 5593.

Richard, J. M., 2003, Phys. Rev. A **67**, 034702.

Rittenhouse, S. T., J. von Stecher, J. P. D'Incao, N. P. Mehta, and C. H. Greene, 2011, J. Phys. B **44**, 172001.

Riva, C., F. Peeters, K. Varga, and V. Schweigert, 2002, Phys. Status Solidi B **234**, 50, ISSN 1521-3951.

Riva, C., F. M. Peeters, and K. Varga, 2000, Phys. Rev. B **61**, 13873.

Riva, C., F. M. Peeters, and K. Varga, 2001, Phys. Rev. B **64**, 235301.

Rybak, S., K. Szalewicz, and B. Jeziorski, 1989, J. Chem. Phys. **91**, 4779.

Rybak, S., K. Szalewicz, B. Jeziorski, and M. Jaszunski, 1987, J. Chem. Phys. **86**, 5652.

Rychlewski, J. (ed.), 2003, *Explicitly Correlated Wave Functions in Chemistry and Physics: Theory and Applications* (Kluwer Academic Publishers, The Netherlands).

Rychlewski, J., W. Cencek, and J. Komasa, 1994, Chem. Phys. Lett. **229**, 657.

Rychlewski, J., and J. Komasa, 2003, in *Explicitly Correlated Functions in Chemistry and Physics*, edited by J. Rychlewski (Kluwer, Dordrecht), pp. 91–148.

Ryzhikh, G., and J. Mitroy, 1998a, J. Phys. B **31**, 4459.

Ryzhikh, G. G., and J. Mitroy, 1997, J. Phys. B **30**, 5545.

Ryzhikh, G. G., and J. Mitroy, 1998b, J. Phys. B **31**, 5013.

Ryzhikh, G. G., J. Mitroy, and K. Varga, 1998a, J. Phys. B **31**, L265.

Ryzhikh, G. G., J. Mitroy, and K. Varga, 1998b, J. Phys. B **31**, 3965.

Saito, S., 1969, Prog. Theor. Phys. **41**, 705.

Saito, S. L., and Y.-I. Suzuki, 2001, J. Chem. Phys. **114**, 1115.

Salmon, L., and R. D. Poshusta, 1973, J. Chem. Phys. **59**, 3497.

Salumbides, E. J., G. D. Dickenson, T. I. Ivanov, and W. Ubachs, 2011, Phys. Rev. Lett. **107**, 043005.

Schmidt, J. W., R. M. Gavioso, E. F. May, and M. R. Moldover, 2007, Phys. Rev. Lett. **98**, 254504.

Schwartz, C., 1962, Phys. Rev. **126**, 1015.

Schwartz, C., 2006a, Int. J. Mod. Phys. E **15**, 877.

Schwartz, C., 2006b, ArXiv eprint math-ph/0605018, URL http://arxiv.org/abs/math-ph/0605018.

Schwegler, E., P. M. Kozlowski, and L. Adamowicz, 1993, J. Comput. Chem. **14**, 566.

Scrinzi, A., 1998, Phys. Rev. A **58**(5), 3879.

Seth, P., P. L. Ríos, and R. J. Needs, 2011, J. Chem. Phys. **134**(8), 084105.

Sharkey, K. L., S. Bubin, and L. Adamowicz, 2011a, J. Chem. Phys. **134**, 044120.

Sharkey, K. L., S. Bubin, and L. Adamowicz, 2011b, Phys. Rev. A **83**, 012506.

Sharkey, K. L., S. Bubin, and L. Adamowicz, 2011c, J. Chem. Phys. **134**, 194114.

Shima, T., S. Naito, Y. Nagai, T. Baba, K. Tamura, T. Takahashi, T. Kii, H. Ohgaki, and H. Toyokawa, 2005, Phys. Rev. C **72**, 044004.

Shiozaki, T., M. Kamiya, S. Hirata, and E. F. Valeev, 2009, J. Chem. Phys. **130**, 054101.

Shumway, J., and D. M. Ceperley, 2001, Phys. Rev. B **63**(16), 165209.

Silvestre-Brac, B., and V. Mathieu, 2007, Phys. Rev. **76**, 046702.

Silvestre-Brac, B., and V. Mathieu, 2008, Phys. Rev. E **77**, 036706.

Sims, J. S., and S. Hagstrom, 1971, Phys. Rev. A **4**, 908.

Sims, J. S., and S. A. Hagstrom, 2011, Phys. Rev. A **83**(3), 032518.

Singer, K., 1960, Proc. R. Soc. London, Ser. A **258**, 412.

Spall, J. C., 2003, *Introduction to Stochastic Search and Optimization* (Wiley).

Sprecher, D., J. Liu, C. Jungen, W. Ubachs, and F. Merkt, 2010, J. Chem. Phys. **133**, 111102.

Stanke, M., S. Bubin, M. Molski, and L. Adamowicz, 2009a, Phys. Rev. A **79**, 032507.

Stanke, M., D. Kędziera, S. Bubin, and L. Adamowicz, 2007a, Phys. Rev. A **75**, 052510.

Stanke, M., D. Kędziera, S. Bubin, and L. Adamowicz, 2007b, Phys. Rev. Lett. **99**, 043001.

Stanke, M., D. Kędziera, M. Molski, S. Bubin, M. Barysz, and L. Adamowicz, 2006, Phys. Rev. Lett. **96**, 233002.

Stanke, M., D. Kędziera, S. Bubin, and L. Adamowicz, 2008, Phys. Rev. A **77**, 022506.

Stanke, M., D. Kędziera, S. Bubin, M. Molski, and L. Adamowicz, 2007, Phys. Rev. A **76**, 052506.

Stanke, M., D. Kędziera, M. Molski, S. Bubin, M. Barysz, and L. Adamowicz, 2006, Phys. Rev. Lett. **96**, 233002.

Stanke, M., J. Komasa, S. Bubin, and L. Adamowicz, 2009b, Phys. Rev. A **80**, 022514.

Stanke, M., J. Komasa, D. Kędziera, S. Bubin, and L. Adamowicz, 2008, Phys. Rev. A **78**, 052507.

Stanke, M., J. Komasa, D. Kędziera, S. Bubin, and L. Adamowicz, 2008, Phys. Rev. A **77**, 062509.

Stone, J. A., and A. Stejskal, 2004, Metrologia **41**, 189.

Strasburger, K., and H. Chojnacki, 1998, J. Chem. Phys. **108**, 3218.

Sucher, J., 1958, Phys. Rev. **109**, 1010.

Sundholm, D., 1995, J. Chem. Phys. **102**, 4895.

Suzuki, Y., Y. Fujiwara, W. Horiuchi, H. Matsumura, and M. Orabi, 2007, Nucl. Phys. A **790**, 223c.

Suzuki, Y., and W. Horiuchi, 2009, Nucl. Phys. A **818**, 188.

Suzuki, Y., W. Horiuchi, and K. Arai, 2009, Nucl. Phys. A **823**, 1.

Suzuki, Y., W. Horiuchi, and D. Baye, 2010, Prog. Theor. Phys. **123**, 547.

Suzuki, Y., W. Horiuchi, M. Orabi, and K. Arai, 2008, Few-Body Syst. **42**, 33.

Suzuki, Y., R. Lovas, K. Yabana, and K. Varga, 2003, *Structure and reactions of light exotic nuclei* (Taylor & Francis, London).

Suzuki, Y., H. Matsumura, M. Orabi, Y. Fujiwara, P. Descouvemont, M. Theeten, and D. Baye, 2008, Phys. Lett. B **659**, 160.

Suzuki, Y., and K. Varga, 1998, *Stochastic variational Approach to Quantum-Mechanical Few-Body Problems*, 172 (Springer, New York).

Szalewicz, K., 2011, Wiley Interdisciplinary Reviews–Computational Molecular Science DOI: 10.1002/wcms.86.

Szalewicz, K., and B. Jeziorski, 1979, Mol. Phys. **38**, 191.

Szalewicz, K., and B. Jeziorski, 2010, Mol. Phys. **108**, 3091.

Szalewicz, K., B. Jeziorski, H. J. Monkhorst, and J. G. Zabolitzky, 1982, Chem. Phys. Lett. **91**, 169.

Szalewicz, K., B. Jeziorski, H. J. Monkhorst, and J. G. Zabolitzky, 1983a, J. Chem. Phys. **78**, 1420.

Szalewicz, K., B. Jeziorski, H. J. Monkhorst, and J. G. Zabolitzky, 1983b, J. Chem. Phys. **79**, 5543.

Szalewicz, K., B. Jeziorski, H. J. Monkhorst, and J. G. Zabolitzky, 1984, J. Chem. Phys. **81**, 2723.

Szalewicz, K., K. Patkowski, and B. Jeziorski, 2005, Structure and Bonding **116**, 43.

Theeten, M., H. Matsumura, M. Orabi, D. Baye, P. Descouvemont, Y. Fujiwara, and Y. Suzuki, 2007, Phys. Rev. C **76**, 054003.

Thompson, D., M. Lemere, and Y. Tang, 1977, Nucl. Phys. A **286**, 53 .

Tornow, W., 2011, Few-Body Syst. **50**, 443.

Truemper, J., W. Pietsch, C. Reppin, W. Voges, R. Staubert, and E. Kendziorra, 1978, Astrophys. J. Lett. **219**, L105.

Tung, W. C., M. Pavanello, and L. Adamowicz, 2010, J. Chem. Phys. **133**, 124106.

Tung, W. C., M. Pavanello, and L. Adamowicz, 2011, J. Chem. Phys. **134**, 064117.

Usukura, J., Y. Suzuki, and K. Varga, 1999, Phys. Rev. B **59**, 5652.

Usukura, J., K. Varga, and Y. Suzuki, 1998, Phys. Rev. A **58**, 1918.

Varga, K., 1999, Phys. Rev. Lett. **83**, 5471.

Varga, K., 2011, Few-Body Syst. **50**, 175.

Varga, K., S. Fleck, and J. M. Richard, 1997, Europhys. Lett. **37**, 183.

Varga, K., P. Navratil, J. Usukura, and Y. Suzuki, 2001, Phys. Rev. B **63**, 205308.

Varga, K., and Y. Suzuki, 1995, Phys. Rev. C **52**, 2885.

Varga, K., Y. Suzuki, and R. G. Lovas, 1994, Nucl. Phys. A **571**, 447.

Varga, K., Y. Suzuki, and I. Tanihata, 1995, Phys. Rev. C **52**, 3013.

Varga, K., Y. Suzuki, and J. Usukura, 1998, Few-Body Syst. **24**, 81.

Varga, K., J. Usukura, and Y. Suzuki, 1998, Phys. Rev. Lett. **80**, 1876.

Vincke, M., and D. Baye, 1989, J. Phys. B **22**, 2089.

Viviani, M., A. Deltuva, R. Lazauskas, J. Carbonell, A. C. Fonseca, A. Kievsky, L. E. Marcucci, and S. Rosati, 2011, ArXiv e-prints eprint 1109.3625.

Viviani, M., A. Kievsky, and S. Rosati, 1995, Few-Body Syst. **18**, 25.

Volosniev, A. G., D. V. Fedorov, A. S. Jensen, and N. T. Zinner, 2011, Phys. Rev. Lett. **106**, 250401.

von Stecher, J., 2010, J. Phys. B **43**, 101002.

von Stecher, J., 2011, Phys. Rev. Lett **107**, 200402.

von Stecher, J., J. P. D'Incao, and C. H. Greene, 2009, Nature Phys. **5**, 417.

von Stecher, J., and C. H. Greene, 2007, Phys. Rev. Lett. **99**, 090402.

von Stecher, J., and C. H. Greene, 2009, Phys. Rev. A **80**, 022504.

von Stecher, J., C. H. Greene, and D. Blume, 2007, Phys. Rev. A **76**, 053613.

von Stecher, J., C. H. Greene, and D. Blume, 2008, Phys. Rev. A **77**, 043619.

Wang, L. M., Z.-C. Yan, H. X. Qiao, and G. W. F. Drake, 2011a, Phys. Rev. A **83**, 034503.

Wang, X., and H. Qiao, 2008, Phys. Rev. A **77**, 043414.

Wang, Y., J. P. D'Incao, and C. H. Greene, 2011b, Phys. Rev. Lett. **106**, 233201.

Wenzel, K. B., J. G. Zabolitzky, K. Szalewicz, B. Jeziorski, and H. J. Monkhorst, 1986, J. Chem. Phys. **85**, 3964.

Werner, F., and Y. Castin, 2006a, Phys. Rev. A **74**, 053604.

Werner, F., and Y. Castin, 2006b, Phys. Rev. Lett. **97**, 150401.

Wheeler, J. A., 1946, Ann. N.Y. Acad. Sci. **48**, 219.

Williams, H. L., T. Korona, R. Bukowski, B. Jeziorski, and K. Szalewicz, 1996, Chem. Phys. Lett.

262, 431.

Wiringa, R. B., S. C. Pieper, J. Carlson, and V. R. Pandharipande, 2000, Phys. Rev. C **62**, 014001.

Wiringa, R. B., V. G. J. Stoks, and R. Schiavilla, 1995, Phys. Rev. C **51**, 38.

Witała, H., and W. Glöckle, 1999, Phys. Rev. C **60**, 024002.

Wojs, A., and P. Hawrylak, 1996, Phys. Rev. B **53**, 10841.

Wright, G. L., M. Charlton, G. Clark, T. C. Griffith, and G. R. Heyland, 1983, J. Phys. B **16**, 4065.

Yahiro, M., M. Nakano, Y. Iseri, and M. Kamimura, 1982, Prog. Theo. Phys. **67**, 1467.

Yan, Z., J. Zhang, and Y. Li, 2003, Phys. Rev. A **67**, 062504.

Yan, Z. C., J. F. Babb, A. Dalgarno, and G. W. F. Drake, 1996, Phys. Rev. A **54**, 2824.

Yan, Z. C., and G. W. F. Drake, 1995, Phys. Rev. A **52**(5), 3711.

Yan, Z.-C., and G. W. F. Drake, 2003, Phys. Rev. Lett. **91**, 113004.

Yan, Z. C., and Y. K. Ho, 1999, Phys. Rev. A **59**, 2697.

Yan, Z.-C., W. Nörtershäuser, and G. W. F. Drake, 2008, Phys. Rev. Lett. **100**, 243002.

Yannouleas, C., and U. Landman, 1999, Phys. Rev. Lett. **82**(26), 5325.

Yuan, J., B. D. Esry, T. Morishita, and C. D. Lin, 1998, Phys. Rev. A **58**, R4.

Zaccanti, M., B. Deissler, C. D'Errico, M. Fattori, M. Jona-Lasinio, S. Müller, G. Roati, M. Inguscio, and G. Modugno, 2009, Nature Phys. **5**, 586.

Zhang, J. Y., and J. Mitroy, 2007, Phys. Rev. A **76**, 014501.

Zhang, J. Y., and J. Mitroy, 2008, Phys. Rev. A **78**, 012703.

Zhang, J. Y., and J. Mitroy, 2011, Phys. Rev. A **83**, 022711.

Zhang, J. Y., J. Mitroy, and K. Varga, 2008, Phys. Rev. A **78**, 042705.

Zhang, J.-Y., J. Mitroy, and K. Varga, 2009, Phys. Rev. Lett. **103**, 223202.

Zhang, S., and H. Krakauer, 2003, Phys. Rev. Lett. **90**, 136401.

Zhukov, M. V., B. V. Danilin, D. V. Fedorov, J. M. Bang, I. S. Thompson, and J. S. Vaagen, 1993, Phys. Rep. **231**, 151.

Zumbühl, D. M., C. M. Marcus, M. P. Hanson, and A. C. Gossard, 2004, Phys. Rev. Lett. **93**, 256801.